



**Universidad
Europea**

UNIVERSIDAD EUROPEA DE MADRID

ESCUELA DE ARQUITECTURA, INGENIERÍA Y DISEÑO

DEGREE IN AEROSPACE ENGINEERING

FINAL PROJECT REPORT

**PRELIMINARY DESIGN OF A VARIABLE
AREA PROPELLING NOZZLE FOR AN
AFTERBURNING MILITARY AIRCRAFT
ENGINE**

Christopher Fernandez

YEAR 2023-2024

TITLE: Preliminary Design of a Variable Area Propelling Nozzle for an Afterburning Military Aircraft Engine

AUTHOR: Christopher Fernandez Torres

SUPERVISOR: Rafael Pax

DEGREE: Aerospace Engineering

DATE: 09/06/2024

ABSTRACT

This project presents the preliminary design of a variable area propelling nozzle for an afterburning military aircraft engine. The study begins with an engine cycle analysis using a Python script to iterate through various flight speeds and altitudes, simulating engine performance with and without afterburners. Key parameters such as thrust, thrust specific fuel consumption (TSFC), total pressure, total temperature at the nozzle, and exit area were analyzed and validated against a reference engine. A simple nozzle geometry, trapezoidal in shape, was designed to facilitate pressure and temperature distribution calculations along its length. Structural analyses, including 2D force and moment distributions, were conducted to ensure the nozzle's integrity. A 3D CFD analysis provided detailed internal flow characteristics, which were then used in a 3D structural simulation to obtain stress distributions. Design optimization and material selection were performed iteratively. Finally, bell-crank design and actuator force calculations were completed to ensure the nozzle's operational functionality. The project concludes with the identification of suitable actuators to handle the required forces, as well as the future works required to improve and continue upon the project.

Keywords: Preliminary Design, Variable area nozzle, Afterburners, Engine cycle, Actuators, Multi-physical analysis.

RESUMEN

Este proyecto presenta el diseño preliminar de una tobera de propulsión de área variable para un motor de aeronave militar con postcombustión. El estudio comienza con un análisis del ciclo del motor utilizando un script en Python para iterar a través de varias velocidades de vuelo y altitudes, simulando el rendimiento del motor con y sin postcombustores. Se analizaron y validaron contra un motor de referencia parámetros clave como el empuje, el consumo específico de combustible (TSFC), la presión total, la temperatura total en la tobera y el área de salida. Se diseñó una geometría simple de la tobera, de forma trapezoidal, para facilitar los cálculos de distribución de presión y temperatura a lo largo de su longitud. Se realizaron análisis estructurales, incluyendo distribuciones de fuerzas y momentos en 2D, para asegurar la integridad de la tobera. Un análisis CFD en 3D proporcionó características detalladas del flujo interno, que luego se utilizaron en una simulación estructural 3D para obtener distribuciones de tensiones. La optimización del diseño y la selección de materiales se realizaron de manera iterativa. Finalmente, se completaron los cálculos de diseño de la manivela y la fuerza del actuador para asegurar la funcionalidad operativa de la tobera. El proyecto concluye con la identificación de actuadores adecuados para manejar las fuerzas requeridas, así como los trabajos futuros necesarios para mejorar y continuar el proyecto.

Palabras Clave: Diseño preliminar, Tobera de área variable, Postcombustión, Ciclo del motor, Actuadores, Análisis multifísico.

ACKNOWLEDGMENTS

Firstly, I want to thank my supervisor, Rafael Pax. He provided me with unconditional help whenever I needed it and went further and beyond to explain to me several propulsion and structural concepts that were not included in either subject of the degree and where necessary for a proper development of such project. Additionally, he aroused in me a strong interest in developing this project and gave me significant ideas of where I could take it when I first introduced it to him. For this, I am truly grateful.

I would also like to express my infinite gratitude to my father, for whom without his continuous moral and economic support, I would not be able to be anywhere close to this point of my life academically, physically, and mentally. For this, I am forever in debt.

Finally, I want to thank myself for not giving up during these last 4 tough years of study, handling each situation, problem, exam, project, presentation, setback one at time with the same mindset; get it done regardless of how you feel about it.

CONTENTS

ABSTRACT	3
RESUMEN.....	4
ACKNOWLEDGMENTS.....	5
CONTENTS.....	6
FIGURES.....	9
TABLES.....	12
1. INTRODUCTION.....	13
1.1. Problem Approach.....	13
1.2. Project Objectives.....	14
1.3. Methodology.....	14
1.3.1. Engine Cycle Analysis.....	14
1.3.2. Mechanical & Structural Nozzle Definition.....	15
1.3.3. 3D CFD & Structural Analysis.....	16
1.3.4. Actuator & Linkage System Definition.....	16
2. BACKGROUND FOR ENGINE CYCLE ANALYSIS.....	18
2.1. History of Afterburner Technology.....	19
2.2. Implications of Afterburner Use.....	21
2.2.1. Thrust Augmentation.....	21
2.2.2. Required Control Systems.....	21
2.2.3. Thermal Challenges.....	22
2.2.4. Fuel Consumption.....	23
2.3. Nozzles Designs Enabling Afterburner Use.....	24
2.3.1. Axisymmetric Nozzles.....	24
2.3.2. Bi-Dimensional Nozzles.....	25
2.4. Reference Engine: RB199.....	26
2.4.1. Design & Development.....	28
2.4.2. Specifications.....	28
3. ENGINE THERMODYNAMIC CYCLE ANALYSIS.....	30
3.1. Engine Model for Analysis.....	30
3.2. Analytical Analysis.....	33

3.2.1.	Ambient Conditions.....	33
3.2.2.	Inlet.....	34
3.2.3.	Fan (LPC).....	36
3.2.4.	Core Compressor (HPC).....	36
3.2.5.	Combustion Chamber.....	37
3.2.6.	High-Pressure Turbine (HPT).....	38
3.2.7.	Low-Pressure Turbine (LPT).....	38
3.2.8.	Nozzle (without afterburner).....	39
3.2.9.	Nozzle (with afterburner).....	40
3.2.10.	Final Calculations.....	40
3.3.	Numerical & Iterative Analysis.....	42
3.3.1.	Thrust & Thrust Augmentation	43
3.3.2.	Nozzle Exit Area & Area Increase.....	45
3.3.3.	Nozzle Exit Total Pressure	46
	47
3.3.4.	Thrust Specific Fuel Consumption & Consumption Increase.....	47
3.3.5.	Nozzle Pressure Ratio.....	49
4.	PRELIMINARY NOZZLE DESIGN.....	51
4.1.	Theoretical Background.....	51
4.1.1.	Nozzle Functions.....	51
4.1.2.	Nozzle Types.....	52
4.1.3.	Nozzle Efficiencies & Thrust.....	54
4.1.4.	Nozzle Losses.....	56
4.1.5.	Nozzle Performance based on Nozzle Type.....	62
4.1.6.	Nozzle Flow Equations	66
4.2.	Conceptual Design	69
4.2.1.	Nozzle Concept Selection.....	69
4.2.2.	Nozzle Conceptual Design	70
4.3.	Nozzle Preliminary Design.....	75
4.3.1.	Mechanical Conceptual Design, Initial Sizing & 2D Analysis.....	75
4.3.2.	3D CFD, Structural Analysis & Pressure and Temperature Loads Design Optimization.....	89
4.3.3.	Derivation of Actuator Requirements & Preliminary Selection.....	97
5.	CONCLUSIONS & FUTURE WORKS	101

5.1. Conclusions.....	101
5.2. Future Works.....	102
REFERENCES.....	105
APPENDICES.....	107

FIGURES

Figure 2.1. Schematic of afterburning components and functionality at the tail end of a jet engine (Rolls Royce [1]).....	18
Figure 2.2. Campini Caproni C.C.2, 1940, early jet engine, WWII Italy (Phil DeFer).....	19
Figure 2.3. F-89 Scorpion (top), F6U Pirate (left) & F-94 Starfire (right) (USAF & USN).....	20
Figure 2.4. Thrust augmentation ratio in relation to the temperature ratio (Rolls Royce [1]).....	21
Figure 2.5. Simplified schematics of an afterburner control system (Rolls Royce [1]).....	22
Figure 2.6. SFC comparison between normal engine operation and 70% thrust augmentation with afterburner at different Mach numbers as a function of altitude (Rolls Royce [1]).....	23
Figure 2.7. Axisymmetric exhaust nozzle fitted onto the F/A-18 Hornet.....	25
Figure 2.8. Bi-Dimensional exhaust nozzle fitted onto the F-22 Raptor.....	26
Figure 2.9. RB199 engine on display at the Royal Air Force Museum Hendon [4] (top). Panavia Tornado GR4 under training [5] (bottom).....	27
Figure 3.1. Engine model schematics diagram.....	31
Figure 3.2. Engine stages diagram.....	31
Figure 3.3. ISA model [10].....	33
Figure 3.4. Thrust vs Flight Speed graph for the model engine at different altitudes with and without afterburners.....	43
Figure 3.5. Exit Area vs Flight Speed graph for the model engine at different altitudes with and without afterburners.....	45
Figure 3.6. Nozzle Exit Total Pressure vs Flight Speed graph for the model engine at different altitudes with and without afterburners.....	47
Figure 3.7. Thrust Specific Fuel Consumption vs Flight Speed graph for the model engine at different altitudes with and without afterburners.....	48
Figure 3.8. Nozzle Pressure Ratio vs Flight Speed graph for the model engine at different altitudes with and without afterburners.....	50
Figure 4.1. Turbojet Brayton Cycle with and without afterburners (NASA, 1990) [11].....	51
Figure 4.2. Convergent (top) & Convergent-Divergent (bottom) nozzles examples.....	54
Figure 4.3. Divergence factor as a function of α for a conical exit (NASA, 1990) [11].....	57
Figure 4.4. Nozzle thrust efficiency as a function of NPR for a fixed-area-ratio CD nozzle (NASA, 1990) [11].....	58
Figure 4.5. Overexpanded nozzle pressure distribution & illustration (NASA, 1990) [11].....	59
Figure 4.6. Underexpanded nozzle pressure distribution & illustration (NASA, 1990) [11].....	60

Figure 4.7. Typical NPRs as a function of freestream Mach number (AIAA, 2002) [12].....	60
Figure 4.8. Ratio of convergent nozzle gross thrust to ideal gross thrust vs NPR (AIAA, 2002) [12].....	61
Figure 4.9. Variation of nozzle efficiency for fixed-geometry nozzles (NASA, 1990). [11].....	62
Figure 4.10. Convergent nozzle correction coefficients as a function of convergence half-angle (NASA, 1990). [11].	64
Figure 4.11. Choked convergent nozzle discharge coefficient as a function of convergence half-angle (NASA, 1990). [11].....	65
Figure 4.12. Area ratio vs Mach number for air with $\gamma = 1.4$	68
Figure 4.13. Nozzle geometrical concept design.....	71
Figure 4.14. Local temperature, pressure, and velocity along the nozzle for the dry engine (top) and the wet engine (bottom) at Sea-Level-Static.....	74
Figure 4.15. Nozzle-actuator mechanical configuration (Side View).....	75
Figure 4.16. Nozzle-actuator mechanical configuration (Top View).....	76
Figure 4.17. Nozzle-actuator mechanical configuration (Front View).....	76
Figure 4.18. Nozzle plate load diagram	77
Figure 4.19. Nozzle plate loading case Free-Body-Diagram.	78
Figure 4.20. Nozzle plate Shear Force diagram.....	80
Figure 4.21. Nozzle plate Bending Moment diagram.	80
Figure 4.22. Convergent nozzle plate diagram drawing.....	81
Figure 4.23. Nozzle plate and stiffeners front view initial dimensions drawing.	85
Figure 4.24. Nozzle plate and stiffeners side view initial dimensions drawing.	86
Figure 4.25. Nozzle plate and stiffeners front view final design.....	87
Figure 4.26. Nozzle plate and stiffeners side view final design.....	87
Figure 4.27. Nozzle plate and stiffeners isometric view final design.....	88
Figure 4.28. Nozzle fluid domain definition in ANSYS DM.....	89
Figure 4.29. Nozzle flow simulation results of (top) Mach number contours and (bottom) Mach number plot along the length.....	91
Figure 4.30. Nozzle flow simulation results of (top) static temperature contours and (bottom) static temperature plot along the length.....	92
Figure 4.31. Nozzle flow simulation results of (top) static pressure contours and (bottom) static pressure plot along the length.....	93
Figure 4.33. Nozzle plate imported pressure loads.....	94
Figure 4.32. Nozzle plate and stiffener configuration with fixed supports definition.....	94
Figure 4.34. Nozzle plate resultant total deformation side (top) and front (bottom) views.....	95

Figure 4.35. Nozzle plate resultant total stress (Von-Misses) isometric view.....	95
Figure 4.36. Nozzle plate resultant stress concentration around rod and stiffeners.....	96
Figure 4.37. General diagram of an arbitrary bell crank link.....	97
Figure 4.38. Force diagram of nozzle plate and bell crank linkage.....	98
Figure 4.39. MTS DuraGlide 244 hydraulic actuator picture (MTS) [16].....	100
Figure 4.40. MTS DuraGlide 244 drawing (top) and specifications sheet (bottom) (MTS) [16].....	100

TABLES

Table 3.1. Thrust Augmentation Ratio expressed as % increase for different Altitudes at Mach 0.....	44
Table 3.2. Exit Area Augmentation expressed as % increase for different Altitudes at Mach 0.....	46
Table 3.3. TSFC Augmentation expressed as % increase for different Altitudes at Mach 0.....	49
Table 4.1 Static equilibrium resultants and Max BM & SF for the convergent plate with wet and dry convergence angles at SLS conditions.....	82
Table 4.2. Resultant Actuator Output & Input Forces for the Different Nozzle Convergence Angles.....	99

1. INTRODUCTION

Inside the realm of aviation, the driving force that enables aircraft to takeoff from the ground, soar the skies and travel thousands of miles over the globe at incredibly high speeds and altitudes is, without argument, the engine. With well over 100 years of development, aircraft engines have evolved from simple reciprocating, internal combustion engines to highly complex turbine-powered reaction engines. These powerplants are considered a critical subsystem of the complete aircraft and very special care is given to their design, manufacturing, testing, and integration considering the aircraft's mission requirements.

1.1. Problem Approach

In the case of military, combat-ready aircraft, engine requirements involve characteristics far from those required by commercial jetliners, which focus on low carbon footprint, lower consumption, and overall higher efficiencies. On the other hand, military aircraft such as: multipurpose fighter aircraft (e.g. F-35, F-22, F-16, Eurofighter) or high speed, high altitude strategic reconnaissance aircraft (e.g. SR-71, MiG-25) are required to have high maneuverability capabilities at high speeds, supersonic flight capabilities, high flight ceilings, and stealth. For this purpose, these aircraft don't employ high bypass, ultra efficient turbofan engines. Instead, designers cleverly incorporate engines that are capable of offering high thrust-to-weight ratios, enabling and sustaining supersonic flight, and reducing the radar detectability of the aircraft.

One of the main characteristics of engines designed for military aircraft is the integration of afterburner technology for the purpose of significantly increasing thrust during short periods of time. The use of afterburners has several effects and implications at a physical level besides the thrust augmentation. This project embarks on a multifaceted study, delving into the nuanced interactions between engine thermodynamics, nozzle area adjustments, and the exigencies of varying altitudes in order to paint an overall yet detailed picture of the effects that afterburner use has on engine and aircraft performance and arrive at an accurate design of a variable area propelling nozzle while remaining under the scope of a last year project of bachelor's degree in aerospace engineering.

1.2. Project Objectives

The main objective of this project is to perform and validate a comprehensive, multi-disciplinary analysis and preliminary design of an engine nozzle enabling afterburner use. This includes analyzing the thermodynamics that take place during afterburner use of an operating engine, the effects that altitude has on performance, and the mechanism that are required to ensure proper functionality of the afterburner. For this purpose, the following specific objectives will be developed and expressed in the coming chapters.

- Engine thermodynamic cycle analysis as a function of altitude and flight speed.
- Comparison of engine performance (from cycle analysis) with and without the afterburner use with reference engine available data.
- Analysis of the impact of altitude variation on engine performance with and without afterburner.
- Conceptual and preliminary definition and validation of a nozzle design enabling afterburner use considering resultant nozzle pressure distribution (from cycle analysis).
- Preliminary mechanical design of a variable exhaust area propelling nozzle and derivation of actuator requirements.

1.3. Methodology

1.3.1. Engine Cycle Analysis

To begin the preliminary design of a variable area propelling nozzle for an afterburning military aircraft engine, a comprehensive engine cycle analysis was conducted. The methodology involved the following steps:

- Reference engine selection.

- Definition of model engine based on reference engine data.
- Analytical analysis of all engine components in a similar manner to propulsion system problems.
- Python script written considering equations from analytical analysis to iterate through various flight speeds and altitudes to obtain relevant engine cycle results and graph them.
- Analysis of engine cycle results and validation with available data from reference engine.

1.3.2. Mechanical & Structural Nozzle Definition

Considering the defined assumptions and resultant total pressures and temperatures of the engine cycle analysis, a definition of a nozzle geometry was chosen with certain criteria to obtain the static pressure, temperature and velocity distribution along the nozzle's length and define a mechanical and structural design suitable for sustaining the fluid pressure loads in a 2D manner. The methodology involved the following steps:

- General nozzle shape was chosen together with the cross-sectional shape considering the defined entry and exit areas required for afterburner and non-afterburner operation; obtained from the cycle analysis for the Sea Level Static case.
- Using the defined nozzle geometry and results from cycle analysis, pressure, temperature, and velocity inside the nozzle were obtained for discrete defined points.
- Based on the pressure distributions obtained, resultant forces on the nozzle wall were calculated in a 2D context.
- By setting fixed pivot points, resultant forces, moments, shear force distribution, and bending moment distribution along the nozzle were determined, and overall shear and bending moment stress were calculated for an arbitrary defined nozzle plate.
- Definition of mechanical nozzle design considering actuator configuration placement and stiffener placement was chosen.

- Nozzle material selection was performed considering typical materials used in aerospace industry for similar applications.

1.3.3. 3D CFD & Structural Analysis

The nozzle plate structure was defined in a 3D manner, as well as the fluid domain inside the nozzle in order to simulate the exact same behavior in a 3D manner and obtain overall stress and deflection distribution considering the same mechanical design. The methodology involved the following steps:

- A 3D CFD analysis was conducted using ANSYS Fluent to simulate the internal flow through the defined nozzle geometry, and the same parameters and nozzle inlet flow speed results as the engine cycle analysis were employed.
- The pressure distribution obtained from the 3D CFD analysis was imported into ANSYS Static Structural to study the 3D stress and deflection distribution of the nozzle plate mechanical structure considering actuator placement. The same fixed points were considered as the 2D analysis.
- Iterations of the design were performed by adjusting dimensions and configurations in order to minimize overall stress and stress concentration along edges with the defined material selection.

1.3.4. Actuator & Linkage System Definition

Finally, an actuator-linkage system was defined considering the placement and resultant moments enabling static equilibrium of the plate and rotation for afterburner operation. The methodology involved the following steps:

- Definition of bell-crank mechanism enabling translation of actuator force in one direction to another direction with a mechanical advantage; considering nozzle mechanical design dimensions.
- Required actuator forces were derived from the force and moment analysis.

- Based on the calculated forces and further changes to the actuator configuration, a commercial actuator suitable to withstand the loads was chosen.

2. BACKGROUND FOR ENGINE CYCLE ANALYSIS

Within the field of aerospace engineering, the incorporation of afterburner technology into aircraft engines is a tribute to human resourcefulness and the unwavering quest for improved performance. The afterburner, sometimes referred to as reheat or "burner cans," is an essential part of military aircraft propulsion systems that gives them unmatched performance, maneuverability, acceleration, and short takeoff capabilities.

Using the unburned oxygen in the exhaust stream to enable combustion, afterburning is the process of adding and burning fuel between the engine turbine and the jet pipe propelling nozzle. The temperature of the exhaust gas rises as a result, increasing the jet's velocity as it exits the propelling nozzle and raising engine thrust (Rolls Royce, 1986) [1].

The technology of afterburners is important because it provides aircraft with brief bursts of increased thrust, which allow them to reach supersonic speeds and perform maneuvers during operations. When performing air-to-air dogfights, ground assault missions, or surveillance sorties, military aircraft fitted with afterburners have an unparalleled tactical advantage due to their unrivaled speed and agility.

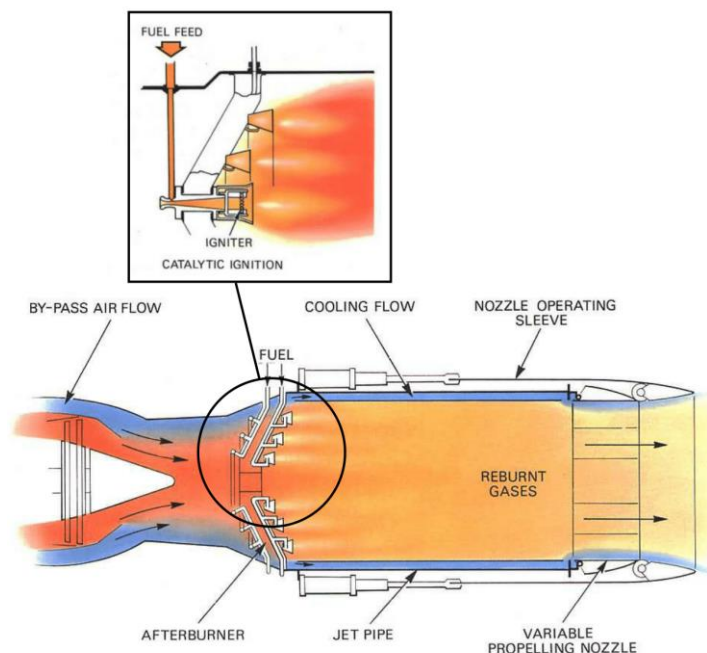


Figure 2.1. Schematic of afterburning components and functionality at the tail end of a jet engine (Rolls Royce [1]).

2.1. History of Afterburner Technology

The origins of afterburner technology may be found in the years following World War II, which saw substantial developments in jet propulsion and aviation as an industry. Engineers looked for creative ways to push aircraft beyond the supersonic threshold in their pursuit of increased performance and speed. During this period, the afterburner became a ground-breaking idea that revolutionized jet engine performance and opened the door for the creation of high-performance military aircraft.

The Caproni Campini C.C.2 Motorjet, the first aircraft to incorporate what would be considered as the first attempt at implementing a thrust augmentation system similar to an afterburner, had its maiden flight on April 11, 1941. Soon after, allied powers began exploring and experimenting with the idea of an afterburner.



Figure 2.2. Campini Caproni C.C.2, 1940, early jet engine, WWII Italy (Phil DeFer).

As Cyril Elliott described in the book *Fast Jets, The History of Reheat Development at Derby* (2002), the first British afterburner experiments were conducted in late 1944 on a Rolls-Royce W2/B23 in a Gloster Meteor I and followed in mid-1945 on a Power Jets W2/700 engine on the ground. This engine was intended for the later discarded supersonic aircraft project, Miles M.52 [2].

NACA (current NASA), conducted an early study on the idea as well. As a result, the article *Theoretical Investigation of Thrust Augmentation of Turbojet Engines by Tail-pipe Burning* was published in January

1947 [3]. This led to the first implementation of afterburners into American-produced aircraft such as the Vought F6U "Pirate", the Lockheed F-94 "Starfire", and the Northrop F-89 "Scorpion" (figure 2.3.)



Figure 2.3. F-89 Scorpion (top), F6U Pirate (left) & F-94 Starfire (right) (USAF & USN).

2.2. Implications of Afterburner Use

2.2.1. Thrust Augmentation

The engine's thrust production with and without afterburner activation is compared in the thrust augmentation ratio, which provides an indication of the extent of power improvement possible with this technology. The thrust augmentation ratio, which is commonly expressed as a percentage increase, demonstrates the dynamic capabilities of aircraft equipped with afterburners during high-speed flight and fast acceleration.

The thrust increase during afterburning operation is solely caused by the significant increase in total temperature after the re-combustion occurs. This increase in total temperature is thermodynamically related to a direct increase in jet exhaust velocity by the square root of the temperature augmentation ratio, which directly increases thrust linearly by this same magnitude, as shown in figure 2.4.

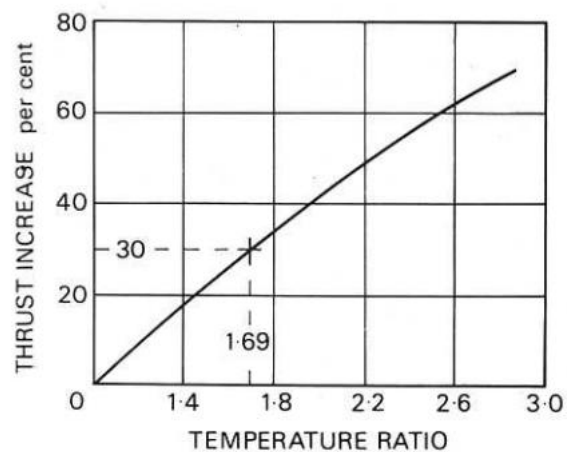


Figure 2.4. Thrust augmentation ratio in relation to the temperature ratio (Rolls Royce [1])

2.2.2. Required Control Systems

In addition to providing unmatched thrust capabilities, the incorporation of afterburner technology into military aircraft engines raises a number of issues that have a significant impact on operational strategies and engine design. The key to using afterburners, while preventing pressure build ups that may lead to surges and engine failures, is to dynamically modify the nozzle exhaust area as the fuel flow rate of the afterburner is increased.

Thus, as Rolls Royce has stated, it is clear that for the afterburner system to operate satisfactorily, two functions, fuel flow and exhaust nozzle area, must be coordinated. By making the nozzle area reliant on the fuel flow at the afterburners or vice versa, both functions are therefore connected. In combination with a jet pipe pressure sensor device (a pressure ratio control unit), the pilot is able to regulate the nozzle area or the afterburner fuel flow. The nozzle area grows with an increase in afterburner fuel flow and reduces with a reduction in afterburner fuel flow. Regardless of the nozzle area and fuel flow, the pressure ratio control unit makes sure the pressure ratio across the turbine is constant and that the afterburning process has no effect on the engine (Rolls Royce, 1986) [1].

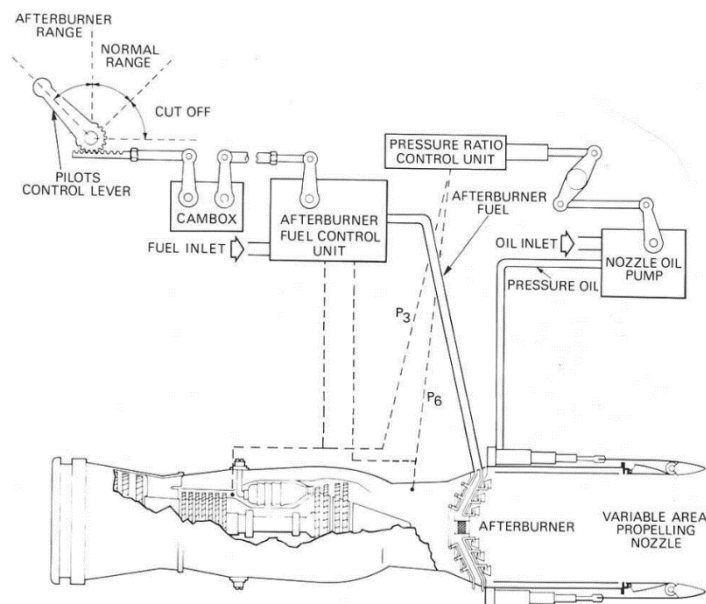


Figure 2.5. Simplified schematics of an afterburner control system (Rolls Royce [1])

2.2.3. Thermal Challenges

Aircraft engines must adhere to strict maintenance guidelines since afterburner operation increases thermal and mechanical loads. Afterburner-equipped aircraft must undergo routine inspections, component replacements, and extensive testing procedures to maintain their airworthiness and operational readiness. Due to the high temperatures of continuous afterburning employment, both

passive and active cooling techniques are employed in order to prevent complete engine degradation and malfunction. Furthermore, this implies that the capability to increase thrust with afterburner use is directly limited by the inability to sustain higher temperatures in the combustion chamber and nozzle. Material selection and insulation plays a critical role in enabling the use of afterburners, as well as active cooling systems.

2.2.4. Fuel Consumption

Perhaps the most obvious and prominent implication (and limitation) of afterburner use is its increase in fuel consumption. This is the main reason why afterburners are generally limited to short periods of operation.

The gas stream has to be filled with more fuel in order to reach the necessary temperature ratio. The fuel is not burned as effectively as it would be in the engine combustion chamber because the temperature rise does not happen at the peak of the compression, requiring a greater fuel consumption.

Fuel consumption rates are often expressed in terms of specific fuel consumption (SFC). The use of afterburners may increase this parameter by two to three times the standard cruise SFC. Altitude also has a significant effect on both cruise SFC and afterburner SFC, due to the reduced intake temperatures with increased altitude.

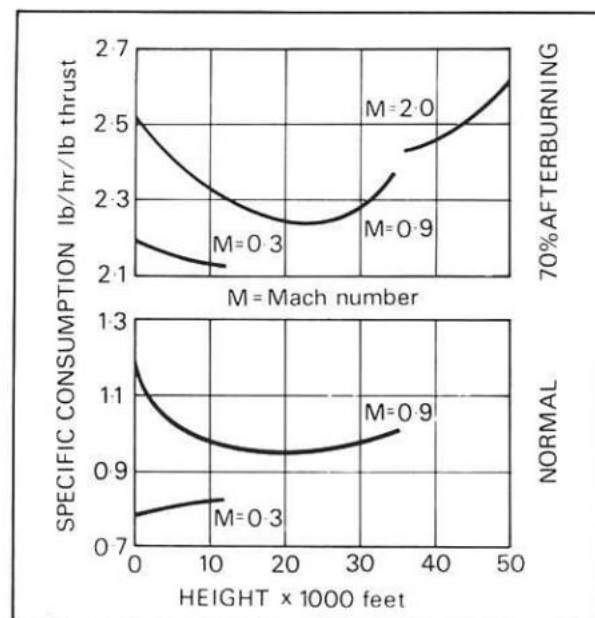


Figure 2.6. SFC comparison between normal engine operation and 70% thrust augmentation with afterburner at different Mach numbers as a function of altitude (Rolls Royce [1]).

2.3. Nozzles Designs Enabling Afterburner Use

The efficient application of afterburner technology is largely dependent on the design of jet engine nozzles, which offer a way to regulate exhaust flow, maximize thrust production, and improve engine efficiency for different flight conditions by modifying the exhaust area dynamically as required. To meet the demands of afterburner operations, a variety of nozzle designs and technical advancements have been created, each specifically suited to the needs of various aircraft and engine combinations.

Besides the different use cases of Converging-Diverging (CD) nozzles or converging only nozzles, which are explained in a separate chapter, generally only two geometric types of nozzle design are implemented on fighter aircraft depending on their mission requirements; Axisymmetric (conical) and Bi-Dimensional (2D) nozzles.

2.3.1. Axisymmetric Nozzles

Axisymmetric (conical) jet engine exhaust nozzles have been a cornerstone of jet propulsion systems for decades. Their circular cross-section and smooth, pro-convergent-divergent design allow for efficient and versatile exhaust flow control in different conditions.

In terms of flight dynamics and maneuverability, the round shape can be fitted with actuators to swivel around in any direction. This gives the nozzle thrust vectoring capabilities on both the pitch and yaw axis. Additionally, the rounded shape allows the material to efficiently withstand the pressure forces of the exhaust gases and outside ambience, making it lighter, simpler, and less costly.

In terms of the actuators required for enabling afterburner use, the axisymmetric nozzle requires significantly more complex control systems that fit the rounded shape of the exhaust and provide support for the change in area. A clear example of this nozzle type can be seen on the GE F404 engines fitted onto the F/A-18 Hornet (figure 2.7).



Figure 2.7. Axisymmetric exhaust nozzle fitted onto the
F/A-18 Hornet.

2.3.2. Bi-Dimensional Nozzles

Bi-Dimensional, or squared-shaped, jet engine exhaust nozzles represent a more advanced and tailored approach to exhaust flow control. These nozzles feature a rectangular or square cross-section and are designed to control exhaust flow in two dimensions.

In contrast with axisymmetric nozzles, bi-dimensional nozzles require more complex designs and more robust materials in order to withstand the operational loads encountered during flight and the pressure differential caused by the exhaust gases. This makes the nozzles heavier and more expensive.

These nozzles, generally, only offer thrust vectoring around the pitch axis only due to their 2-dimensional nature, although if used in a twin-engine configuration, the nozzle is able to offer roll maneuverability by asymmetric controls.

The most significant and only clear advantage of squared-shaped nozzles over axisymmetric nozzles is its enhanced radar and infrared capabilities. This allows aircraft, such as the F-22 Raptor (figure 2.8), to be designed for greater stealth capabilities as the nozzle can be aligned to prevent radar reflection, while shielding the exhaust gases from view to decrease the infrared detectability of the aircraft.

In terms of the actuators required for enabling afterburner use, the Bi-Dimensional nozzle requires less complex and much simpler & redundant control systems to provide the required area change, as it only moves up or down.



Figure 2.8. Bi-Dimensional exhaust nozzle fitted onto the F-22 Raptor.

2.4. Reference Engine: RB199

For the purposes of the comprehensive analysis, an engine thermodynamic cycle needs to be performed, following the definition of an engine model that will be described in the following section. This engine model will be based on a reference engine for the purpose of obtaining key engine parameters and performance data for performing the analysis and comparing it with available literature.

For this purpose, the selected reference engine is the *Turbo-Union RB199*. This is a turbofan type engine built in the 1970s for the *Panavia Tornado* (figure 2.9) and was employed for the development of the Eurofighter Project [6].



Figure 2.9. RB199 engine on display at the Royal Air Force Museum Hendon [4] (top). Panavia Tornado GR4 under training [5] (bottom).

2.4.1. Design & Development

The RB199 engine, developed and produced in collaboration by MTU Aero Engines, Rolls-Royce, and Aeritalia (current Avio Aero), powers the multi-role combat aircraft Tornado. Throughout the 1970s and 1980s, Europe's biggest and most prosperous military aircraft program was the *Panavia Tornado*. Over seven million flight hours have been logged by the engine since its delivery. A three-shaft configuration with a thrust reverser and afterburner was selected to fulfill the various mission requirements of the Tornado, particularly the operations at extremely low altitudes. This engine is also the only military engine with an integrated thrust reverser in the world (MTU Aero [7]).

Rolls-Royce chose a bypass ratio of around 1.2 and three shafts as the general design idea for the global collaboration effort. The bypass ratio was selected to provide low fuel consumption over a long distance, especially when the throttle was decreased. Additionally, the chosen BPR produced a greater reheat increase than lesser values on engines that were comparable. Rolls-Royce also designed and manufactured the fan, combustor, high pressure turbine, and the afterburner stages. Aeritalia was in charge of the design and manufacturing of the low-pressure turbine and the nozzle stages, while MTU developed the intermediate and high-pressure compressors, the intermediate pressure turbine, and the thrust reverser system.

On September 27, 1971, the RB199 made its debut test at Patchway, UK. An Avro Vulcan with the engine mounted in a nacelle resembling that of a Tornado aircraft was used for the test flights. 1972 saw RB199 maiden flight aboard the Vulcan.

2.4.2. Specifications

These specifications are provided by the manufacturers (Rolls Royce & MTU Aero).

General Characteristics:

- Length = 3.2m
- Fan Diameter = 0.72m
- Dry Weight = 976kg

Performance:

- BPR = 1.2
- OPR = 23.5
- Mass flow rate (air) = 70kg/s
- Turbine Inlet Temperature = 1600K
- Max Thrust = 40kN (dry), 73kN (wet)
- Thrust-to-Weight = 7.6 (with afterburner)
- TSFC = 0.063 kg/N·hr (dry), 0.224 kg/N·hr (wet)

These values will be employed for establishing an engine model for the purpose of thermodynamic cycle analysis.

3. ENGINE THERMODYNAMIC CYCLE ANALYSIS

3.1. Engine Model for Analysis

As mentioned before, an engine model needs to be defined for the purpose of performing the engine cycle analysis and therefore obtaining relevant data and input parameters for the proper design of the nozzle. For this reason, the RB199 engine will serve as a reference engine for comparison of the results and validation of the analysis. In other words, the objective is to obtain the most accurate to reality results of thrust and TSFC values (only values found for the engine) as a function of altitude and flight speed while considering a simplified version of the reference engine and several important assumptions.

First of all, it's important to establish the general schematics and components of the engine that the flow will follow to complete the cycle. The RB199 features a three-spool arrangement that connects the Low-Pressure Compressor (LPC), Intermediate-Pressure Compressor (IPC), and High-Pressure Compressor (HPC) with their respective counterparts in the turbine sections (HPT, IPT, LPT). This arrangement will be simplified into a two-spool configuration where a fan will serve as the low-pressure compressor driving the complete flow inside the engine and a core compressor will prepare the primary air flow for combustion and its subsequent expansion. The engine model schematics diagram can be seen in the following figure.

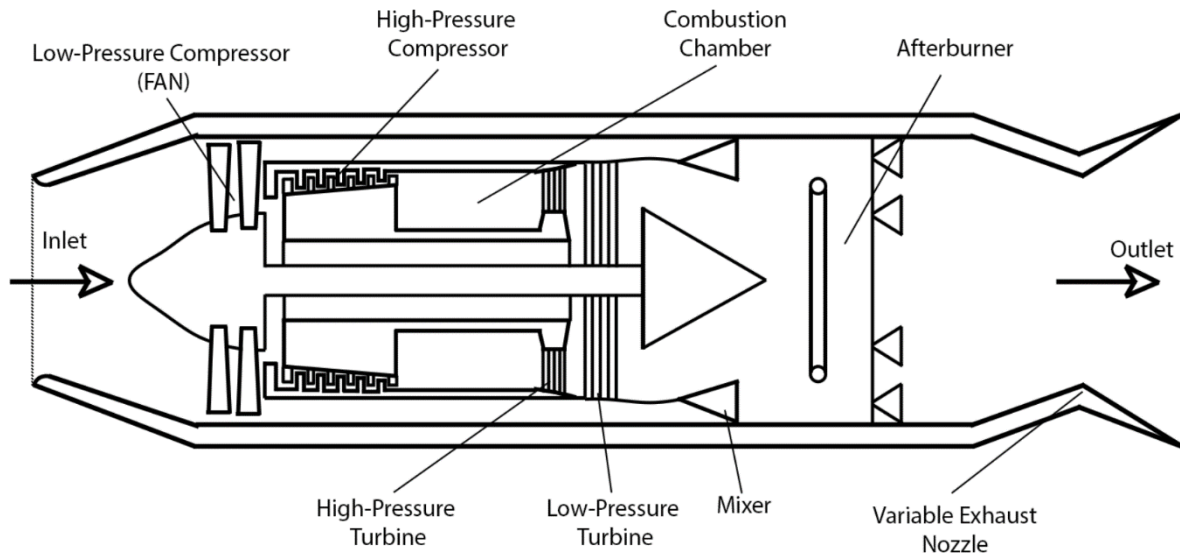


Figure 3.1. Engine model schematics diagram.

In addition to the engine model schematics, a stages diagram is shown in the following figure in order to define the different stages of the engine to perform the analysis in conjunction with additional information.

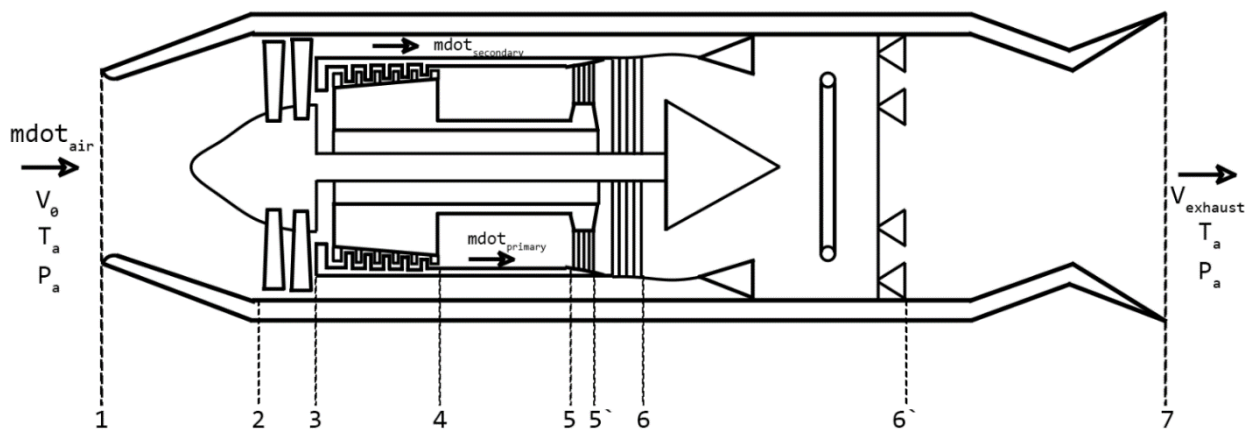


Figure 3.2. Engine stages diagram.

Figures 3.1 and 3.2 clearly define and establish the engine model and its stages in order to perform the cycle analysis by considering each stage separately. These diagrams show how the Fan and the LPT stages are directly connected by the main shaft, while the core compressor and turbine are connected by an outside shaft that guides the primary flow of air into the combustion chamber where fuel is added and ignited. Before any post-combustion occurs, the secondary flow and the primary flow are mixed once the secondary flow has been used for cooling purposes. Finally, the engine outlet features the variable exhaust nozzle that is used in order to maintain the functionality of the engine during afterburner activation.

In addition to the schematics, several parameters, idealizations, and assumptions are established based on the reference engine in order to define the initial conditions required for the analysis:

- Specific Heat Ratio is constant for air: $\gamma = 1.4$
- Ideal Gas Constant for air is assumed constant for all conditions: $R = 287 \text{ J/kg} \cdot \text{K}$
- Specific Heat at constant pressure for cold air: $C_{P \text{ cold}} = 1005 \text{ J/kg} \cdot \text{K}$
- Specific Heat at constant pressure for hot air: $C_{P \text{ hot}} = 1170 \text{ J/kg} \cdot \text{K}$
- Heating Value of kerosene (jet fuel): $L = 44 \cdot 10^6 \text{ J/kg}$
- By-Pass Ratio: $BPR = 1.2$
- Overall Pressure Ratio: $OPR = 23.5$
- Compression Ratio of the Fan (assumed): $r_{c \text{ fan}} = 1.2$
- Fan Diameter: $D = 0.72 \text{ m}$
- Turbine Inlet Temperature: $TIT = 1600 \text{ K}$
- Afterburner Temperature: $ABT = 2500 \text{ K}$
- Compressor Adiabatic Efficiency (LPC and HPC) (assumed): $\eta_a = 82\%$
- Turbine Adiabatic Efficiency (LPT and HPT) (assumed): $\eta_a = 87\%$

- 5% pressure losses on combustion
- 8% pressure losses on post-combustion
- Ideal exhaust nozzle (no pressure losses)
- Ideal inlet (no pressure nozzles)
- Pressure losses in inlet during supersonic flight following Military Specifications [8].
- 18% air bleed after high-pressure compressor.
- Isentropic behavior of the flow.

3.2. Analytical Analysis

This section deals with the analytical analysis of each of the stages in order to obtain the required equations for iterating the analysis in different initial conditions. In other words, the following section will define the thermodynamic equations in coherence with the defined engine model and sections. These equations are the ones studied and used during the propulsion system course and are based on the class's reference bibliography: *Fundamentals of Aircraft & Rocket Propulsion* by Ahmed F. El-Sayed [17].

3.2.1. Ambient Conditions

Before introducing any engine stage or component, consideration should be given to establishing the ambient conditions for the analysis. This will be done by following the International Standard Atmosphere (ISA) static atmospheric model that defines

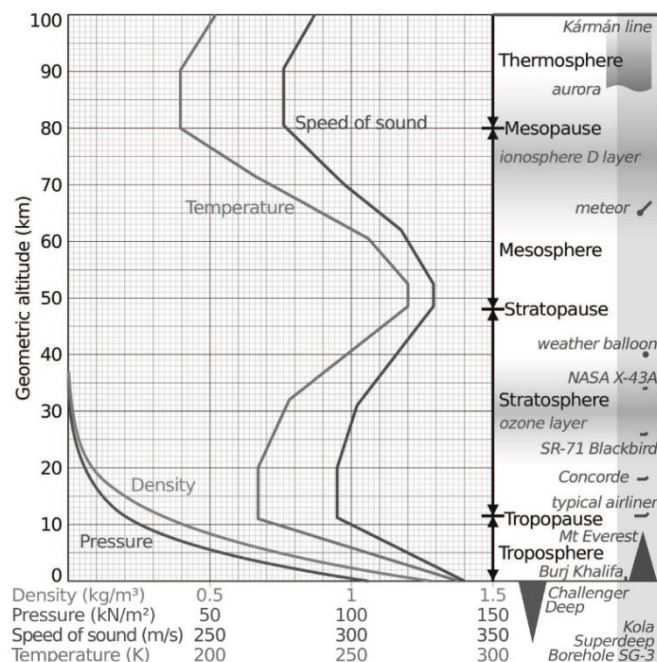


Figure 3.3. ISA model [10].

air pressure, density, viscosity, and temperature as a function of altitude. This model was first defined by the International Organization for Standardization (ISO) which published this model as an international standard under the ISO 2533 of 1975 [9]. This atmospheric model can be seen in figure 3.3.

Thus, the equations for ambient temperature, pressure, and density are defined following the established model:

- For the Troposphere ($0m \leq h \leq 11000m$):

$$T_a [K] = 288.15 - 0.0065 \cdot h \quad (1)$$

$$P_a [Pa] = 101325 \cdot (1 - 22.558 \times 10^{-6} \cdot h)^{5.2559} \quad (2)$$

$$\rho_a [kg/m^3] = 1.225 \cdot (1 - 22.558 \times 10^{-6} \cdot h)^{4.2559} \quad (3)$$

- For the Tropopause and the inferior part of the Stratosphere ($11000m \leq h < 20000m$):

$$T_a [K] = 216.65 \quad (4)$$

$$P_a [Pa] = 0.3639e^{-157.69 \times 10^{-6}(h-11000m)} \quad (5)$$

$$\rho_a [Pa] = 22632e^{-157.69 \times 10^{-6}(h-11000m)} \quad (6)$$

This way, the ambient conditions can be estimated following the worldwide accepted ISA model considering the changes from the Troposphere to the Tropopause and Stratosphere.

3.2.2. Inlet

Before defining the equations for the inlet, considerations must be taken in order to recognize the dynamic compressibility effect of air at high speeds. This is known as the RAM effect and is present in

all aircraft (or objects) that are in motion through the air. The equations for this effect are expressed in terms of an Isentropic evolution as there is not heat nor work at this stage:

$$T_{01} = \left(1 + \frac{\gamma - 1}{2} M^2\right) T_a \quad (7)$$

$$P_{01} = \left(1 + \frac{\gamma - 1}{2} M^2\right)^{\gamma/\gamma-1} P_a \quad (8)$$

These equations show that lower flight speeds would result in negligible increases of total temperature and pressure from ambient conditions due to air's dynamic compressibility. However, as the flight speed increases (over Mach 0.3) the effect drastically increases its effectiveness with the square of the Mach number. The equations also show how at 0 Mach (0 m/s) the total temperature and pressure is equal to the ambient conditions.

Following this, the inlet section of the engine will be considered as an ideal inlet. This implies that the adiabatic efficiency is 1 (100%), thus there are no pressure losses before the air reaches the fan section. However, in order to define a more accurate model of such a complex component of the engine while remaining under the objective scope of this project, NASA's *Inlet Pressure Recovery* (IPR) following Military Specifications [8] is considered:

- For $M \leq 1$:

$$P_{02} = \eta_{inlet} \cdot P_{01} \quad (9)$$

- For $M > 1$:

$$P_{02} = \eta_{inlet} \cdot (1 - 0.75[M - 1]^{1.35}) \cdot P_{01} \quad (10)$$

For subsonic flight speeds, the losses are reduced to the inlet efficiency losses (in this case none). While for supersonic flight speeds, there are additional losses created by shockwaves that are employed for reducing the flow's velocity before entering the compressor stages.

Finally, because there is no heat or work at this stage, the total temperature remains constant between the inlet and the fan stage:

$$T_{02} = T_{01} \quad (11)$$

3.2.3. Fan (LPC)

The fan section considers the assumed compression ratio of the fan following similar engine configurations to calculate the total pressure after the stage, and with the assumed compressor efficiency the total temperature after the stage can be calculated:

$$P_{03} = P_{02} * r_{c fan} \quad (12)$$

$$T_{03} = \left[\frac{r_{c fan}^{\gamma-1/\gamma} - 1}{\eta_{compressor}} + 1 \right] * T_{02} \quad (13)$$

Right after the fan stage, the flow is divided into the core, or primary, flow and the bypass, or secondary, flow. This way, it's important to calculate the amount of air mass flow entering the core of the engine and the amount of air mass flow that is bypassed and used for cooling purposes:

$$\dot{m}_p = \frac{\dot{m}_a}{BPR + 1} \quad (14)$$

$$\dot{m}_s = \frac{\dot{m}_a}{1 + 1/BPR} \quad (15)$$

3.2.4. Core Compressor (HPC)

Similarly to the fan, the core compressor uses the same approach for calculating the total pressure and temperature after the stage with the outputs from the previous fan stage. However, first the ratio of compression of the core compressor is calculated considering the given Overall Pressure Ratio (OPR) of the engine's compressors and the assumed fan compression:

$$r_c = OPR/r_{c\ fan} \quad (16)$$

$$P_{04} = P_{04} * r_c \quad (17)$$

$$T_{04} = \left[\frac{r_c^{\gamma-1/\gamma} - 1}{\eta_{compressor}} + 1 \right] * T_{03} \quad (18)$$

Finally, right after the core compressor an 18% air bleed is considered (assumed) for use in other aircraft systems. Thus, the air mass flow rate that enters the combustion chamber is decreased:

$$\dot{m}_p = \dot{m}_p * 0.82 \quad (19)$$

3.2.5. Combustion Chamber

Because the Turbine Inlet Temperature (TIT) is a given constant, the combustion stage is used to estimate the required fuel mass flow rate and the Fuel-to-Air Ratio (f) to sustain those temperatures considering the properties of the fuel (L) and the specific heat of air at a hotter temperature:

$$f = \frac{(TIT - T_{04}) \cdot C_{P\ hot}}{L - (TIT - T_{04}) \cdot C_{P\ hot}} \quad (20)$$

$$\dot{m}_f = f \cdot \dot{m}_p \quad (21)$$

It's important to highlight the use of the primary air mass flow rate to perform this calculation as the rest of the air (secondary mass flow rate) does not enter the combustion chamber, and thus is not mixed with the fuel.

Finally, with the assumed pressure losses of 5% due to the combustion process, the total pressure at the end of this stage can be calculated:

$$P_{05} = P_{04} * 0.95 \quad (22)$$

3.2.6. High-Pressure Turbine (HPT)

In the HPT stage the *Coupling Equation* is employed to estimate the HPT exit total temperature. This equation expresses the power relationship between the connected stages. In this case the HPT drives the HPC, therefore the power produced by the HPT must be equal to the power required to move the HPC:

$$T'_{05} = TIT - \frac{T_{04} - T_{03}}{1 + f} \frac{C_{P \text{ cold}}}{C_{P \text{ hot}}} \quad (23)$$

Once this temperature is obtained, similarly to the compressor stages, the HPT exit pressure can be estimated considering the turbine's efficiency:

$$P'_{05} = \left[\frac{T'_{05}/TIT - 1}{\eta_{turbine}} + 1 \right]^{\gamma/\gamma-1} \cdot P_{05} \quad (24)$$

3.2.7. Low-Pressure Turbine (LPT)

Similarly, for the LPT, the *Coupling Equation* is employed for calculating the LPT exit temperature, and with this value and the turbine efficiency, the pressure at the exit of this section is calculated. However, in this case the LPT drives the fan stage which moves the complete air flow (not just the primary air flow as is the case with the HPC), thus the equation has additional considerations:

$$T_{06} = T'_{05} - (T_{03} - T_{02}) * \frac{BPR + 1}{1 + f} \frac{C_{P \text{ cold}}}{C_{P \text{ hot}}} \quad (25)$$

$$P_{06} = \left[\frac{T_{06}/T'_{05} - 1}{\eta_{turbine}} + 1 \right]^{\gamma/\gamma-1} \cdot P'_{05} \quad (26)$$

3.2.8. Nozzle (without afterburner)

These equations are representative of the performance of the nozzle when no post-combustion takes place. In general, the nozzle is assumed to be ideal thus no pressure losses are present. In addition, no heat or work is added, thus the total temperature of the exit of the LPT is maintained constant through the nozzle. In addition, this stage features the mixing of the primary and secondary flows which will become relevant later.

$$P'_{06} = P_{06} = P_{07} \quad (27)$$

$$T'_{06} = T_{06} = T_{07} \quad (28)$$

Then, by assuming (establishing this condition) that the flow is choked at the nozzle exit (Mach = 1), the static pressure and temperature of the exhaust gases can be estimated, and the exhaust speed and density can be then calculated for their later use.

- If $M_e = 1$:

$$\frac{T_{07}}{T_7} = \left(1 + \frac{\gamma - 1}{2} M_e^2\right) = 1.2 \rightarrow T_7 = T_e = EGT = \frac{T_{07}}{1.2} \quad (29)$$

$$\frac{P_{07}}{P_7} = \frac{1}{\frac{T_{07}}{T_7}^{\gamma/\gamma-1}} = 1.893 \rightarrow P_7 = P_e = \frac{P_{07}}{1.893} \quad (30)$$

$$V_e = a * M_e = 1 \cdot \sqrt{EGT \cdot R \cdot \gamma} \quad (31)$$

$$\rho_e = \frac{P_e}{R \cdot EGT} \quad (32)$$

3.2.9. Nozzle (with afterburner)

These equations now represent the thermodynamic behavior of the nozzle when post-combustion takes place. In this case, the temperature is increased to the constant afterburner total temperature assumed, and this post-combustion causes an 8% loss in total pressure:

$$T'_{06} = T_{07} = ABT \quad (33)$$

$$P'_{06} = P_{07} = P_{06} * 0.92 \quad (34)$$

As mentioned before, in this stage the primary flow is mixed with the secondary (bypassed) flow prior to the post-combustion. This will have a direct effect on the calculation of Thrust and nozzle exit area that will be defined in the following section. However, this also implies the use of a mixing equation in the post-combustion in order to determine the Fuel-to-Air ratio and fuel mass flow rate of the post-combustion:

$$f_{ab} = \frac{(1 + BPR)C_{P\ hot} \cdot ABT}{L} - \frac{T_{06} \cdot C_{P\ hot}}{L} - \frac{BPR \cdot C_{P\ cold} \cdot T_{03}}{L} \quad (35)$$

$$\dot{m}_{fab} = f_{ab} \cdot \dot{m}_p \quad (36)$$

Finally, the exit parameters can be calculated using equations (29, 30, 31, 32) and assuming the choked flow condition at the nozzle exit, just as before.

3.2.10. Final Calculations

Once the complete engine cycle is completed, exit area, thrust, and Thrust Specific Fuel Consumption (TSFC) can be calculated for both cases: with and without afterburner.

a) No post-combustion:

$$A_e = (\dot{m}_p + \dot{m}_s + \dot{m}_f) \cdot \frac{\sqrt{T_{07}}}{P_{07}} \cdot \sqrt{\frac{R}{\gamma}} \cdot \left(\frac{\gamma + 1}{2}\right)^{\frac{\gamma+1}{2(\gamma-1)}} \quad (37)$$

As it is seen, the equation for nozzle exit area is derived from the mass flow rate equation considering the total conditions at the nozzle exit, with isentropic relations, and assuming that the Mach number is 1.

$$T = (\dot{m}_p + \dot{m}_s + \dot{m}_f)V_e - \dot{m}_a \cdot V_0 + (P_e - P_a)A_e \quad (38)$$

In this case, the thrust equation considers the additional mass flow rate of the fuel and the mixed flow at the exit, in addition to the thrust coming from the pressure difference at the exit. Finally, once the thrust is known, the TSFC can be calculated:

$$TSFC = \frac{\dot{m}_f}{T} \quad (39)$$

b) With post-combustion:

In the case with the post-combustion, the equations are the same, however, different parameters at the exit are used and fuel flow rates from the post-combustion are considered:

$$A_{e\ ab} = (\dot{m}_p + \dot{m}_s + \dot{m}_f + \dot{m}_{f\ ab}) \cdot \frac{\sqrt{ABT}}{P_{07}} \cdot \sqrt{\frac{R}{\gamma}} \cdot \left(\frac{\gamma + 1}{2}\right)^{\frac{\gamma+1}{2(\gamma-1)}} \quad (40)$$

$$T_{ab} = (\dot{m}_p + \dot{m}_s + \dot{m}_f + \dot{m}_{f\ ab})V_{e\ ab} - \dot{m}_a \cdot V_0 + (P_{e\ ab} - P_a)A_{e\ ab} \quad (41)$$

$$TSFC_{ab} = \frac{\dot{m}_f + \dot{m}_{f\ ab}}{T_{ab}} \quad (42)$$

3.3. Numerical & Iterative Analysis

Following the model engine and equations established in the previous sections, a Python script was written in order to iterate through the equations for different altitudes and Mach numbers and graph the relevant results (Thrust, Exit Area, TSFC, Nozzle Total Pressure, etc.) as a function of flight speed for both cases with and without afterburners. The goal with this is to obtain results that mimic the engine behavior and performance at sea level (available data) and observe how both altitude and flight speed have an impact on the performance and the calculated values. It's important to highlight that because of the scope of this project and the many idealizations and assumptions of the engine model, the results are not truly representative of the real behavior of an engine, as it would be too complex and lengthy for a Bachelor's Final Project to include the complex equations of the independent components of the engine as a function of altitude and flight speed separately.

All the coding done for this program is included in the *Annex* section, as it is too lengthy to be included here. The results obtained are shown in the following sections.

Before expressing and analyzing the results, it's important to note that the dotted curves represent the results with afterburners while the solid curves represent the results without afterburners. For this reason, the solid curves finish at Mach 0.9 as further results don't make sense given that the use of afterburners enables higher speed flight (up to Mach 2.5). Furthermore, each curve is given a color and a marker, identifying the altitude of the computation. Curves with the same marker but different line style represent the same altitude. This is true for all the graphs.

3.3.1. Thrust & Thrust Augmentation

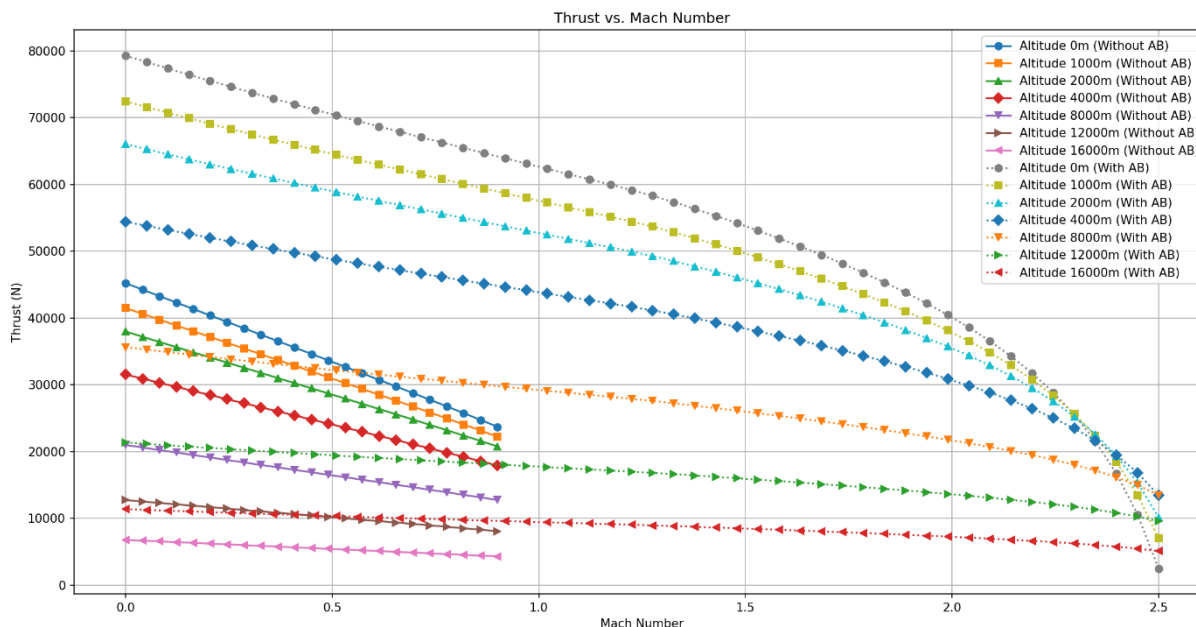


Figure 3.4. Thrust vs Flight Speed graph for the model engine at different altitudes with and without afterburners.

This first graph shows, clearly, how thrust decreases with increasing altitude and increasing airspeed. The case of sea level conditions and no flight speed is represented by the first point of the circle-marked lines. In the case with afterburners, the thrust is almost 80kN while in the case with no afterburners the thrust is around 45kN. These values are slightly higher than the reference values of the RB199 of 73kN and 40kN with and without afterburners, respectively. These two represent an average error of 11.05% with respect to the reference values. This is expected and accepted, as the many idealizations and assumptions taken for this analysis are the reason for the resultant increased thrust values for the model engine.

In terms of the thrust augmentation ratio with the afterburners on, the following table expresses these results only for the first points of the curves (Mach = 0).

Table 3.1. Thrust Augmentation Ratio expressed as % increase for different Altitudes at Mach 0.

Altitude	Thrust Dry	Thrust Wet	Thrust Augmentation
0m	45kN	80kN	77.7%
1000m	41.5kN	72.5kN	74.7%
2000m	38kN	66kN	73.7%
4000m	31.5kN	54.5kN	73%
8000m	21kN	35.5kN	69%
12000m	12.7kN	21.3kN	67.7%
16000m	6.8kN	11.4kN	67.64%

Table 3.1 indicates that the thrust augmentation ratio expressed as a percentage increase decreases slightly as altitude increases. This is because at higher altitudes less thrust is produced by the engine, however the required thrust to fly is also lowered as drag is also a function of air density. Compared with the reference engine, which available data indicates that the thrust augmentation is 82.5% at sea level, this model engine has a higher overall thrust but a lower thrust augmentation. Although normal thrust augmentation values lie between 40% to 60%.

3.3.2. Nozzle Exit Area & Area Increase

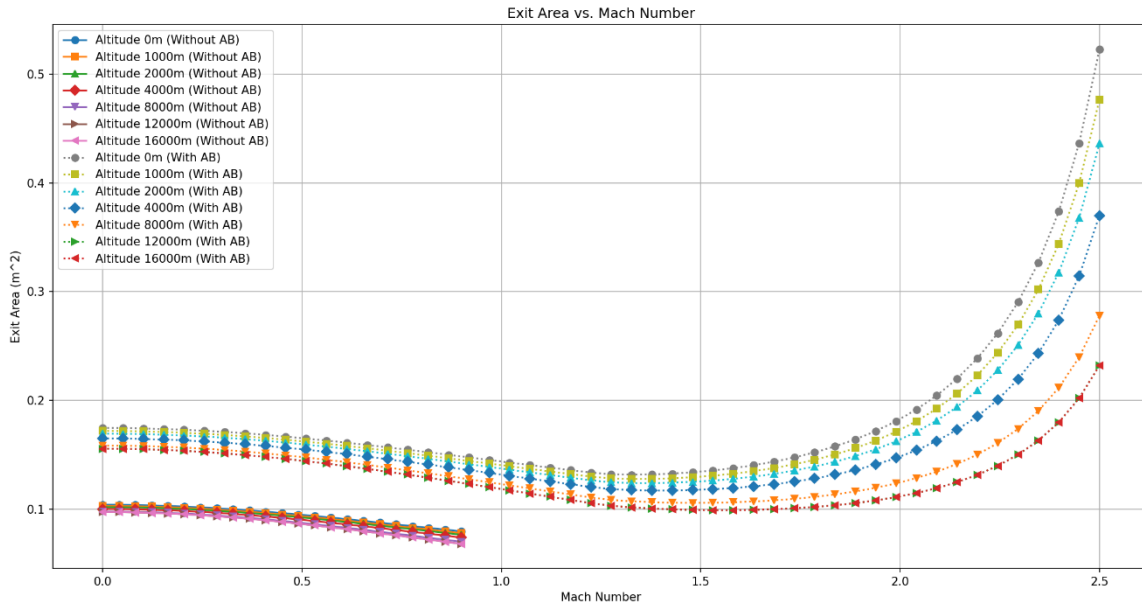


Figure 3.5. Exit Area vs Flight Speed graph for the model engine at different altitudes with and without afterburners.

There is no reference data to compare these results to, however it has been established that the exit area of the engine's nozzle must increase during afterburner operations to maintain the functionality of the engine and avoid engine surges. This is the exact behavior shown in figure 3.5. Clearly, the exit area obtained for the case where no afterburner is present is significantly lower than the case where the afterburners are present.

Furthermore, the curves show how the area decreases with increased flight speed. This can be understood as increasing flight speed increases RAM pressure and temperature, reducing the need for a larger exit area downstream. However, in the case of the afterburner's curves, at around Mach 1.3 the exit nozzle exit area begins reversing and shooting up parabolically. This is caused by the increasing effect of the reduced Inlet Pressure Recovery established for the inlet Military Specifications. This results in a significant reduction in inlet pressure which causes the need to increase exit area with supersonic flight.

In terms of the exit area increase with the afterburners on, the following table expresses these results only for the first points of the curves (Mach = 0).

Table 3.2. Exit Area Augmentation expressed as % increase for different Altitudes at Mach 0.

Altitude	Exit Area Dry	Exit Area Wet	Area Augmentation
0m	0.1042m ²	0.174725m ²	67.68%
1000m	0.10305m ²	0.172m ²	66.91%
2000m	0.102m ²	0.1695m ²	66.17%
4000m	0.1002m ²	0.1651m ²	64.77%
8000m	0.098m ²	0.1585m ²	61.73%
12000m	0.09745m ²	0.1557m ²	59.77%
16000m	0.09745m ²	0.1557m ²	59.77%

Table 3.2 shows how the exit area ratio with and without afterburner decreases slightly for an increase in altitude. Thus, being conservative, the design of the nozzle must account for area increases of up to 70% when operating with afterburners compared with the dry engine.

3.3.3. Nozzle Exit Total Pressure

In order to properly design the engine nozzle, one of the most important input parameters is the nozzle exit total or stagnation pressure. As it was expressed while defining the engine model for the analysis, the nozzle is assumed ideal thus the total pressure at the exit of the LPT remains constant throughout the nozzle. However, in the case of the afterburners, there is a slight pressure loss due to the post-combustion of 8%. Thus, the total pressure should be higher in the case where no post-combustion occurs. Figure 3.6 shows this loss and the development of the total pressure as the flight speed is increased for the different altitudes.

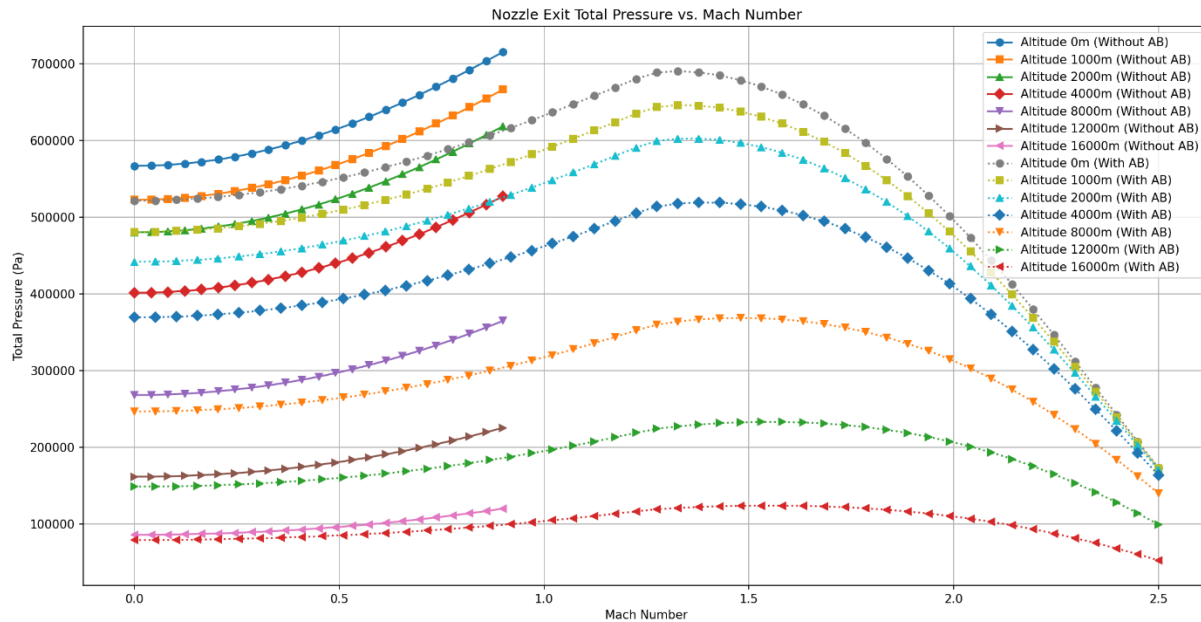


Figure 3.6. Nozzle Exit Total Pressure vs Flight Speed graph for the model engine at different altitudes with and without afterburners.

It can be clearly seen that with increased altitude, the total pressure at the nozzle decreases following ambient conditions. However, as flight speed increases this pressure increases due to the RAM effect up to supersonic speeds (only seen with afterburners). With the already stated Inlet Pressure Recovery effect, the total pressure at the nozzle is shown to be decreasing with increased flight speed. Similarly to the exit area results, this effect becomes significant at around Mach 1.3.

3.3.4. Thrust Specific Fuel Consumption & Consumption Increase

Even though fuel consumption is not a relevant input parameter for the design of the nozzle, it is insightful data to compare and validate its behavior with what is to be expected from the reference.

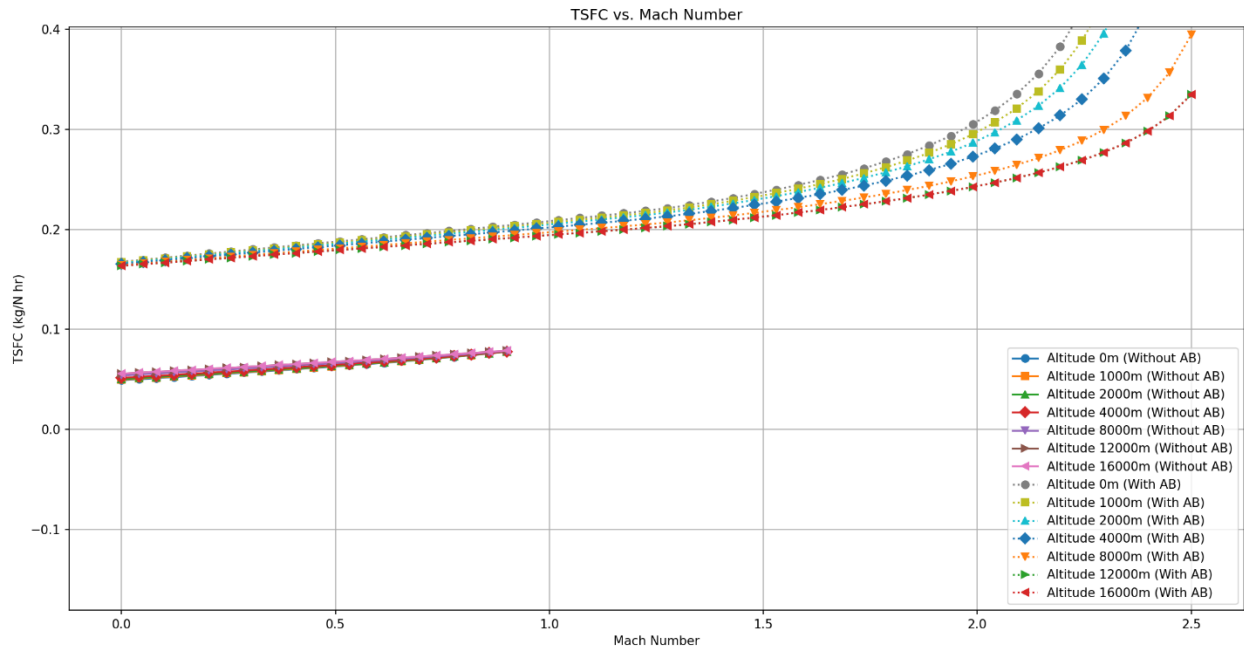


Figure 3.7. Thrust Specific Fuel Consumption vs Flight Speed graph for the model engine at different altitudes with and without afterburners.

As it is seen in figure 3.7, a significant increase in fuel consumption is experienced during afterburner operations. In addition, both cases show how TSFC is increased with increasing flight speed. This is directly correlated with the decrease in thrust with increasing flight speed shown in figure 3.4. In terms of the fuel consumption increase with the afterburners on, the following table expresses these results only for the first points of the curves (Mach = 0).

Table 3.3. TSFC Augmentation expressed as % increase for different Altitudes at Mach 0.

Altitude	TSFC Dry	TSFC Wet	TSFC Augmentation
0m	0.04905 kg/N·hr	0.16765 kg/N·hr	241.8%
1000m	0.04965 kg/N·hr	0.167 kg/N·hr	236.35%
2000m	0.05025 kg/N·hr	0.16645 kg/N·hr	231.1%
4000m	0.0514 kg/N·hr	0.1655 kg/N·hr	221.98%
8000m	0.0539 kg/N·hr	0.1641 kg/N·hr	204.45%
12000m	0.0557 kg/N·hr	0.1635 kg/N·hr	193.5%
16000m	0.0557 kg/N·hr	0.1635 kg/N·hr	193.5%

Comparing the cases at sea level and Mach 0 with the reference values obtained for the RB199, the error is roughly 23.6% and 25% for the dry and wet cases, respectively. This is normal and expected given the idealizations and assumptions of the model engine resulting in an increased overall thrust, lowering thrust specific fuel consumption compared to the reference values.

Finally, for the case of the engine operating dry, the highest TSFC is obtained at the highest altitude (16,000m). On the other hand, for the case of the engine operating wet, the highest TSFC is obtained at the lowest altitude (0m). This results in the TSFC augmentation decreasing with increasing altitude. In other words, the expected increase in fuel consumption when using the afterburner is overall decreased while flying at higher altitudes.

3.3.5. Nozzle Pressure Ratio

Another very important input parameter for the design of the nozzle is the nozzle pressure ratio (NPR). This represents the ratio between the nozzle total pressure to the ambient pressure conditions.

$$NPR = \frac{P_t}{P_a}$$

Given that the ambient conditions are known, as well as the pressure conditions inside the nozzle, the NPR can be computed for each altitude and flight speed for both cases.

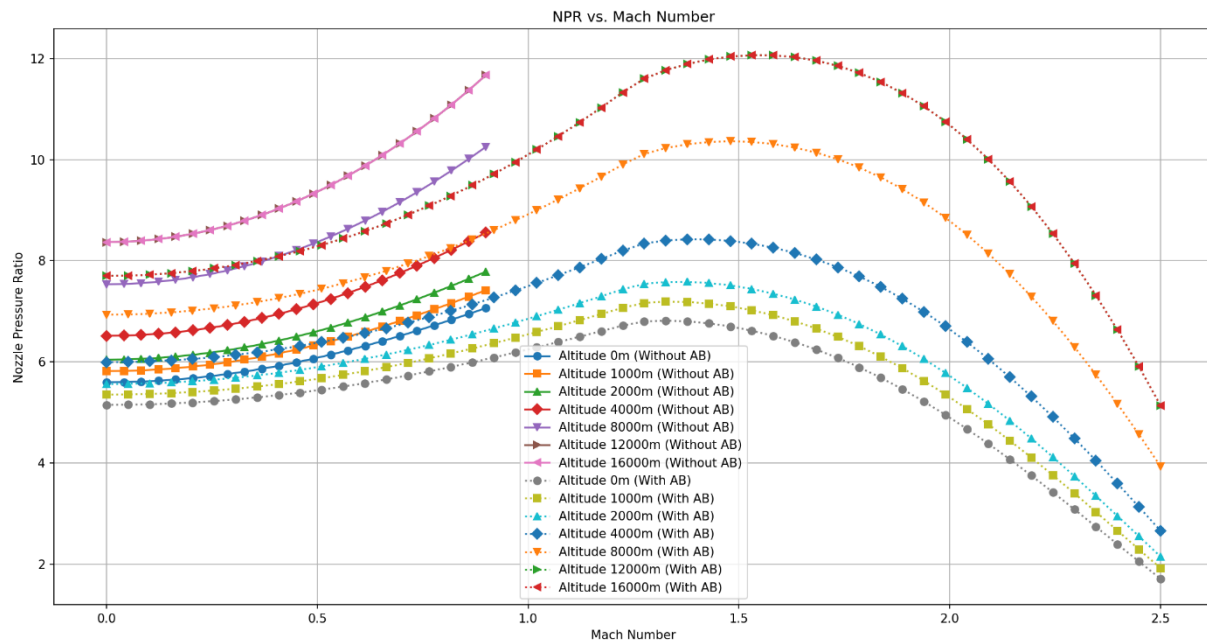


Figure 3.8. Nozzle Pressure Ratio vs Flight Speed graph for the model engine at different altitudes with and without afterburners.

Figure 3.8 clearly shows how NPR increases with increasing flight speed, in congruence with the increase in nozzle exit total pressure (figure 3.6). In addition, it is clear that the inlet Military Specification also has a significant effect on the evolution of NPR through supersonic speeds, in the same manner as the total pressure. Furthermore, there is a slight difference between curves of the same altitude but different cases due to the stated pressure loss during the re-combustion. Finally, the graph clearly indicates the effect of altitude; as ambient pressure decreases significantly, NPR becomes larger at higher altitudes.

4. PRELIMINARY NOZZLE DESIGN

This chapter deals with, what can be considered as the 2nd and main part of this project, the conceptual and preliminary design of a variable area propelling nozzle based on the model engine and outputs from the thermodynamic cycle analysis established in the previous chapter. For this purpose, a further analysis of nozzle requirements and background literature is defined before diving into the complete preliminary design development.

4.1. Theoretical Background

4.1.1. Nozzle Functions

The main objective of an engine exhaust nozzle is relatively simple, to convert excess potential energy in the form of temperature and pressure into useful kinetic energy that provides thrust for the complete vehicle (be it a rocket or an aircraft). As explained by Leonard E. Stitt in NASA's publication *Exhaust Nozzles for Propulsion Systems With Emphasis on Supersonic Cruise Aircraft* [11], the nozzle achieves this by expanding the flow between two predetermined pressure and temperature levels, from the high nozzle intake total pressure to the low free-stream static pressure. The nozzle throat area must be adjusted, as expressed in a previous chapter, to correspond with the temperature rise if the propulsion system is capable of afterburning. The variable nozzle's throat area has to allow temperature changes in the exhaust gas while keeping the turbine inlet temperature constant. This main nozzle

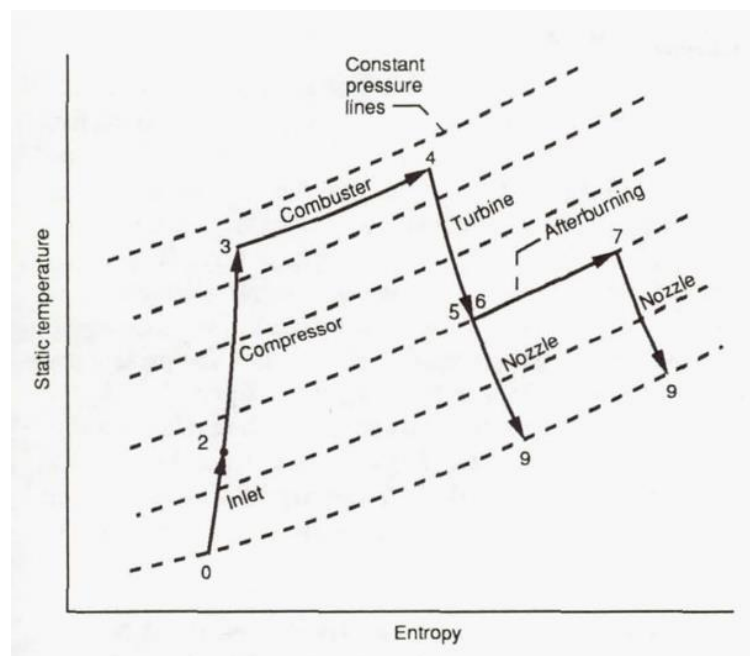


Figure 4.1. Turbojet Brayton Cycle with and without afterburners (NASA, 1990) [11].

function is shown in a T-S Diagram of a Brayton Cycle for a Turbojet type engine (figure 4.1). Thus, the maximum uninstalled thrust for any particular engine is achieved when the exit pressure (P_e) matches the ambient pressure (P_a), and the expansion process is controlled by the pressure ratio across the nozzle, which in turn will vary with varying local nozzle area and area ratio.

Furthermore, as expressed in the American Institute of Aeronautic & Astronautics' (AIAA) book, *Aircraft Engine Design* [12], a summary of the nozzle's functions is described in the following list:

- Accelerate the flow to a high velocity with minimum total pressure loss.
- Match exit and atmospheric pressure as closely as desired.
- Permit afterburner operation without affecting main engine operation.
- Allow for cooling of walls if necessary.
- Mix core and bypass streams of turbofan if necessary.
- Allow for thrust reversing if desired.
- Suppress jet noise, radar reflection, and infrared radiation (IR) if desired.
- Two-dimensional and axisymmetric nozzles, thrust vector control if desired.
- Do all of the above with minimal cost, weight, and boattail drag while meeting life and reliability goals.

4.1.2. Nozzle Types

Two basic nozzle types are currently employed for jet engines: convergent nozzles and convergent-divergent (CD) nozzles (figure 4.2). Each nozzle type is further complicated with the addition of variable exhaust and throat areas. Thus, inside each nozzle type, there are various configurations depending on the aircraft mission and requirements, as described by the AIAA in their 2004 publication *Nozzle Selection and Design Criteria* [13]:

- Fixed-Area Convergent Nozzles:

The fixed-area convergent nozzle, as the name implies, is a simple duct that converges towards the exit and is normally employed for subsonic commercial aircraft that don't employ afterburners. Variation in the throat size is not necessary for optimal engine performance in subsonic applications. Furthermore, the expansion ratio variation offers negligible benefit because the nozzle pressure ratio ($NPR = P_{0e}/P_a$) is typically less than 2. Fixed convergent nozzles are a good fit for subsonic applications because of these factors.

- Variable-Area Convergent Nozzles:

When operating at high subsonic or transonic Mach numbers, tactical aircraft usually use afterburning to get the necessary thrust to overcome the high drag in these conditions while keeping the engine size to a minimum. Because NPR for these conditions is often less than 4, expansion ratio adjustments are used to generate minimal thrust enhancement, allowing for the employment of a reasonably simple variable throat area convergence nozzle without a divergent section.

Variable area convergent nozzles are employed in situations where transonic flight is infrequent and has a secondary focus on mission objectives. When the flight speed Mach number exceeds 2, the variable convergent nozzle performs inadequately compared to a CD nozzle.

- Convergent-Divergent Nozzles:

As the name suggests, the CD nozzle is a convergent duct that is followed by a divergence section. If properly designed and implemented, the convergent section expands the flow to sonic speed (Mach = 1) at a minimum area known as the throat area, while the divergence section continues to expand the flow up to ambient conditions and thus supersonic speeds are reached the nozzle exit, as it has been established.

The majority of convergent-divergent nozzles found in aircraft are made up of variable geometries and other aerodynamic elements rather than being straightforward ducts. In situations when the nozzle pressure ratio is large, the convergent-divergent nozzle is utilized as further expansion is required to increase exhaust speed and improve nozzle performance. Supersonic aircraft with high-performance engines typically have a convergent-divergent nozzle in one form or another. To generate the highest possible uninstalled thrust, the exit area must be continuously adjusted to meet the internal and

external static pressures at the exit for different flow conditions. In addition, if the engine has an afterburner, it is designed with a variable exit nozzle area in order to maintain the engine's operational parameters upstream of the afterburner constant.

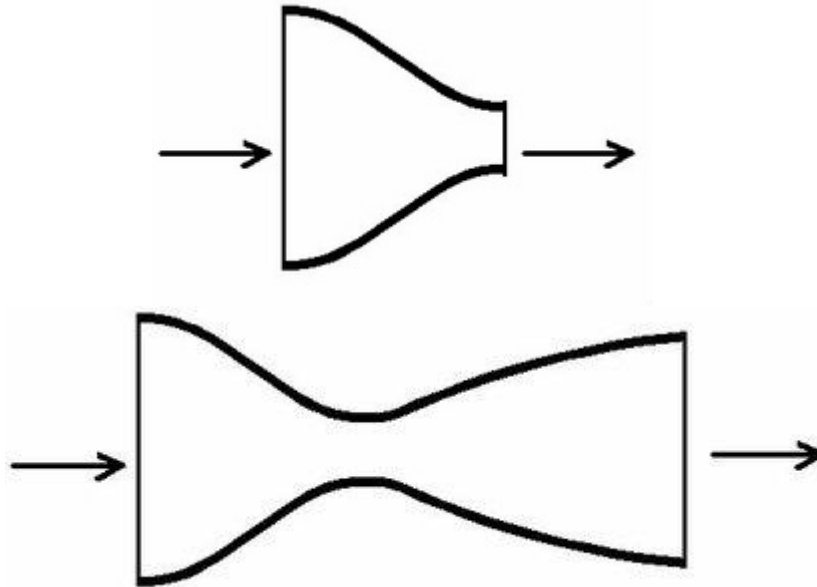


Figure 4.2. Convergent (top) & Convergent-Divergent (bottom) nozzles examples.

4.1.3. Nozzle Efficiencies & Thrust

Theoretically, the nozzle expands the exhaust gases isentropically (no losses) to realize the largest change in enthalpy over a given pressure ratio. This yields the greatest, or ideal, exit velocity, and therefore the greatest, or ideal thrust. However, in reality the expansion process experiences losses due to friction and entropy increases for various reasons. For this purpose, the adiabatic efficiency factor is defined as the ratio between the actual enthalpy change to the ideal enthalpy change of an adiabatic expansion:

$$\eta_a = \frac{\text{Actual Enthalpy Change}}{\text{Ideal Enthalpy Change}} \quad (43)$$

Similarly, a velocity coefficient can be defined as the ratio between the actual exit flow velocity and the ideal exit flow velocity after an isentropic expansion to ambient pressure:

$$C_v = \frac{\text{Actual Velocity}}{\text{Ideal Velocity}} \quad (44)$$

This coefficient represents the effect of frictional loss in the boundary layer of the nozzle and is a measure of the nozzle's efficiency.

Furthermore, as it was established, the ideal, or maximum uninstalled, thrust for any given engine is obtained when the nozzle exit static pressure equals the ambient pressure:

$$F_i = \dot{m}_e \cdot V_e$$

This can be rewritten as:

$$F_i = \gamma \cdot P_a \cdot M_e^2 \cdot A_e$$

This equation can then be turned into a thrust coefficient by dividing it by the total pressure and area at the nozzle throat:

$$C_F = \frac{F_i}{P_{0e} \cdot A_t} = M_e^2 \left(\frac{P_a}{P_{0e}} \right) \left(\frac{A_e}{A_t} \right) \gamma \quad (45)$$

However, in many cases, the expansion is not completed, and the thrust coefficient is expressed in terms of the gross thrust:

$$F_g = \dot{m}_e \cdot V_e + (P_e - P_a)A_e \quad (46)$$

Thus, the thrust coefficient becomes:

$$C_{Fg} = \frac{F_{g \text{ actual}}}{F_{g \text{ ideal}}} \quad (47)$$

It's important to note that the ideal mass flow rate also differs from the actual mass flow rate due to leakage of flow through the nozzle walls, thus also affecting the ideal thrust by a factor known as discharge coefficient:

$$C_d = \frac{\text{Actual flow rate}}{\text{Ideal flow rate}} \quad (48)$$

This coefficient can be shown to be identically equal to the ratio of the effective one-dimensional flow area actually required to pass the total nozzle flow ($A_{t \text{ effective}}$) to the ideal nozzle throat area (A_t) of the engine cycle calculations as follows (AIAA, 2002) [12]:

$$C_d = \frac{\rho_t V_t A_t}{\rho_t V_t A_{t \text{ effective}}} = \frac{A_t}{A_{t \text{ effective}}} \quad (49)$$

The nozzle throat area is sized using the discharge coefficient to allow passage for the required mass flow rate.

Finally, because the objective of the nozzle is to maximize thrust, a nozzle thrust efficiency can also be defined by relating the actual or measured thrust with the ideal thrust:

$$\eta_F = \frac{\text{Actual Gross Thrust}}{\text{Ideal Gross Thrust}} \quad (50)$$

4.1.4. Nozzle Losses

In terms of the total pressure losses due to non-isentropic expansion, the fraction of total pressure loss can be expressed for one-dimensional flow in its differential form as:

$$\frac{dP_0}{P_0} = -\frac{\gamma}{2} M^2 C_f \frac{P_w}{A} dx \quad (51)$$

Where C_f is the friction coefficient and P_w is the wet perimeter of the duct.

Additional losses due to the nonuniform distribution of the velocity vector's magnitude and direction at the exit plane has an impact on a nozzle's thrust efficiency as well. The axial component of

momentum is what generates thrust; the normal component does not. A divergence factor can be used to assess the loss resulting from wall divergence (NASA, 1990) [11]:

$$\lambda = \frac{1 + \cos \alpha}{2} \quad (52)$$

Where α is the nozzle divergence half-angle. The variation of divergence factor with α is shown in figure 4.3.

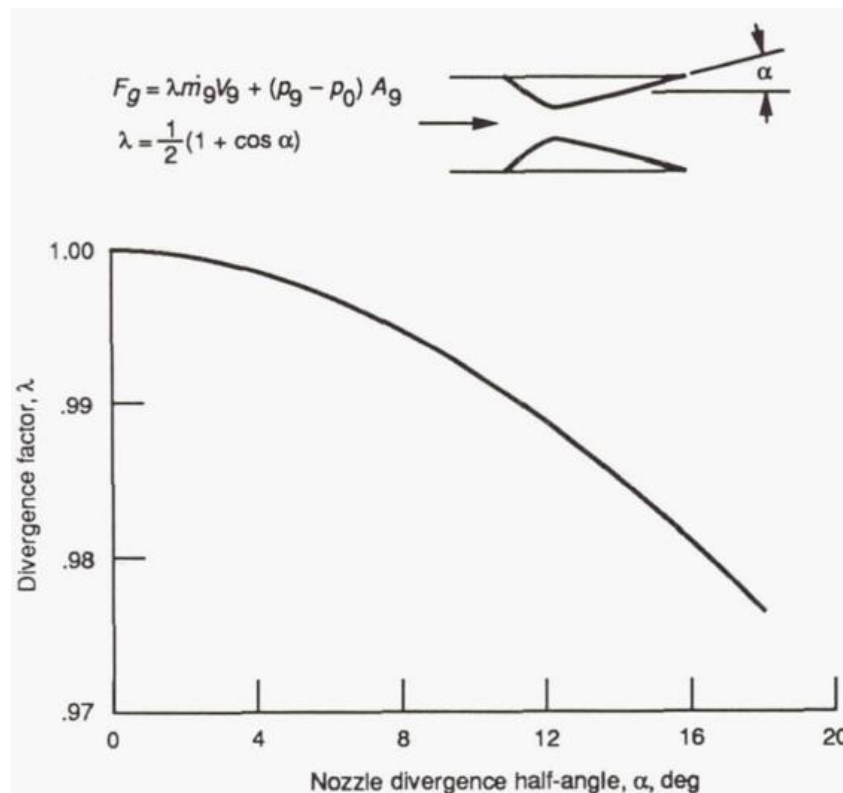


Figure 4.3. Divergence factor as a function of α for a conical exit (NASA, 1990) [11].

In the case of fixed-area-ratio CD nozzles compared with variable-area-ratio CD nozzles, it becomes clear that the variable-area nozzles will always be superior in terms of thrust efficiency because they are designed to perfectly expand the exhaust gases over a range of nozzle pressure ratios. The primary thrust losses then mostly rely on whether the nozzle is operating at a pressure ratio above or below its

design point in a fixed-area-ratio nozzle. As it is shown in figure 4.4, these losses are due to the overexpansion or underexpansion of the exhaust jet.

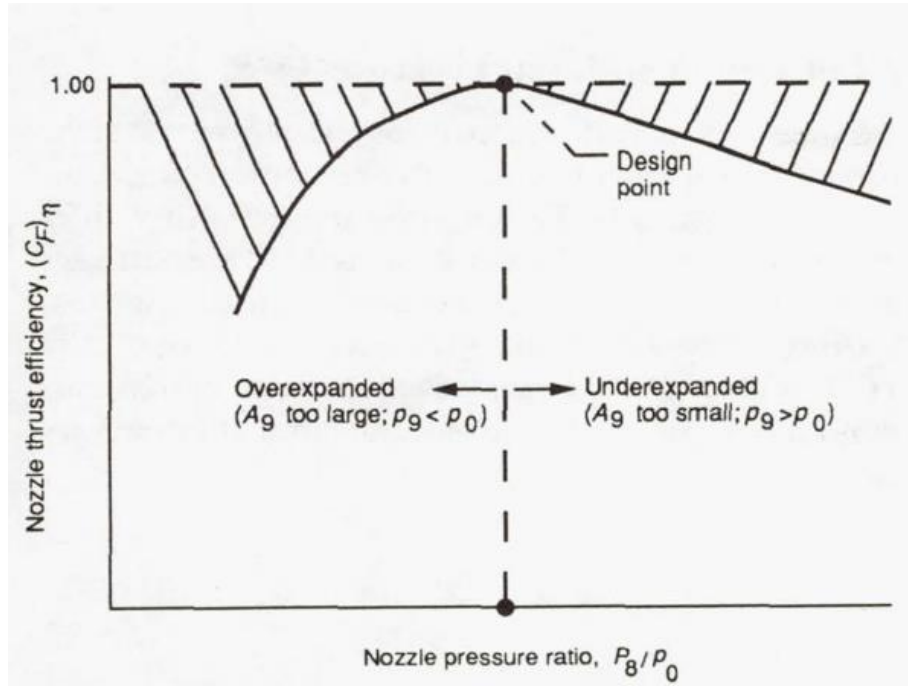


Figure 4.4. Nozzle thrust efficiency as a function of NPR for a fixed-area-ratio CD nozzle (NASA, 1990) [11].

- Overexpansion:

If a nozzle is functioning at a pressure ratio lower than its design value, it is considered overexpanded. There is a point between the nozzle throat and exit stations where the nozzle flow expands to free-stream pressure. Nevertheless, the pressure is lower than ambient pressure and the nozzle flow keeps expanding past this limit. The system is dragged by every diverging shroud with pressures lower than ambient. A CD nozzle will typically overexpand and continue to flow continuously until the ratio of the exit to the surrounding static pressure drops below a certain threshold. The nozzle flow pressure will rise to ambient levels as a result of the exhaust gases separating from the nozzle wall, creating a shock wave. The flow will often spin or move around the shroud wall due to the unstable interaction between the shock and the boundary layer. This instability can occasionally cause the shroud wall to shatter or sustain damage. From the perspective of nozzle stability, the most dangerous situation is the overexpanded nozzle

that separates, as it is by far the hardest to foresee and analyze. The overexpanded case is demonstrated by the pressure distribution within the diverging shroud of the nozzle (figure 4.5).

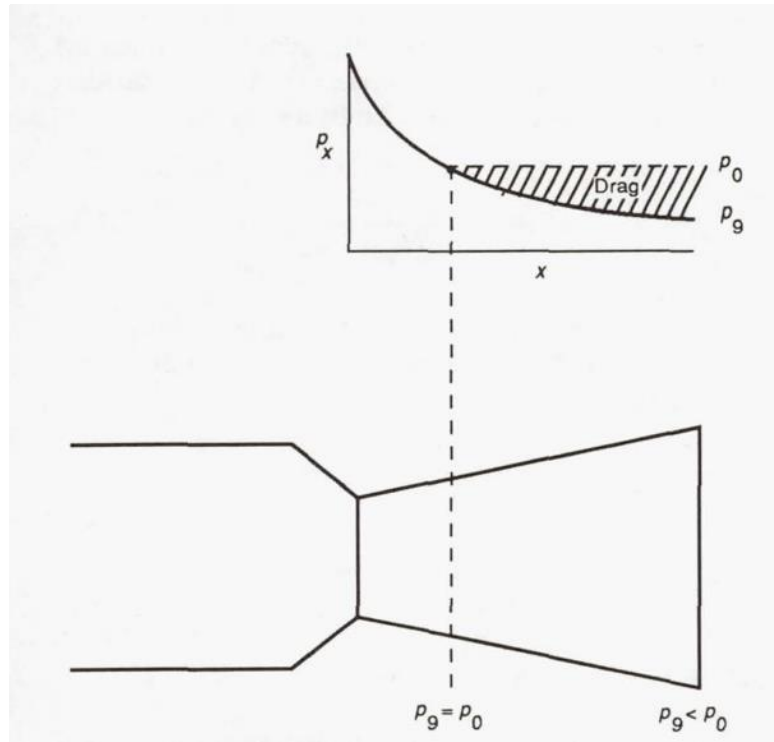


Figure 4.5. Overexpanded nozzle pressure distribution & illustration (NASA, 1990) [11].

- **Underexpansion:**

If a nozzle is running at a pressure ratio higher than its design value, it is considered underexpanded. In this instance, the flow expands to a nozzle exit pressure higher than the ambient pressure because the nozzle area ratio is too low. To get the optimal thrust in this scenario, the nozzle's divergent part would need to be extended. The loss in nozzle thrust efficiency can be attributed to the fraction of potential thrust that is wasted by the shorter nozzle. Since underexpanded nozzles are incapable of allowing flow separation, the underexpanded scenario is the easiest to examine analytically and is desired over an overexpansion inside of the nozzle. The underexpanded case is demonstrated by the pressure distribution within the diverging shroud of the nozzle (figure 4.6).

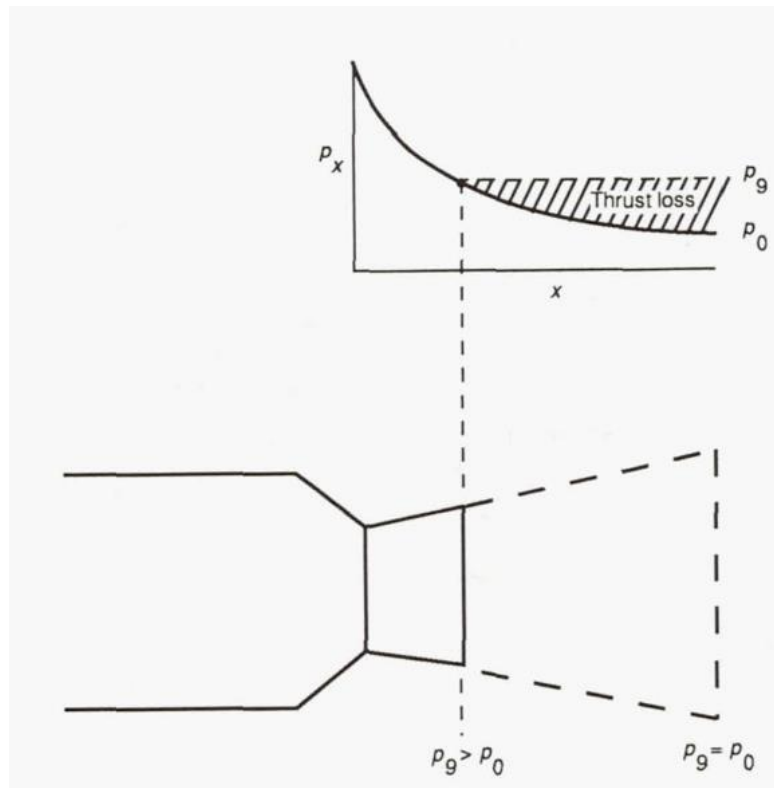


Figure 4.6. Underexpanded nozzle pressure distribution & illustration (NASA, 1990) [11].

Furthermore, for turbofan and turbojet engines operating in the subsonic cruising speed band, the nozzle pressure ratios are around 3 to 5 (figure 4.7). Thus, a subsonic engine's exhaust nozzle is usually convergent.

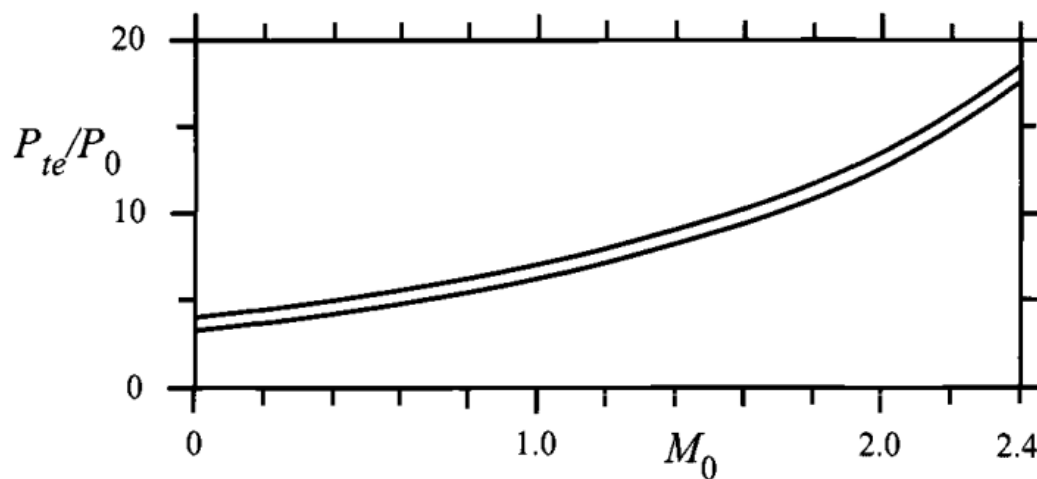


Figure 4.7. Typical NPRs as a function of freestream Mach number (AIAA, 2002) [12].

This is due to the fact that the convergent nozzle gross thrust is around 1-3 percent lower than the peak gross thrust in the 3-5 nozzle pressure range (AIAA, 2002). As a result, for a subsonic cruise turbofan or turbojet engine, there could not be enough gross power gain available to offset the additional drag and weight of a convergent-divergent nozzle.

In certain circumstances, a C-D nozzle is utilized since the convergent nozzle's gross thrust coefficient is too significantly reduced. As the flight Mach number increases, the pressure ratio across the nozzle does as well (figure 4.7). At a Mach number of 2, for instance, the nozzle pressure ratio lies at around 12. As seen in Fig. 4.8, the convergent nozzle gross thrust penalty at this pressure ratio is around 9%. This figure represents the ratio of the gross thrust ($A_e = A_t$) to the peak thrust ($P_e = P_a$) vs NPR of a convergent nozzle.

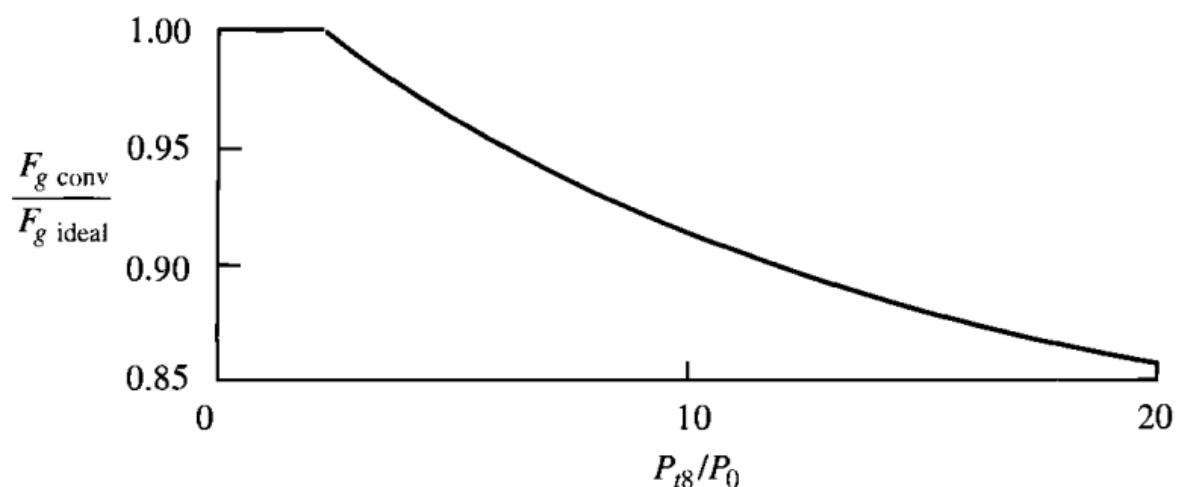


Figure 4.8. Ratio of convergent nozzle gross thrust to ideal gross thrust vs NPR (AIAA, 2002) [12].

Thus, in order to sustain and increase supersonic flight speeds without significantly reducing thrust efficiency, CD nozzles are employed instead of convergent nozzles. Additionally, in order to maintain the nozzle operating at its maximum thrust capacity across all flight conditions, variable-area-ratio nozzles are employed (for both convergent and CD nozzles).

As it has been established, the expansion process inside the nozzle is not really ideal, and this results in overall reduced thrust by reduction in exit velocity or total pressure inside of the nozzle. This directly

affects the nozzle's thrust efficiency. In most cases, empirically derived thrust efficiencies are used, that account for the following losses:

- Thrust loss due to the exhaust velocity vector angularity and/or dispersion.
- Thrust loss due to reduction in velocity magnitude caused by friction in the boundary layers.
- Thrust loss due to loss of mass flow from leakage through the nozzle walls.
- Thrust loss due to flow non-uniformities.

4.1.5. Nozzle Performance based on Nozzle Type

As it has been established, nozzles of many kinds can provide thrust for propulsion systems. From basic fixed-area convergent and fixed-area convergent-divergent (C-D) nozzles to more intricate ejector nozzles with independent control over the throat and exit areas. The more intricate cooling air ejector nozzles are utilized for supersonic military aircraft with afterburning engines, whereas the simpler convergent nozzle has long been employed on commercial subsonic transports. To get the best thrust efficiency for a supersonic cruise aircraft, such as supersonic commercial transport aircraft, the nozzle area ratio has to be continually adjusted throughout the flight. The reason for this is shown in figure 4.9, where nozzle thrust efficiency is graphed as a function of flight speed (Mach number) for fixed-area-ratio convergent and CD nozzles. At takeoff and subsonic speeds, a simple convergent nozzle

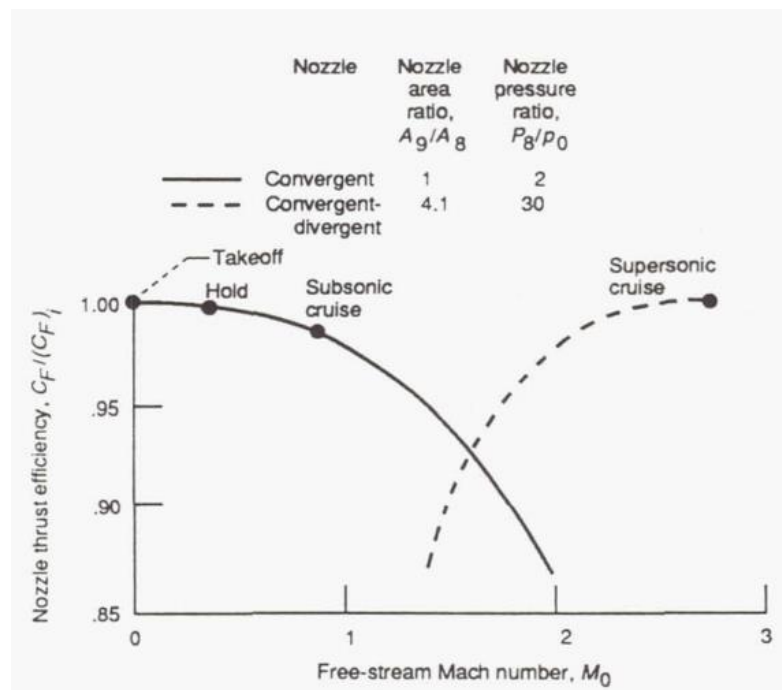


Figure 4.9. Variation of nozzle efficiency for fixed-geometry nozzles (NASA, 1990). [11].

would be preferred, but ineffective at transonic and supersonic speeds. However, at transonic speeds, a fixed convergent-divergent nozzle that performs well during supersonic cruising has significant overexpansion losses. The nozzle area ratio has to be regularly adjusted to ensure good performance under all flying circumstances.

- **Convergent Nozzles:**

The gross thrust of the nozzle is calculated from equation (46), by rewriting it to include correction coefficients due to the defined losses:

$$F_g = C_V C_{\theta} \gamma P_e M_e^2 A_{e, effective} + (P_e - P_a) A_e \quad (53)$$

Then the thrust coefficient can be defined by dividing the equation by total pressure and effective exit area:

$$\frac{F_g}{P_{0e} A_{e, effective}} = C_V C_{\theta} \gamma \frac{P_e}{P_{0e}} M_e^2 + \frac{1}{C_d} \left(\frac{P_e}{P_{0e}} - \frac{P_a}{P_{0e}} \right) \quad (54)$$

Where C_d is given by equation (49).

In addition, the thrust efficiency given by equation (50) can also be expressed in terms of the thrust coefficient:

$$\eta_F = \frac{C_{Fg}}{C_{Fg, ideal}} = \frac{C_V C_{\theta} \gamma \frac{P_e}{P_{0e}} M_e^2 + \frac{1}{C_d} \left(\frac{P_e}{P_{0e}} - \frac{P_a}{P_{0e}} \right)}{\left(\frac{F_i}{P_{0e} A_{e, effective}} \right)} \quad (55)$$

Where:

$$\frac{F_i}{P_{0e} A_{e, effective}} = \left\{ \frac{2\gamma^2}{\gamma - 1} \left(\frac{2}{\gamma + 1} \right)^{\frac{\gamma+1}{\gamma-1}} \left[1 - \left(\frac{P_a}{P_{0e}} \right)^{\frac{\gamma-1}{\gamma}} \right] \right\}^{1/2} \quad (56)$$

As it was mentioned, the correction factors account for losses due to flow non-idealizations and multi-dimensional flow mechanics and have been empirically derived over the years of experimental test programs. These are shown in figures 4.10-4.11.

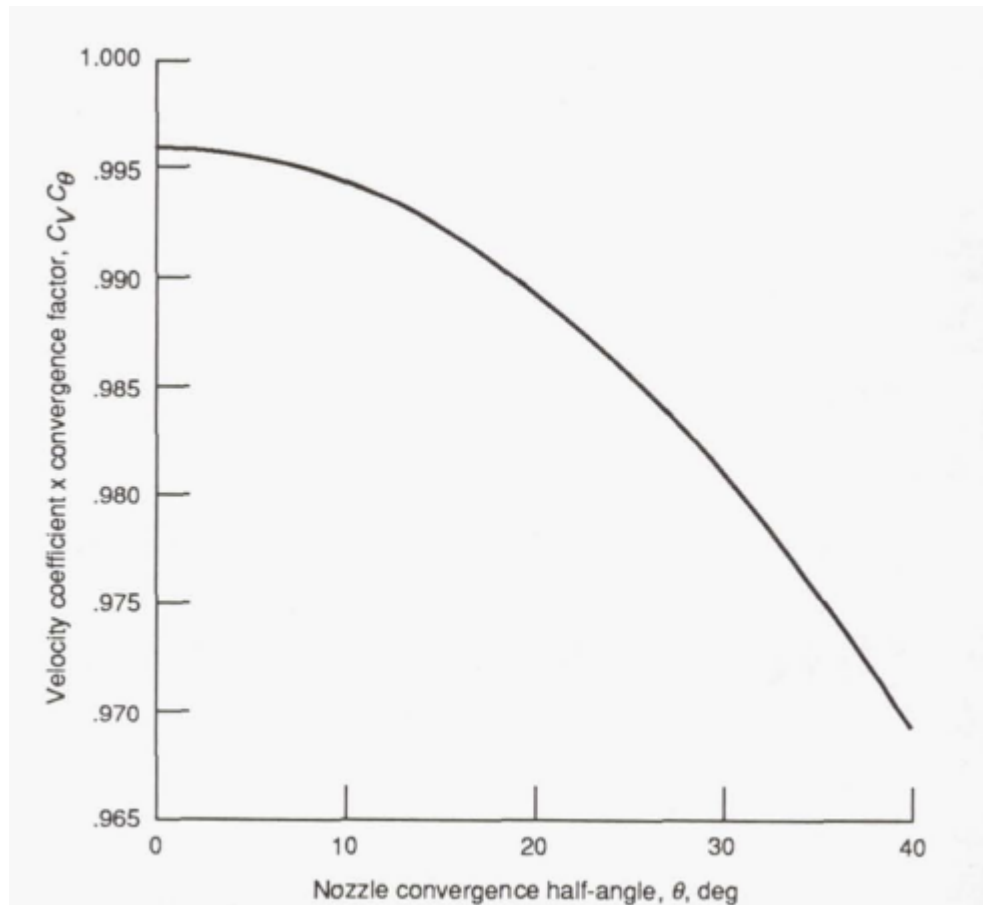


Figure 4.10. Convergent nozzle correction coefficients as a function of convergence half-angle (NASA, 1990). [11].

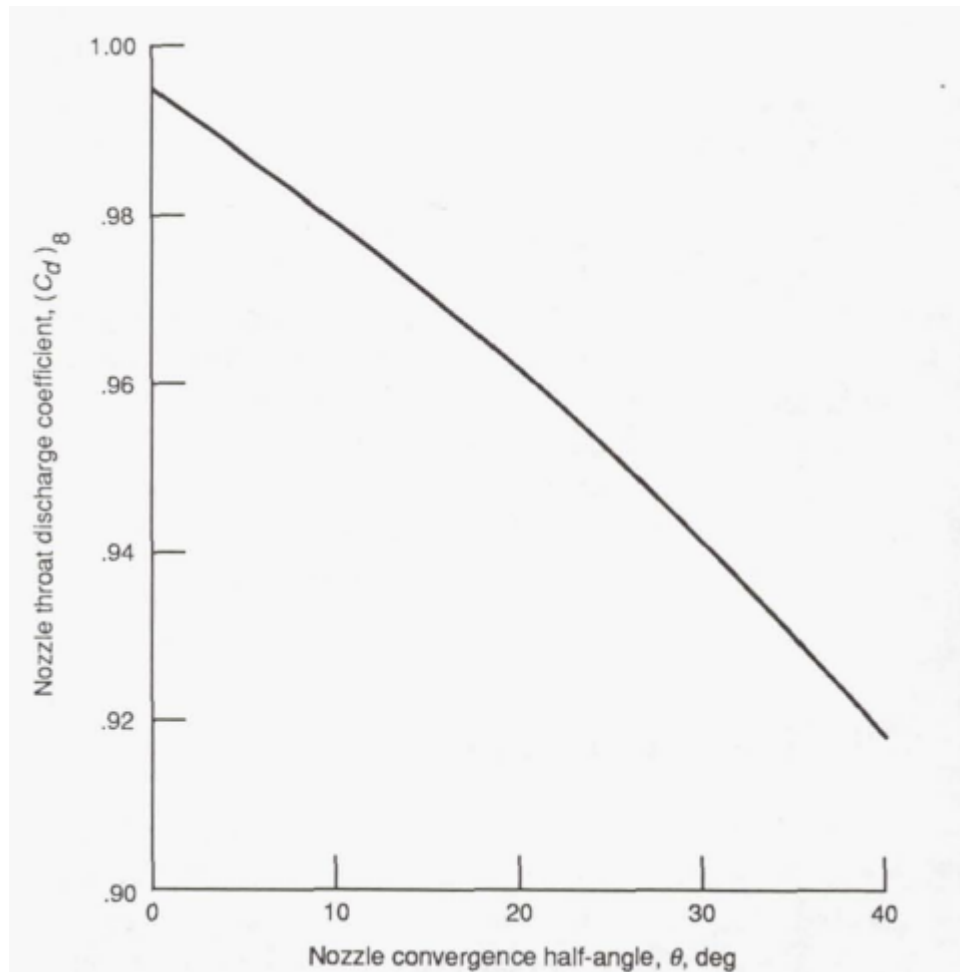


Figure 4.11. Choked convergent nozzle discharge coefficient as a function of convergence half-angle (NASA, 1990). [11].

- Convergent-Divergent Nozzles:

The gross thrust of a CD nozzle is calculated from the conditions at the nozzle exit considering the losses due to friction and angularity, just as equation (53). However, in order to obtain the thrust coefficient, the gross thrust is divided by the geometric and flow conditions at the throat:

$$\frac{F_g}{P_{0t} A_{t, effective}} = C_V \lambda \gamma \frac{P_e}{P_{0t}} \left[\frac{A_{e, effective}}{A_{t, effective}} \right] M_e^2 + \frac{1}{C_{d,t}} \left(\frac{A_e}{A_t} \right) \left(\frac{P_e}{P_{0t}} - \frac{P_a}{P_{0t}} \right) \quad (57)$$

Where λ is given by equation (52).

If the nozzle area ratio is fixed, meaning the nozzle does not feature a variable exit or throat area mechanism, equation (575757575757575757575757575757) can be rearranged:

$$\frac{F_g}{P_{0t}A_{t,effective}} = \left\{ C_V \lambda \gamma \frac{P_e}{P_{0t}} \left[\frac{A_{e,effective}}{A_{t,effective}} \right] M_e^2 + \frac{1}{C_{d,t}} \left(\frac{A_e}{A_t} \right) \left(\frac{P_e}{P_{0t}} \right) \right\} - \frac{1}{C_{d,t}} \left(\frac{A_e}{A_t} \right) \left(\frac{P_a}{P_{0t}} \right) \quad (58)$$

As defined by Leonard E. Stitt (NASA, 1990) [11], in this case, "the value of the coefficient is equal to the terms inside the brackets when the NPR is infinite, this is referred to as the vacuum thrust coefficient."

Similarly to equation (55555555), the thrust efficiency becomes:

$$\eta_F = \frac{C_{Fg}}{C_{Fg,ideal}} = \frac{C_V \lambda \gamma \frac{P_e}{P_{0t}} \left[\frac{A_{e,effective}}{A_{t,effective}} \right] M_e^2 + \frac{1}{C_d} \left(\frac{A_e}{A_t} \right) \left(\frac{P_e}{P_{0t}} - \frac{P_a}{P_{0e}} \right)}{\left(\frac{F_i}{P_{0t}A_{t,effective}} \right)} \quad (59)$$

Where:

$$\frac{F_i}{P_{0t}A_{t,effective}} = \left\{ \frac{2\gamma^2}{\gamma-1} \left(\frac{2}{\gamma+1} \right)^{\frac{\gamma+1}{\gamma-1}} \left[1 - \left(\frac{P_a}{P_{0t}} \right)^{\frac{\gamma-1}{\gamma}} \right] \right\}^{1/2} \quad (60)$$

4.1.6. Nozzle Flow Equations

Given that the nozzle is a component that does not produce or extract either work nor heat, the flow inside of the nozzle, for the purpose of this project, can be assumed to be adiabatic and isentropic. Furthermore, jet exhaust is composed of combustion gases that can be considered to behave as ideal gases ($PV = mRT$). Thus, as expressed by the National Advisory Committee for Aeronautics (NACA) in their 1953 publication, *Equations, Tables, And Charts for Compressible Flow*, the following fundamental thermodynamic and isentropic relations can be made for a continuous 1-dimensional compressible flow of a thermally perfect (ideal) gas [14]:

Temperature:

$$\frac{T_{0i}}{T_i} = 1 + \frac{\gamma - 1}{2} M_i^2 \quad (61)$$

$$T_{0i} = T_i + \frac{1}{2} \frac{v_i^2}{C_p} = \frac{h_{0i}}{C_p} \quad (62)$$

Pressure:

$$\frac{P_{0i}}{P_i} = \left[1 + \frac{\gamma - 1}{2} M_i^2 \right]^{\frac{\gamma}{\gamma - 1}} \quad (63)$$

Temperature-Pressure:

$$\frac{T_{0i}}{T_i} = \left(\frac{P_{0i}}{P_i} \right)^{\frac{\gamma - 1}{\gamma}} \quad (64)$$

Mass flow rate:

$$\dot{m}_i = A_i \sqrt{\frac{\gamma}{R}} \frac{P_{0i}}{\sqrt{T_{0i}}} \frac{M_i}{\left[1 + \frac{\gamma - 1}{2} M_i^2 \right]^{\frac{\gamma + 1}{2(\gamma - 1)}}} \quad (65)$$

Speed of Sound:

$$a = \sqrt{\gamma R T} \quad (66)$$

It's important to highlight that derivations of these equations have been employed for the calculations done in the engine cycle analysis section.

Furthermore, there is a direct relationship between the local area of a nozzle (or any duct where fluids flow) and the flow velocity at that point given by the continuity equation derived from the conservation of mass:

$$\rho v A = cte$$

Expressing this relationship in terms of an isentropic, adiabatic, expansion of a 1D compressible flow of a perfect gas, the ratio between any given local area and the area where the flow becomes sonic (Mach 1) can be obtained:

$$\frac{A^*}{A_i} = M_i \left[\frac{\frac{\gamma + 1}{2}}{1 + \frac{\gamma - 1}{2} M_i^2} \right]^{\frac{\gamma + 1}{2(\gamma - 1)}} \quad (67)$$

In the case of a convergent nozzle, A^* represents the exit area. In the case of a CD nozzle, A^* represents the throat area. This equation clearly is a function of the specific heat ratio (γ) of the fluid. In the case of air considered as a diatomic gas ($\gamma = 1.4$), as it is for this project, the equation yields the following curve:

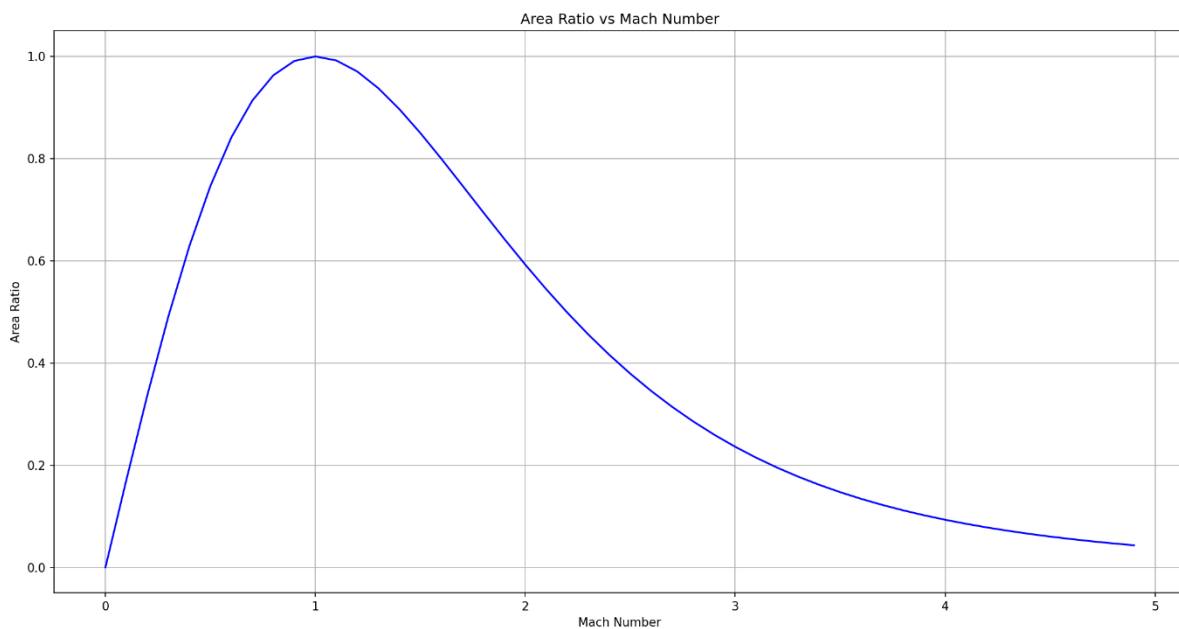


Figure 4.12. Area ratio vs Mach number for air with $\gamma = 1.4$

This clearly represents the expansion of the gas through a converging-diverging duct. Mach number increases up to 1 when the area ratio is equal to 1 and keeps increasing to supersonic speeds after that point, while the area ratio reduces back towards 0 because of the divergent section.

For the case of a convergent only nozzle, the curve in figure 4.12. would only reach Mach 1, if sufficient expansion occurs. In addition, in congruence with the conservation of energy, while the velocity of the flow increases through the length of the nozzle, the static pressure inside of the nozzle reduces (as it is an expansion process) which also drives down the static temperature, which decreases at a lower rate.

4.2. Conceptual Design

This section deals with the conceptual design phase of a nozzle enabling afterburner use for a military aircraft engine. This includes nozzle concept selection based on functional requirements for the defined model engine, in congruence with the established theoretical background, and initial conceptual drawings and calculations before a further-depth complete preliminary design is developed.

4.2.1. Nozzle Concept Selection

The selection of the nozzle type is entirely based on aircraft mission and performance requirements. For any given aircraft program, several nozzle types can be studied and compared to arrive at the most optimal configuration given flight requirements and engine performance and cycle analysis.

In the case of this design, a model engine has already been defined and its cycle analyzed. This model engine is based on a reference engine (RB199), which has been used as the powerplant for the Multirole Combat Aircraft (MRCA) jointly developed and manufactured by Germany, Italy, and the United Kingdom, the *Panavia Tornado* (figure 2.9). Thus, it will be wise to study and understand the mission requirements, role, and capabilities of this aircraft and its variants, as well as the actual engine, in order to derive requirements for the established model engine.

There are three main variants of the Panavia Tornado:

1. Tornado IDS (Interdictor/Striker): fighter-bomber variant meant for striking ground targets and perform low altitude missions.
2. Tornado ECR (Electronic Combat/Reconnaissance): suppression of enemy air defenses (SEAD) variant meant to target and destroy enemy surface-based air defenses, anti-aircraft artillery, and ground radars and telecommunications equipment either through physical destruction or electronic suppression.
3. Tornado ADV (Air Defense Variant): intended to be a long-endurance interceptor aircraft to counter threats from soviet bombers during the Cold War.

These 3 variants have significantly different mission requirements; however, they all use the same engine platform but with different variants for longer ranges or endurances. Thus, in general the Panavia Tornado performance specifications relevant to this design are the following:

- Maximum Speed at 9,000m: 2,400km/h (Mach 2.2)
- Maximum Speed at Sea Level: 1,482 km/h (Mach 1.2)

Given these values of flight speed and the theoretical background defined in the previous section, the most obvious nozzle choice, based purely on best performance (nozzle thrust efficiency), would be a variable geometry convergent-diverging nozzle. However, by analyzing the components of the real engine, RB199, utilized by this aircraft family, it is clear that the nozzle used is a relatively simple variable geometry converging nozzle. In the same manner, it is also clear that the overall engine system design features a variable intake ramp in order for the aircraft to be able to reach supersonic speeds without the need for a CD nozzle (not to mention the afterburner use). However, analysis of intake design effects falls outside the scope of this project. Thus, for the reason being, the nozzle concept for this design will be that of a variable geometry converging nozzle.

This nozzle concept selection will also be in congruence with the performed cycle analysis, as the exit speed of the gases reaches sonic speed (Mach 1) at the exit section. The variable geometry condition is necessary due to the nature of afterburner use, as it has already been established, and it will serve to maintain the exit flow choked through all flight conditions. However, it's important to highlight that this configuration will obviously suffer losses due to the under expansion of the exhaust gases, especially at supersonic flight speeds.

4.2.2. Nozzle Conceptual Design

In terms of the nozzle geometry and shape, for the purpose of maintaining a simple yet usable design, the nozzle geometry will be approximated to that of a trapezoid. In this configuration, the longer base of the trapezoid represents the nozzle intake area, and the nozzle converges towards the opposite, shorter trapezoid base. This configuration is shown in figure 4.13 along with the developed equations and the cross-sectional shape.

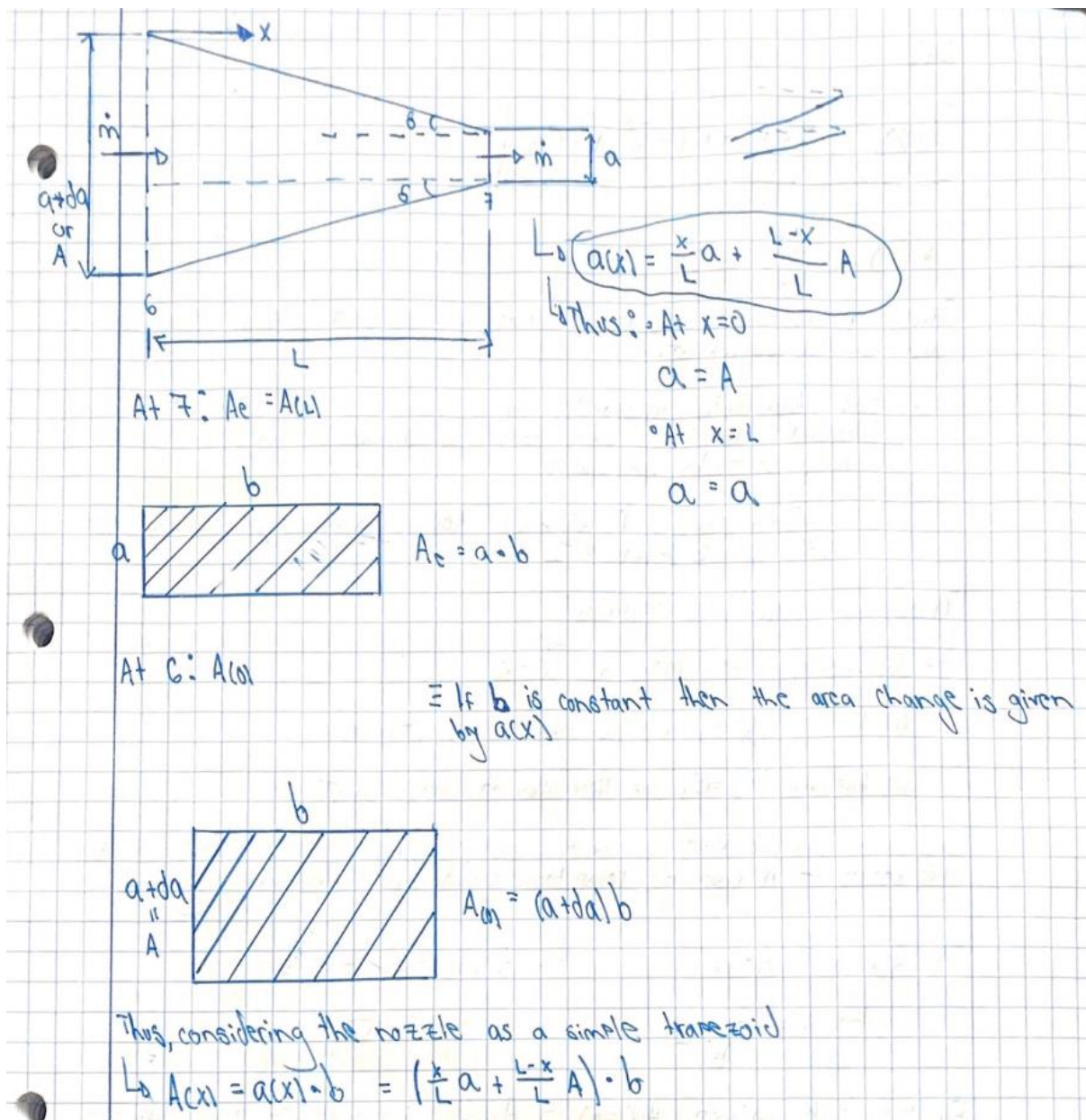


Figure 4.13. Nozzle geometrical concept design.

As it is shown in the above figure, the nozzle cross section is taken to be a rectangular shape, as in the case with 2D nozzles. Although is not the optimal shape for flow losses, structurally, or in terms of weight, this shape will allow to simplify the mechanical design of the variable area using actuator-linkages systems. As shown in figure 4.13, the equation for the internal height of the nozzle as a function of distance x is a simple equation for trapezoids:

$$a(x) = \frac{x}{L}a + \frac{L-x}{L}A \quad (68)$$

In this way, when $x = 0$, the height of the nozzle is given by a constant height (A), and when $x = L$ (the length of the nozzle) the height is given by a constant (a). Furthermore, by considering the width of the nozzle (b) as a constant through the length of the nozzle, the equation for the cross-sectional area of the nozzle can easily be obtained as a function of x :

$$A(x) = a(x)b = \left[\frac{x}{L}a + \frac{L-x}{L}A \right] b \quad (69)$$

However, initially the length of the nozzle is unknown, thus the equation is adimensionalised:

$$\bar{x} = \frac{x}{L}$$

Thus, equation (69) becomes:

$$A(\bar{x}) = [\bar{x}a + (1 - \bar{x})A]b \quad (70)$$

Where the value of (\bar{x}) goes from 0 to 1. Then, the area ratio relevant to obtaining the Mach number (eq 67) at each point along the nozzle's length has the following limits:

$$0 < \frac{A_e}{A(\bar{x})} \leq 1$$

In this way, each area ratio corresponds to a value of \bar{x} (and therefore a value of x along L) up to 1, where the exit area is equal to the local area and the Mach number reaches 1. However, the area ratio may never be 0 as this would imply that the inlet area approaches infinity and therefore the flow speed is 0. This is just not true, thus an assumption at the inlet has to be made in order to define a boundary condition:

- Assume $A(0)$
- Assume $M(0)$

For this design, the area at the inlet of the nozzle will be assumed to be equal to the engine fan area and maintained constant through all flight conditions. Thus, the following boundary conditions apply:

- At $\bar{x} = 0$: $A(0) = A_{fan} = 40715m^2 \rightarrow M(0) = 0.15$
- At $\bar{x} = 1$: $A(1) = A_e = 0.1042m^2 \rightarrow M(1) = 1$

Knowing the area ratio at each point along the nozzle, and utilizing the tables from NACA's *Equations, Tables, And Charts for Compressible Flow* [14], the flow Mach number can be obtained for each discrete point along the nozzle. In addition, by considering the stated boundary conditions and taking the width of the nozzle (b) as the fan diameter, the constant from equation 69 can be estimated:

- At $\bar{x} = 0$: $A(0) = A_{fan} = 40715m^2 = Ab \rightarrow A = 0.565m$
- At $\bar{x} = 1$: $A(1) = A_e = 0.1042m^2 = ab \rightarrow a = 0.14472m$

Thus, the area equation becomes:

$$A(\bar{x}) = [\bar{x} \cdot 0.14472m + (1 - \bar{x}) \cdot 0.565m] \cdot 0.72m$$

It's important to note that the boundary condition at $x = 0$ is maintained constant throughout all flight conditions and afterburner use because the inlet area is constant. However, because the exit area changes with the use of afterburners, the boundary constant (a) has to be calculated for each case and flight conditions, yielding different area equations as a function of x for each change in exit area or ambient conditions. In the case of the equations already defined, this represents the dry case of the engine at Sea Level-Static (SLS) conditions. Doing the same analysis for the case with afterburners SLS (exit area increases), the equation defining the Area as a function of the position along the length of the nozzle becomes:

$$A(\bar{x}) = [\bar{x} \cdot 0.2426m + (1 - \bar{x}) \cdot 0.565m] \cdot 0.72m$$

With these nozzle cross sectional area equations, the static parameters along the length of the nozzle can be obtained and graphed for each of the cases:

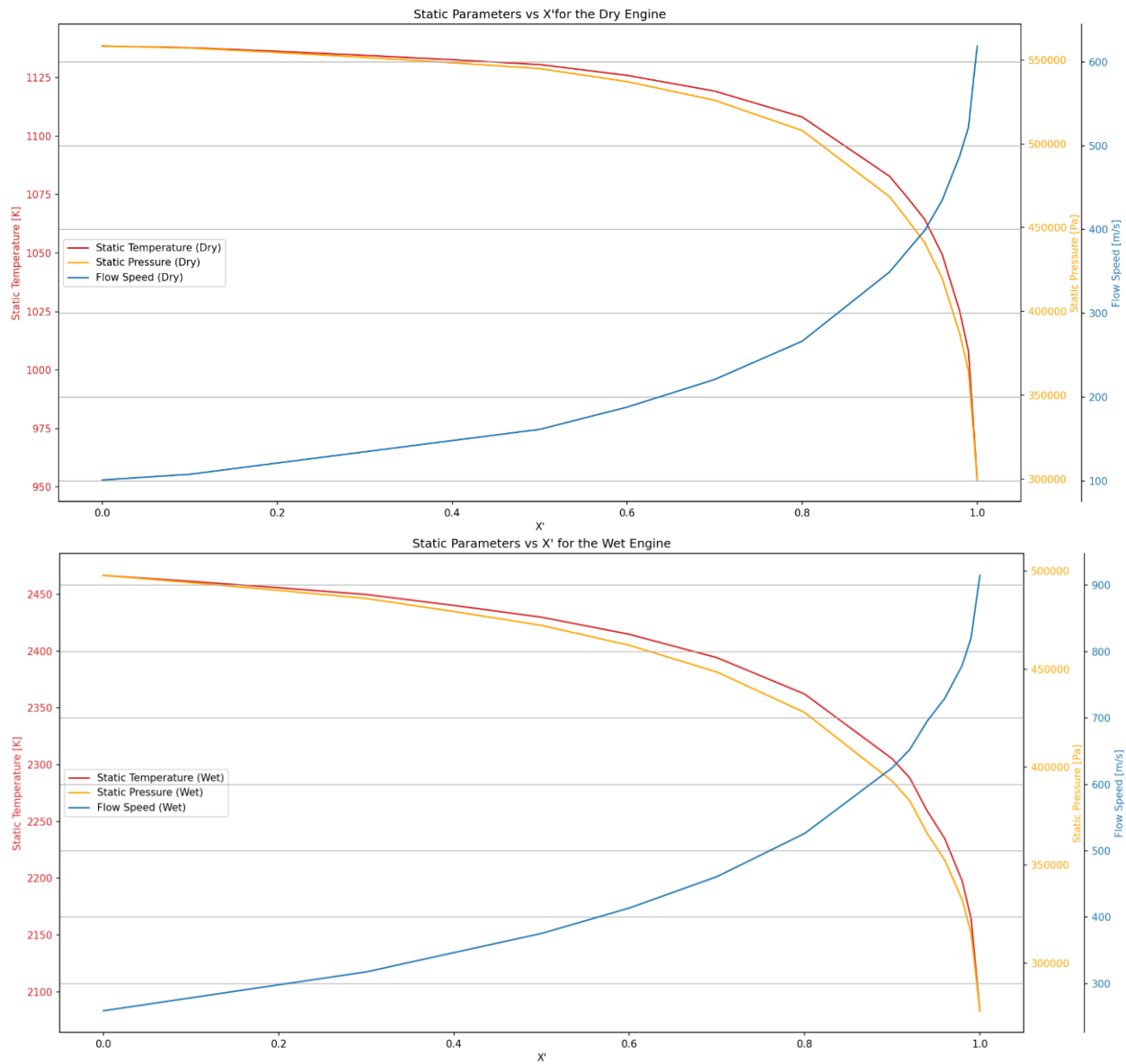


Figure 4.14. Local temperature, pressure, and velocity along the nozzle for the dry engine (top) and the wet engine (bottom) at Sea-Level-Static.

Figure 4.14 clearly shows the static parameters for the flow inside the converging nozzle. Both cases behave as expected; pressure and temperature decreasing parabolically towards the exit while the flow velocity increases up to sonic speed at the exit. Both cases look almost the same, however the wet case (afterburners on) clearly shows a significantly higher velocity and temperature magnitude due to the re-combustion.

4.3. Nozzle Preliminary Design

This section deals with the complete preliminary design phase of a nozzle enabling afterburner use for a military aircraft engine. This includes multi-physical analysis of the nozzle behavior under operation to arrive at a suitable mechanical design of the variable geometry nozzle considering the results from the engine cycle analysis and the defined conceptual design.

4.3.1. Mechanical Conceptual Design, Initial Sizing & 2D Analysis

For the purpose of this analysis, the upper plate of the nozzle will be studied in a 2D fashion, considering it as a straight beam subjected to the pressure loads on the lower side. Because the pressure distribution is not trivial and only discrete values were obtained at different points along the length, the trapezoidal rule must be employed to approximate the resultant force caused by the pressure distribution by obtaining the product between the initial and final values of static pressure and the nozzle's width (b). The mechanical configuration is represented in the following figures.

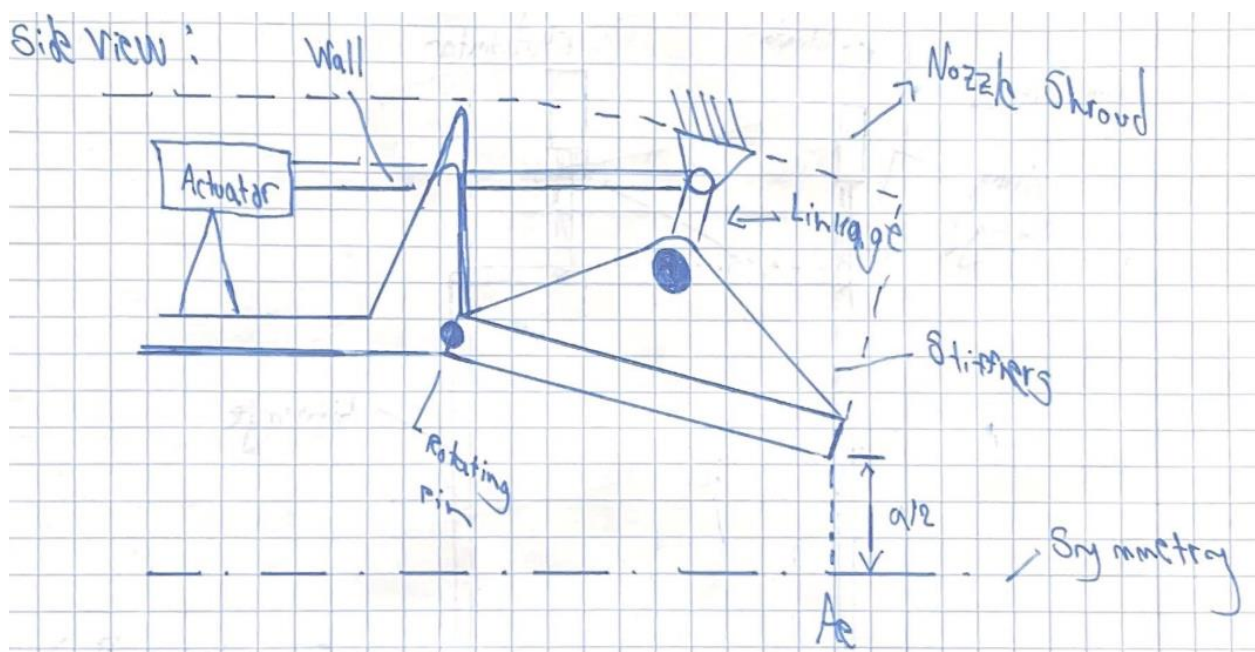


Figure 4.15. Nozzle-actuator mechanical configuration (Side View)

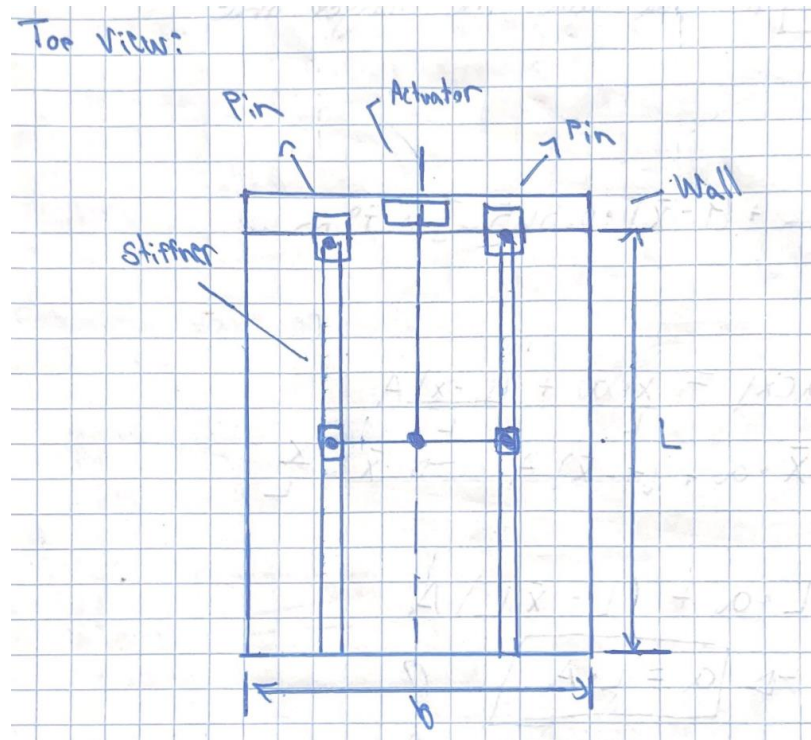


Figure 4.16. Nozzle-actuator mechanical configuration (Top View)

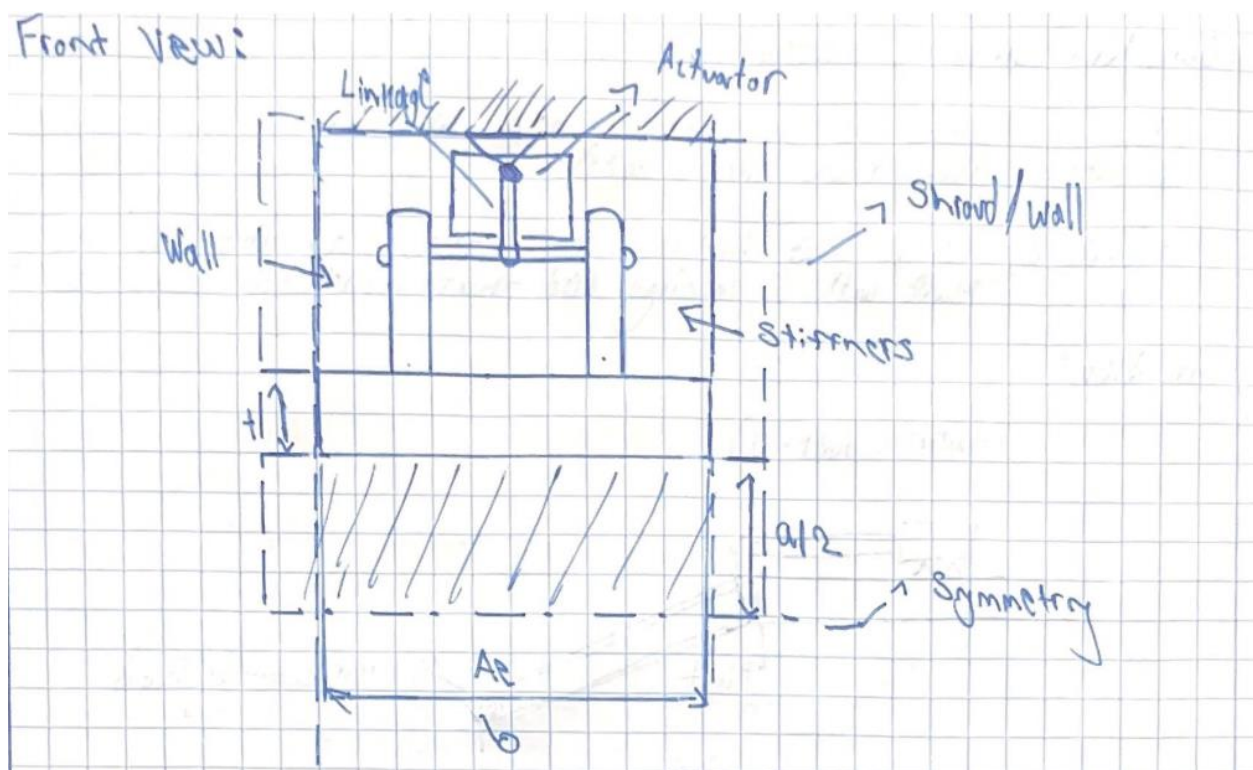


Figure 4.17. Nozzle-actuator mechanical configuration (Front View)

This configuration allows for the modulation of nozzle exit area by the use of a linear actuator directly connected to stiffeners that are placed symmetrically on the plate. The plate itself is joined to the body of the engine via a pinned connection that allows rotation. The actuator transfers its motion with the use of a simple bell-crank linkage that is directly connected at the center of rod that joins both stiffeners and it is fixed at its pivot. This way, the input force of the actuator serves to rotate the plate, increasing or decreasing the exit area by decreasing or increasing the convergence angle, respectively.

Furthermore, the actuator has a perhaps more important task; to maintain static equilibrium of the nozzle plate for as long as required. For this purpose, the following Load Diagram is defined:

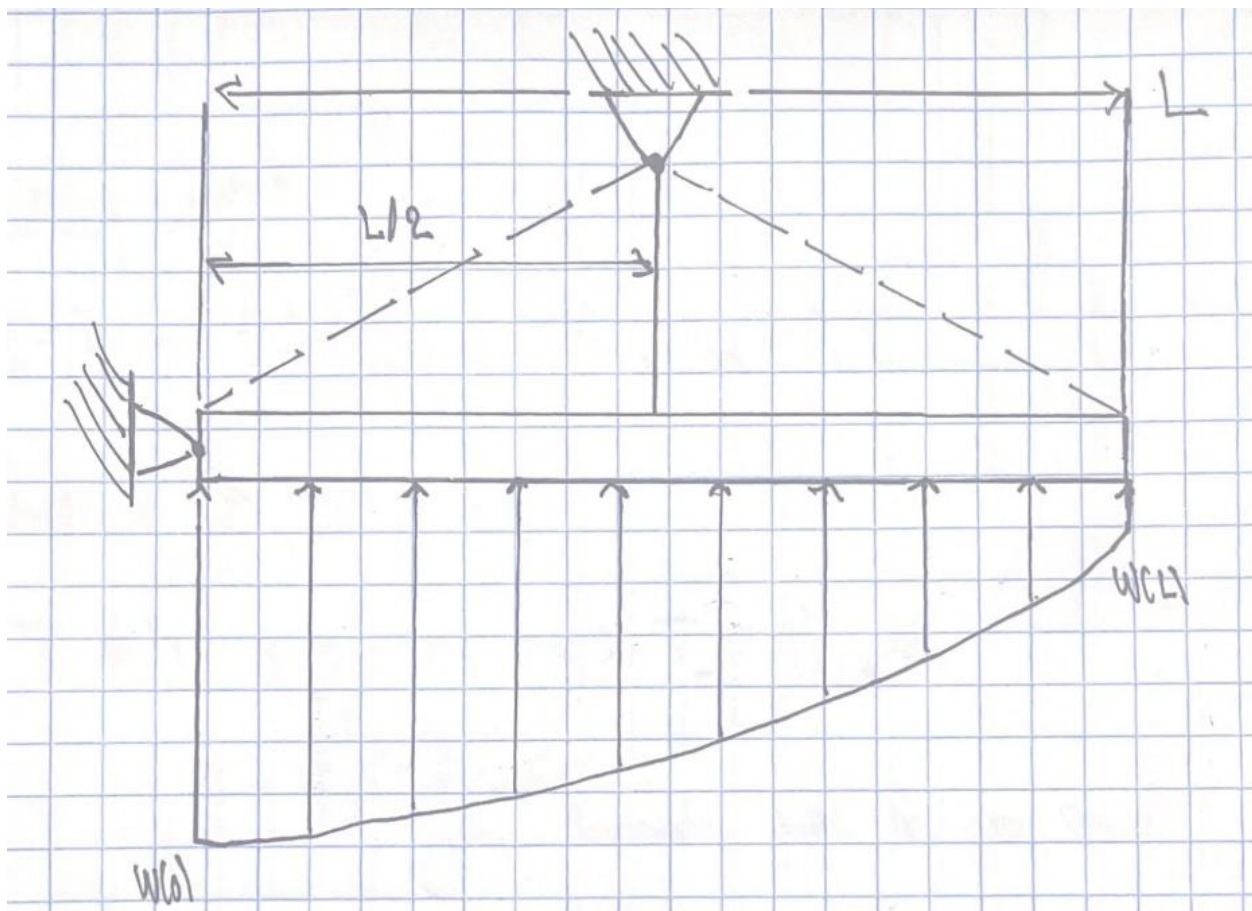


Figure 4.18. Nozzle plate load diagram

In this diagram, the support at (B) is simplified to account for the connection between the actuator, linkage, and the stiffeners. Following the conceptual design, the load case will be assumed to be at Sea-Level-Static conditions and the length of the nozzle plate will be taken as 1 meter. This results in the following simplified Free-Body-Diagram:

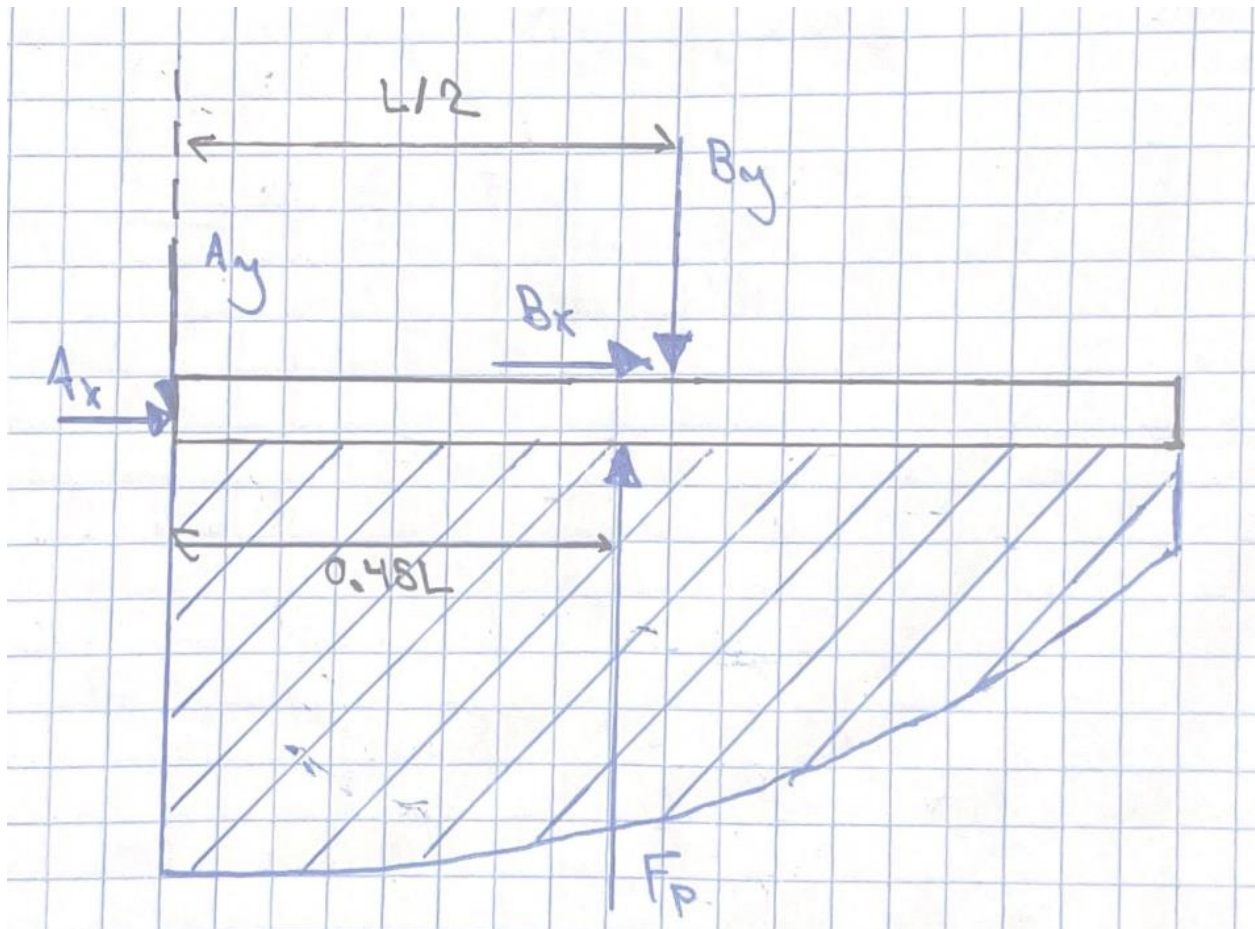


Figure 4.19. Nozzle plate loading case Free-Body-Diagram.

By defining equilibrium equations and taking moments from point A, the resultant forces can be determined:

- $B_y = 0.88F_p$
- $A_y = 0.12F_p$

As mentioned, because the pressure distributions obtained are discrete values along the nozzle's length and not a given expression, definite integration is not possible, thus the trapezoidal rule must be

employed. The trapezoidal rule works by approximating the region under the graph as a trapezoid and calculating its area:

$$\int_a^b f(x)dx \approx \sum_{k=1}^N \frac{f(x_{k-1}) + f(x_k)}{2} \times (x_k - x_{k-1}) \quad (71)$$

Thus, by using the static pressure forces obtained from the engine cycle analysis (figure 4.14) the resultant pressure force and reactions can be obtained:

- $F_p = 368.7\text{kN}$
- $B_y = 324.456\text{kN}$
- $A_y = 44.244\text{kN}$
- $B_x = 0$
- $A_x = 0$

These forces act following the directions defined in the FBD. In the case of the reaction at point (B), this represents the force required to be sustained by the support where the bell crank linkage. Depending on the bell-crank design, the actuator force may be amplified or minimized by it. This relationship is obtained by taking moments from the fixed pivot point and equating them to 0 and assuming that the forces act perpendicular to the connection, yielding the following relationship:

$$P = P' \frac{V}{H} \quad (72)$$

Where P is the actuator force, P' is the linkage output force, H is the horizontal length of the linkage (the connection with the actuator), and V is the vertical length of the linkage (the connection with the stiffeners). Thus, in order to prevent a decrease in the output force, both sides of the bell-crank must be of the same distance, or preferably the horizontal length greater in order to amplify the force of the actuator with the link. However, the design and specific placement of the linkage is limited by the available space which is yet to be determined.

Considering the calculated reactions and the distributed load, a bending moment and shear force diagram can be constructed for this configuration.

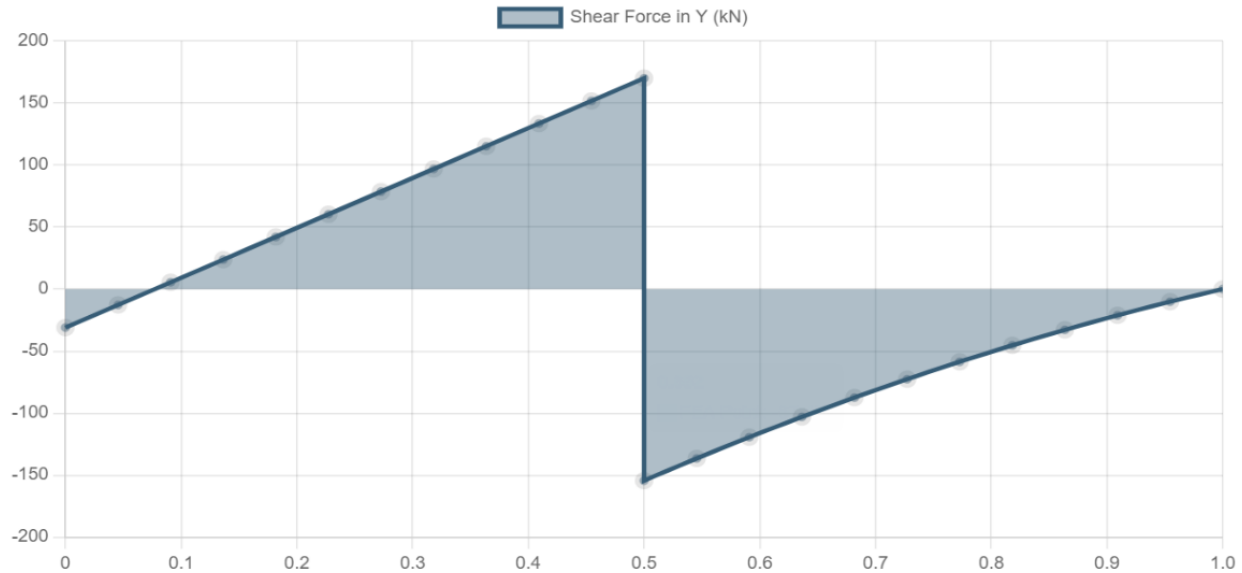


Figure 4.20. Nozzle plate Shear Force diagram.

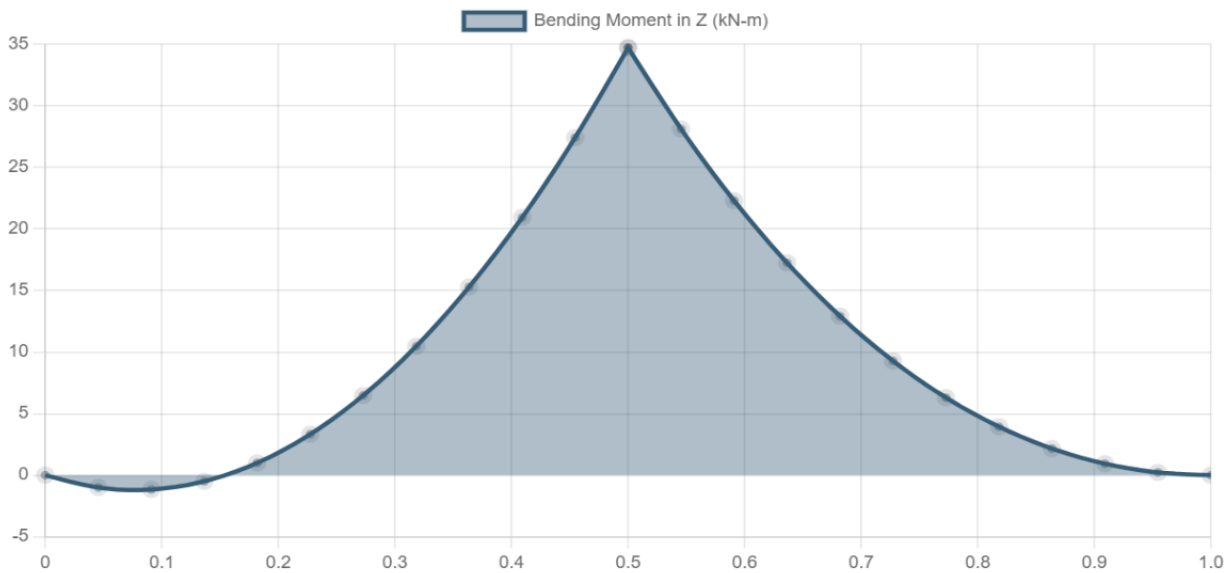


Figure 4.21. Nozzle plate Bending Moment diagram.

These graphs clearly show the maximum bending moment and shear force experienced by the nozzle plate under these load conditions and plate configuration:

- Max Bending Moment: 34.723 kN-m
- Max Shear Force: 169.9 kN

However, the plate should be analyzed while being placed at angle with respect to the horizontal line in order to represent the convergence angle of the nozzle. Just as shown in figure 4.22.

Following the dimensions established for the Sea-Level-Static case of both the wet and dry cases, the convergence angle (θ) can be easily determined trigonometrically for any given exit area required for the proper operation of the engine:

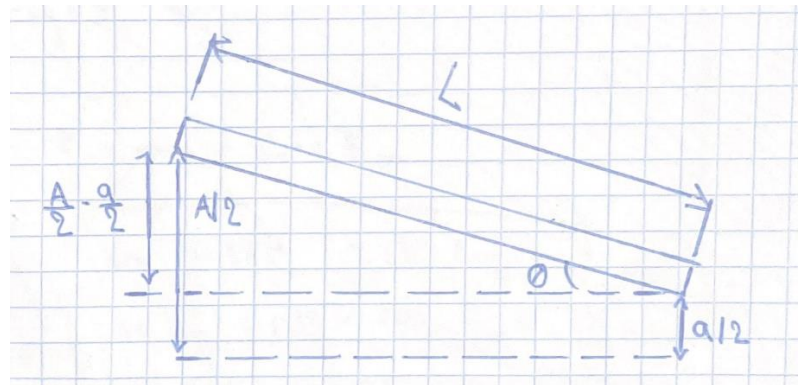


Figure 4.22. Convergent nozzle plate diagram drawing.

$$\theta = \sin^{-1} \frac{A/2 - a/2}{L} \quad (73)$$

At the studied conditions and given the assumed length of the nozzle, the convergence angle for both the dry and wet cases are:

- $\theta_{\text{dry}} = 12.13^\circ$
- $\theta_{\text{wet}} = 9.27^\circ$

As it has been expressed in the nozzle theoretical background, the convergence angle implicitly creates losses that affect the performance of the nozzle. Thus, a balance needs to be found between the length of the nozzle and the overall allowed losses related with the convergence angle.

Performing the static equilibrium analysis with the considered rotation of the plates yields the following results:

Table 4.1 Static equilibrium resultants and Max BM & SF for the convergent plate with wet and dry convergence angles at SLS conditions

Convergence Angle	12.13°	9.27°
Max Bending Moment (z)	33.94 kN-m	34.26 kN-m
Max Bending Moment (y)	7.29 kN-m	5.59 kN-m
Max Shear Force (z)	35.7 kN	27.36 kN
Max Shear Force (y)	166.1 kN	167.68 kN
A _x	9.29 kN	7.12 kN
A _y	43.25 kN	43.66 kN
B _x	68.178kN	52.26 kN
B _y	317.21 kN	320.21 kN

This simply implies that rotating the plate to meet the convergence angle does not affect the resultant reaction forces, bending moments, or shear forces, but it divides them into components in different directions directly proportional to the rotation angle.

Furthermore, a first iteration of the sizing of the mechanical design of the plate can be performed with the obtained results and by assuming a general material for the complete design shown in figures 4.15-4.17.

The plate's length and width have already been defined (1m and 0.72m respectively) and the thickness will be assumed to be 30mm. Given this thickness, the furthest distance from the neutral axis of the plate is 15mm. Thus, given the minimum moment of inertia of the plate only:

$$I_z = \frac{bt^3}{12} = 1,620,000 \text{ mm}^4$$

and the previous calculated maximum bending moment experienced by the plate, the maximum stress can be determined:

$$\sigma_{max} = \frac{M_{max} \cdot c}{I_z} = 321.51 \text{ MPa}$$

Additionally, the resultant shear stress for the plate can also be calculated by considering the maximum shear stress previously calculated:

$$\tau_{max} = \frac{1.5V_{max}}{A} = 11.8 \text{ MPa}$$

With these calculated stresses, an approximation of the resultant Von-Mises stress can be performed for any point on the plate's cross section where the maximum stresses act (L/2):

$$\sigma_{vm} = \sqrt{\sigma_x^2 - \sigma_x\sigma_y + \sigma_y^2 + 3\tau_{xy}^2} \quad (74)$$

Simplifying the equation for this case yields the following result:

$$\sigma_{vm} = \sqrt{\sigma_{max}^2 + 3\tau_{max}^2} = 322.15 \text{ MPa}$$

With this maximum stress for the plate only, a material needs to be selected to be able to withstand without trouble the maximum stress load. Generally, military afterburning jet engines are made of several different materials based on the different component requirements. The most critical of these components, structurally speaking, are the turbine blades and the nozzle due to their high pressure loads and very high temperature operation. For this purpose, engine manufacturers typically use the following materials for exhaust nozzles or a combination of them:

- Ceramic Matrix Composites
- Nickel-Based Superalloys
- Inconel
- Stainless Steel-Based Alloys
- Titanium-Based Alloys
- Clad Metals

- Cobalt-Based Superalloys
- Refractory Metal Alloys
- Niobium Alloys

Obviously, the main considerations of such materials are extreme high temperature performance, excellent mechanical properties, low thermal expansion, high oxidation resistance, good manufacturability, cost, and weight.

Thus, for this application a Silicon Carbide Composite (SiC) will be chosen for the nozzle plate with the following relevant mechanical properties, according to Swiss precision component manufacturer *IMETRA, Inc.* [15]:

- Density: 3100 kg/m³
- Flexural Strength: 550 MPa
- Compressive Strength: 3900 MPa
- Elastic Modulus: 410 GPa
- Poisson's Ratio: 0.14
- Thermal Expansion Coefficient: 4.0 x10⁻⁶/°C

So, considering a safety factor (SF) of 1.5 (generally used through all aviation designs) and the flexural strength being the minimum strength of the material, the allowable stress for maintaining the defined safety margin of the plate is:

$$\sigma_{allowable} = \frac{\sigma_y}{SF} = \frac{550 \text{ MPa}}{1.5} = 366.6 \text{ MPa}$$

Given that the max stress calculated for the plate under the bending moment and shear force conditions (Von-Misses) is 322.15MPa, this implies that the material will be able to safely withstand the loads considering the allowable stress. Furthermore, considering the equation for stress and moment of inertia of a rectangular plate, an expression for the thickness of the plate can be derived:

$$t \geq \sqrt{\frac{6 \cdot M_{max}}{b \cdot \sigma_{allowable}}} \quad (75)$$

Inputting the values into this equation yields a minimum plate thickness of 28.1mm in order to be able to withstand the bending loads with a 1.5 safety margin. Following these estimations, the position and dimensions of the stiffeners need to be defined. Using the stiffeners will ensure proper operation of the design for higher loading conditions as well as to provide a support for the bell-crank and actuator linkage. The following figures show the 2 views that completely define the initial sizing and positioning of the nozzle plate and stiffener configuration:

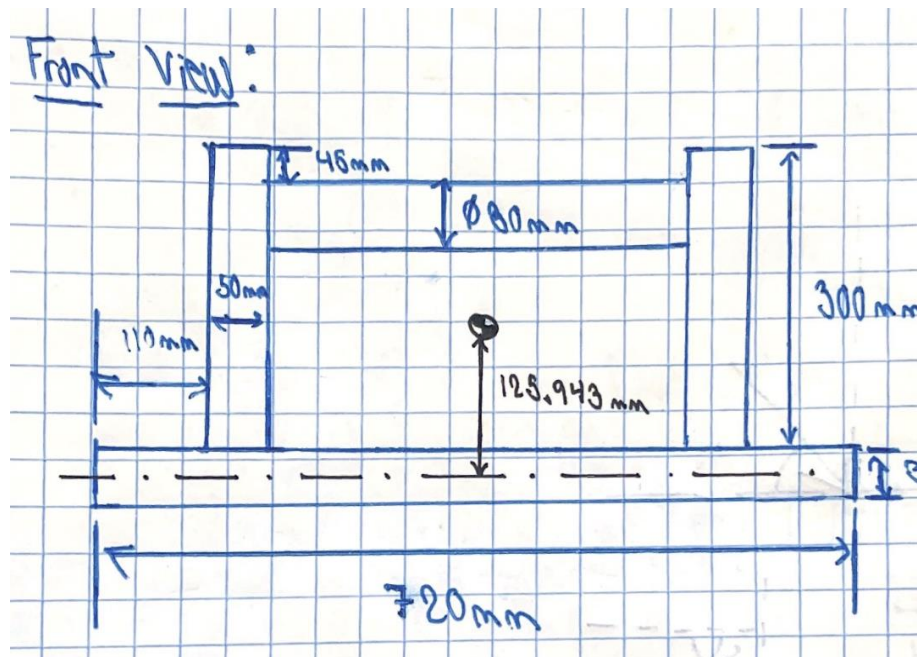


Figure 4.23. Nozzle plate and stiffeners front view initial dimensions drawing.

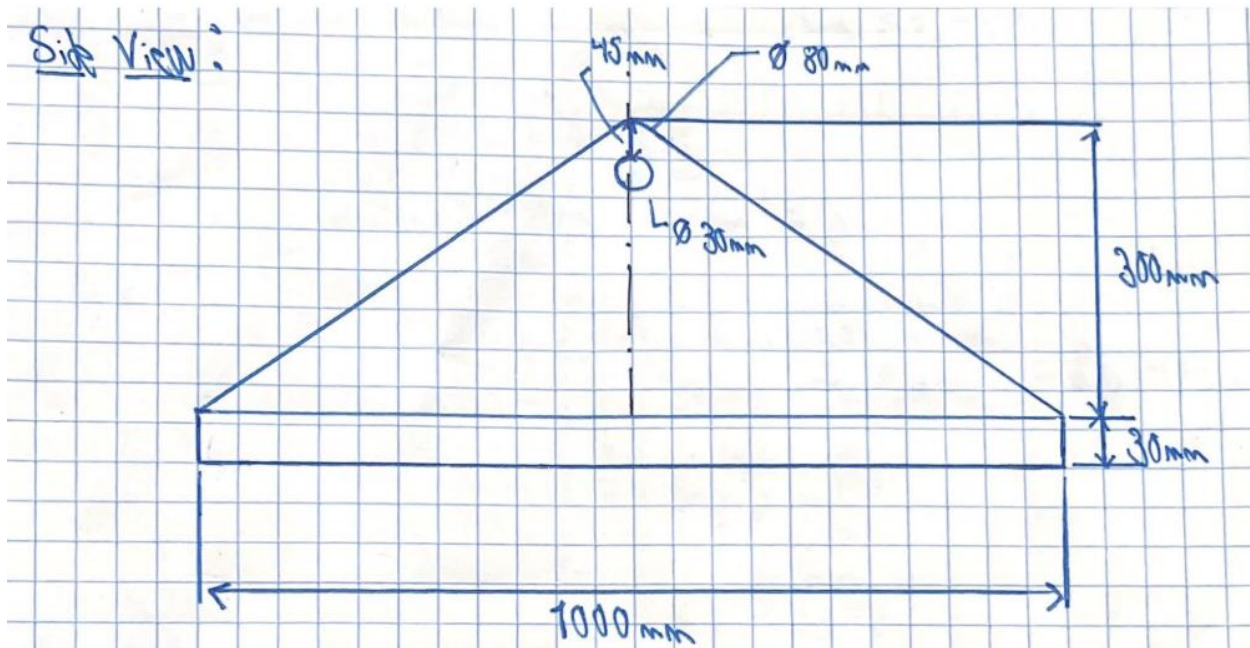


Figure 4.24. Nozzle plate and stiffeners side view initial dimensions drawing.

The drawings, although not drawn to perfect scale, clearly show the different dimensions considered for each of the components of this configuration. The rod was chosen to have a 30mm diameter to match the thickness of the plate, with each stiffener having a thickness of 50mm to provide support and additional inertia. The distance between the midline of the stiffeners is 450mm which was chosen arbitrarily. This configuration has a frontal area of 0.064m² and the following moments of inertia around the principal cross-sectional axes:

- $I_y = 8.158e^8 \text{ mm}^4$
- $I_z = 2.618e^9 \text{ mm}^4$

Given this new configuration, the maximum bending stress and Von-Misses stress are decreased to less than 1. This is clearly an over-engineered design that will result in a very high weight and cost. Thus, considering the maximum bending moment, and the allowable stress of the material, the following estimation of the minimum Moment of Inertia is the following:

$$I_z \geq \frac{M_{max} \cdot c}{\sigma_{allowable}} = 1,420,744.681 \text{ mm}^4$$

This is almost 2,000 less moment of inertia than the resultant configuration has. Thus, various stiffener design iterations will be performed in order to arrive at a suitable configuration that balances structural performance with weight and therefore material cost. The following figures show the final design for the plate and stiffener configuration:

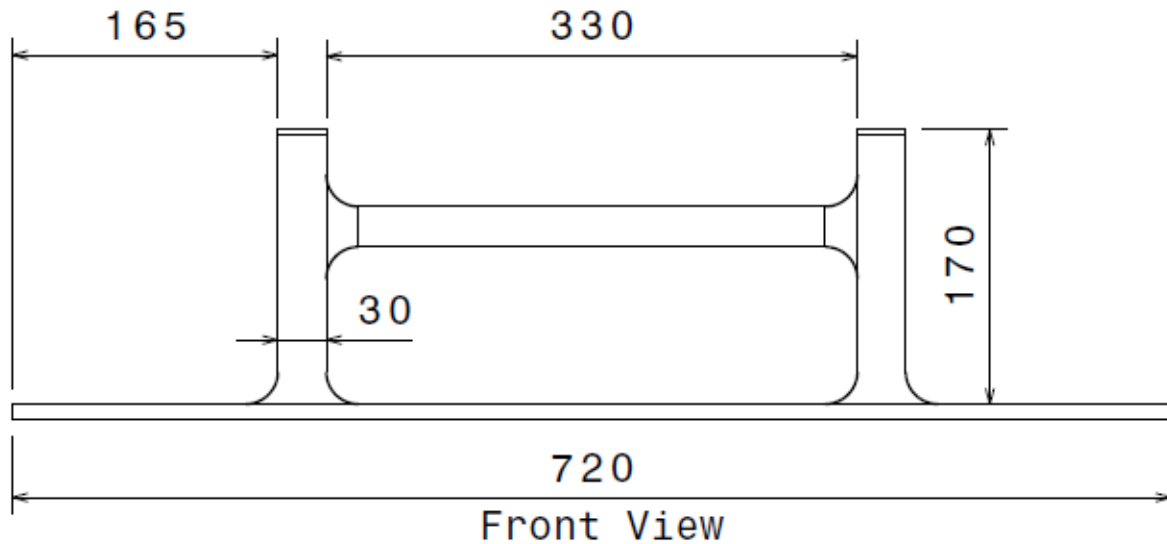


Figure 4.25. Nozzle plate and stiffeners front view final design.

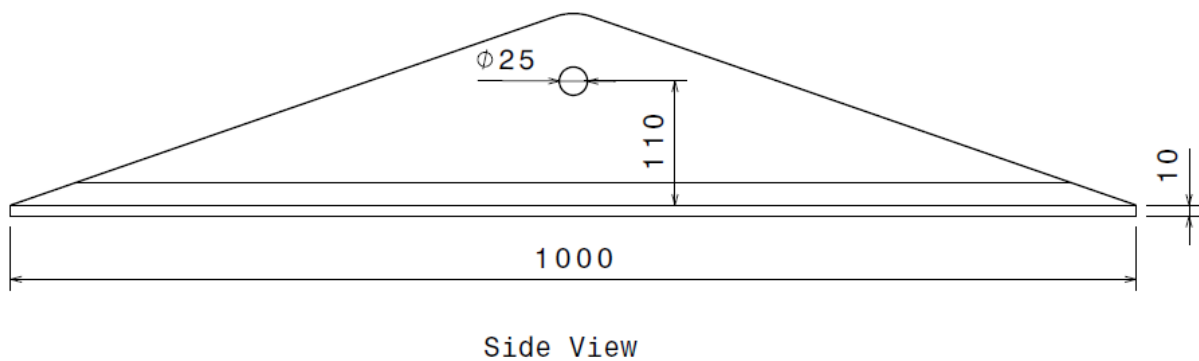
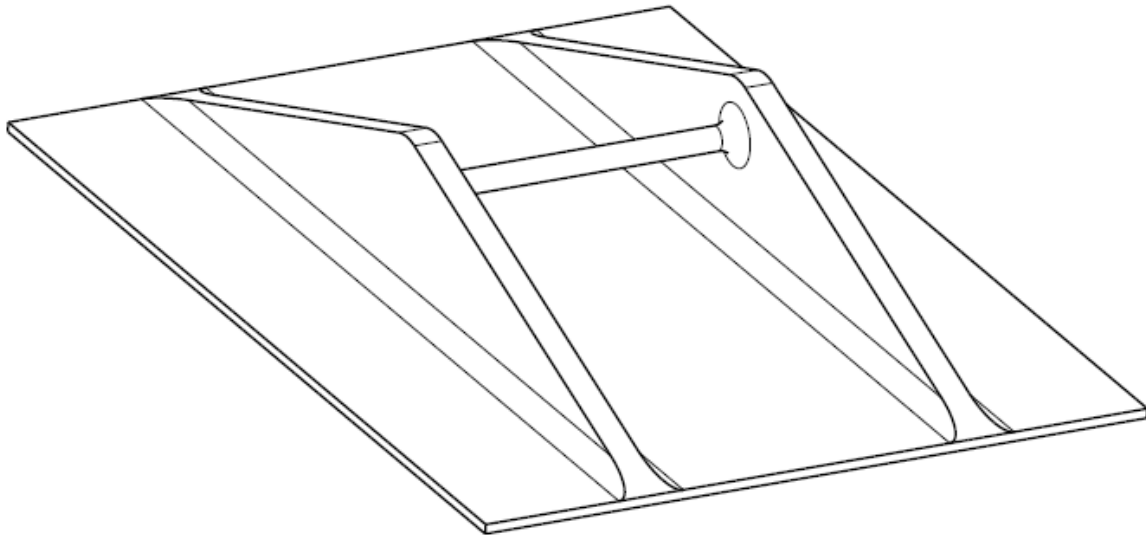


Figure 4.26. Nozzle plate and stiffeners side view final design.



Isometric View

Figure 4.27. Nozzle plate and stiffeners isometric view final design.

In this configuration, everything besides the driven dimensions of the nozzle (length and width) were modified to decrease the resultant moments of inertia and reduce the overall weight and cost of the components. This configuration yields the following main moments of inertia and cross-sectional area:

- $I_y = 7.178e^8 \text{ mm}^4$
- $I_z = 8.27e^7 \text{ mm}^4$
- $A = 0.026 \text{ m}^2$

This resultant moment of inertia is still way above the previous minimum, and the resultant maximum stress is now about 2.1 MPa. This means that the nozzle should be fully capable of withstanding higher-pressure loads related to flying at higher speeds while minimizing the overall weight.

4.3.2. 3D CFD, Structural Analysis & Pressure and Temperature Loads Design Optimization

In conjunction with all the previous design analysis and in order to compare and validate the results, a 3D structural analysis will be performed utilizing *ANSYS Static Structural*. In addition, and prior to obtaining structural loads and deformations, a 3D CFD analysis will be performed utilizing the *ANSYS Fluent* solver in order to obtain the desired pressure distribution under the nozzle plate and validate it with the previous 2D analysis by employing the resultant total pressure and temperature from the engine cycle analysis.

The first operation of the complete conjunction analysis is to define the fluid domain to properly perform the CFD. This domain needs to have the shape and exact dimension as the defined nozzle region

where the jet exhaust is present (length, width, exit area, entry area, and convergence angle). This is done in *ANSYS Design Modeler*, and the resultant domain is seen in figure 4.28. As it is seen, this case represents the nozzle configuration without afterburner use. It's important to note that the model was extruded up to the symmetry line of the nozzle in order to save memory and computational power

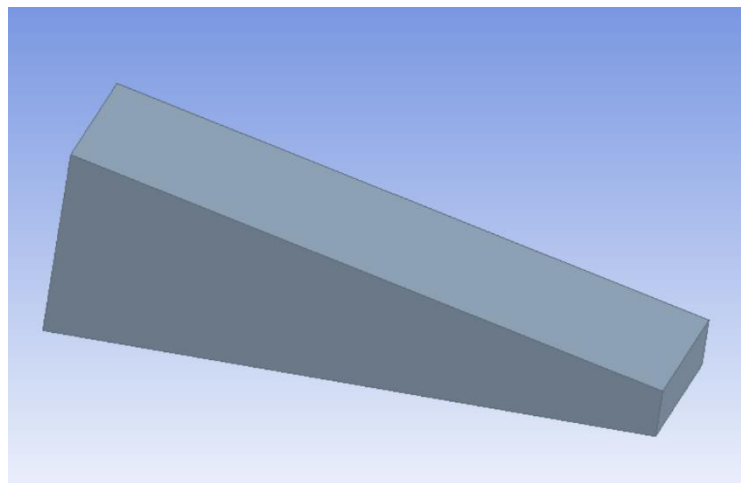


Figure 4.28. Nozzle fluid domain definition in ANSYS DM.

by only simulating the behavior of one of the sides and then applying a symmetry condition to completely visualize the nozzle's interior behavior. This fluid domain is then meshed with elements of 0.005m of size yielding a very high minimum orthogonal element quality (0.97) and over 1 million total elements.

With the fluid domain properly defined and meshed, the Fluent solver can be used to obtain the resultant velocity, temperature, and pressure distributions along the nozzle's length. For this purpose,

models need to be defined that closely resemble the fluid's behavior under these conditions and are also comparable to the previous 2D calculations. Thus, the energy model is used together with the inviscid viscous model. For the purpose of comparing the results, the inviscid model neglects all viscous effects of the jet exhaust flow along the nozzles bounding walls. Although in reality viscosity does have an effect, it is neglected for this analysis for comparative reasons, as mentioned. Finally, boundary conditions are chosen for all boundaries of the domain:

- **Inlet:** the inlet is a velocity inlet where the flow of the exhaust gases is given by the resultant velocity at this point along the nozzle, obtained using the defined sub-sonic area ratio from eq (67) and NASA's tables. Additionally, the total pressure is input as well as the static temperature, both obtained from the engine cycle analysis.
- **Outlet:** the outlet is assumed as a pressure outlet and the gauge (static) pressure at this point is inputted as well as the total backflow temperature, both obtained from the engine cycle analysis and area ratio and Mach number relationships.
- **Nozzle Walls:** the nozzle walls are initialized as walls; this implies that they are not movable and in the case for viscous flows these are selected to have the "No Slip" condition. Flow adjacent to the walls develop a boundary layer that goes from 0 speed to flow speed in this case.
- **Interior Fluid:** the interior fluid refers to the moving jet flow. In this case, the fluid is selected as air with an Ideal-Gas compressibility condition in order to capture its expansion along the nozzle. Additionally, the specific heat at constant pressure (C_p) is changed to a constant value of 1170 J/kg-k in order to have the same value as the engine cycle analysis assumption.
- **Symmetry:** the symmetrical face was initialized as a symmetry boundary. This allows for later visualization of the results.

With the boundary conditions properly defined, initialization of the computation is done from the inlet, and the solver is then able to perform the simulation. A total of 300 iterations were inputted, however the results converged after just 31 iterations. Figures 4.29 through 4.31 show both the contours and plots of the static temperature, pressure, and Mach number along the nozzle's length.

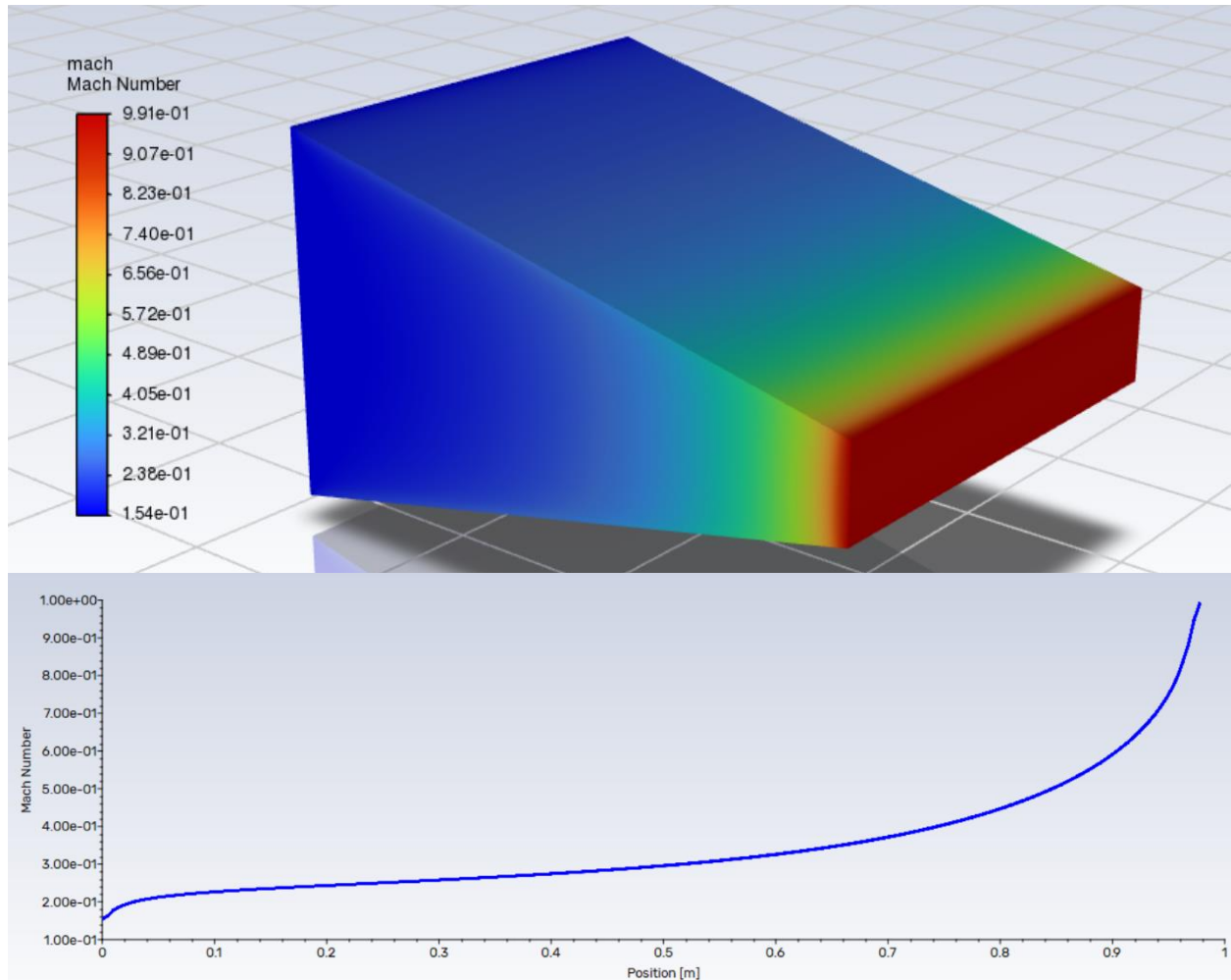


Figure 4.29. Nozzle flow simulation results of (top) Mach number contours and (bottom) Mach number plot along the length.

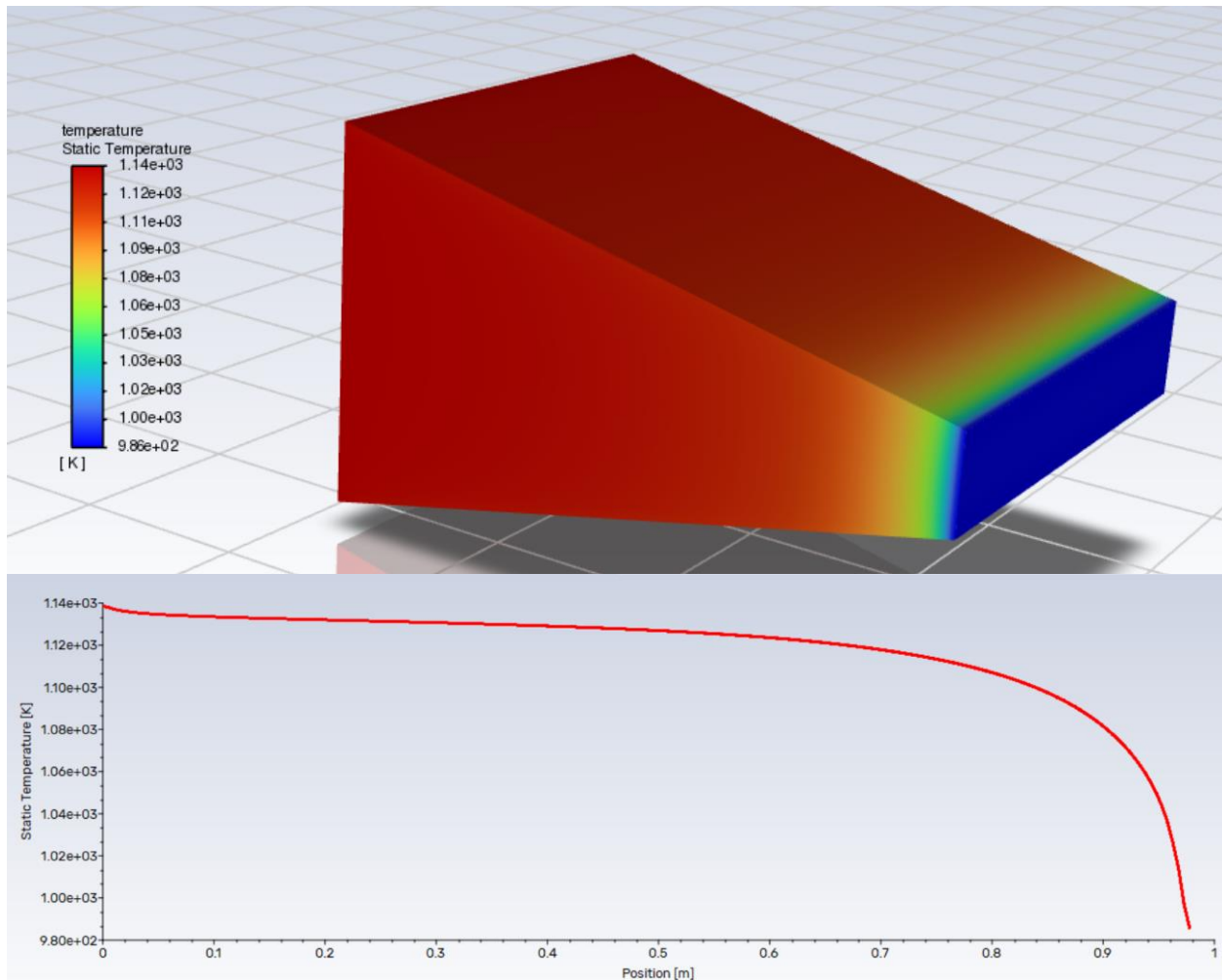


Figure 4.30. Nozzle flow simulation results of (top) static temperature contours and (bottom) static temperature plot along the length.

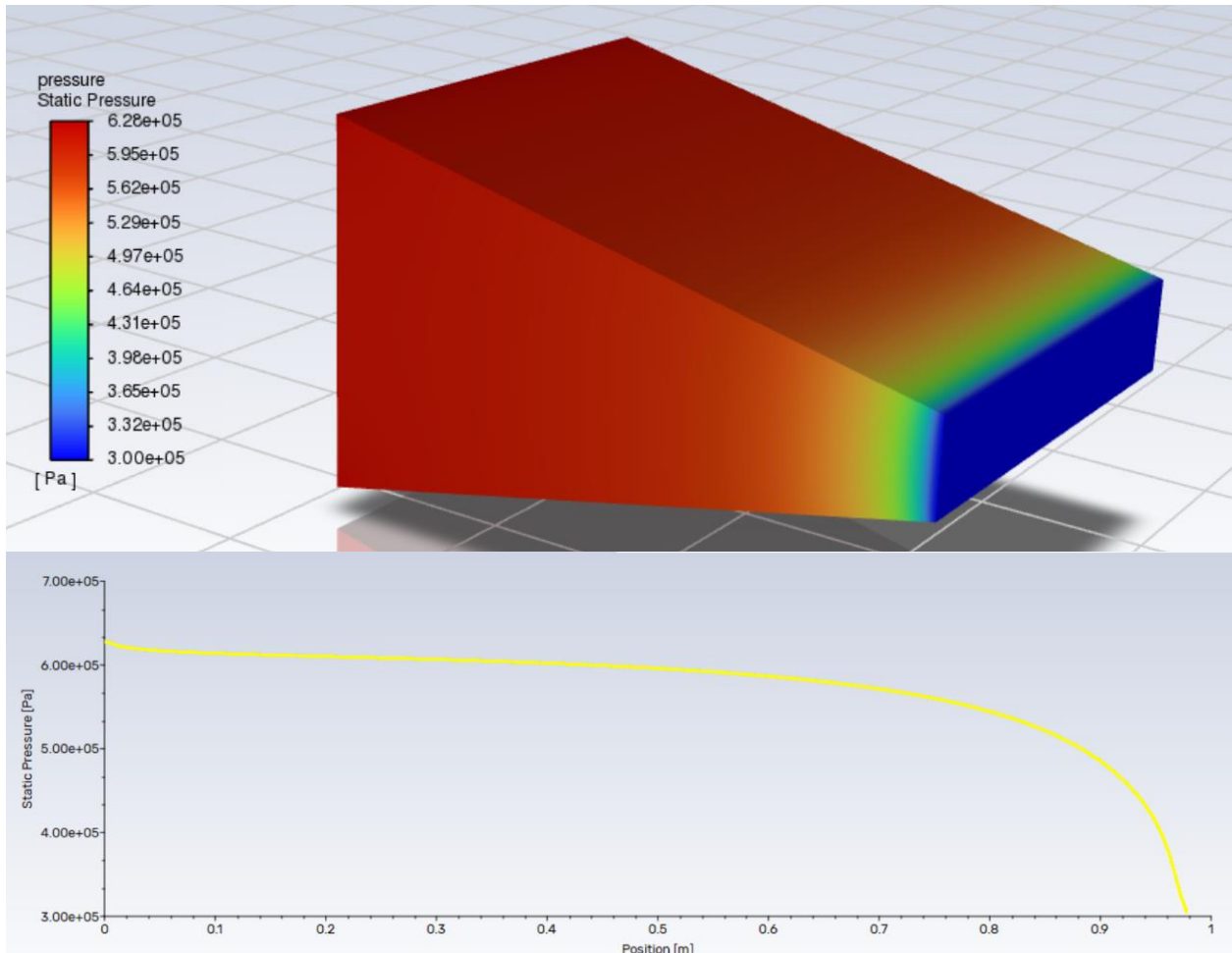


Figure 4.31. Nozzle flow simulation results of (top) static pressure contours and (bottom) static pressure plot along the length.

The resultant distributions are clearly very similar to the ones expected from an expanding flow of jet exhaust through a nozzle and the ones obtained from the cycle analysis and area-ratios (figure 4.14). In this case, the afterburner is not considered, thus the total magnitude of the static temperature is lower, however all three distributions behave as expected. Although it's important to note that all 3 computations do not quite reach the end of the nozzle (position 1m). This might also be the reason why the maximum Mach number reached, shown in figure 4.29, only reaches a value just below 1 (0.991). Nevertheless, these output distributions will serve as inputs for the structural analysis. Additionally, the resultant pressure force obtain is 381.634 kN, which is roughly a 3.5% difference with the calculated value by hand.

For the Static Structural solver, the nozzle plate and stiffener configuration are imported as modeled geometry. Similarly to the CFD simulation, this geometry is then meshed with the same element size (0.005m), yielding a total of 96320 elements with a minimum element quality of 0.14. A material is selected for the complete body, in this case it is Silicon Carbide which was previously defined as a User-Defined Material by using the same properties as the 2D analysis. Then the supports are defined, taking the origin of the nozzle as a fixed support as well as the connecting rod between the stiffeners. This resembles the static equilibrium conditions of the nozzle and actuator-linkage configuration (figure 4.32). Finally, the loads from the CFD solution are properly imported into the lower surface of the nozzle plate (figure 4.33). It's important to note that the temperature loads were input manually as the nozzle is assumed to be refrigerated by cooling secondary airflow through the inside

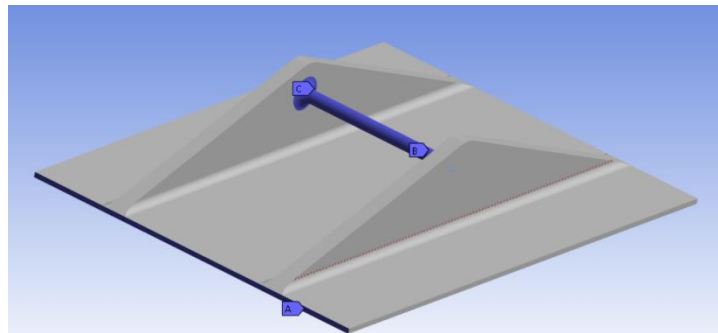


Figure 4.32. Nozzle plate and stiffener configuration with fixed supports definition.

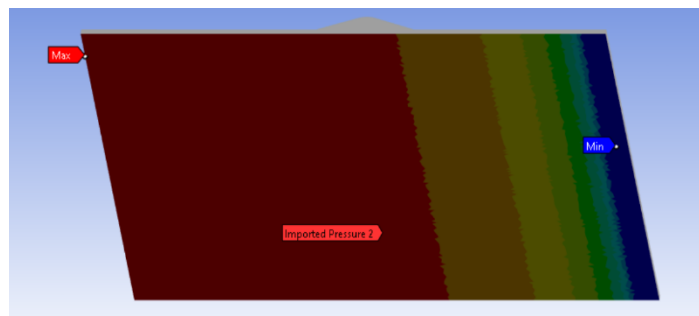


Figure 4.33. Nozzle plate imported pressure

of the nozzle and another ambient flow intake over the nozzle. Thus, the resultant body temperature was assumed to be 800°C. However, this does not result in suitable stress distribution as it's only affected by temperature gradients. Thus, the resultant distribution only represents the pressure loads and the material properties at this temperature. In addition, ambient pressure loads were neglected; these loads mitigate some of the jet exhaust loads on the plate. With everything properly defined, the simulation is able to solve stresses and deformations in all directions. The following figures show the results:

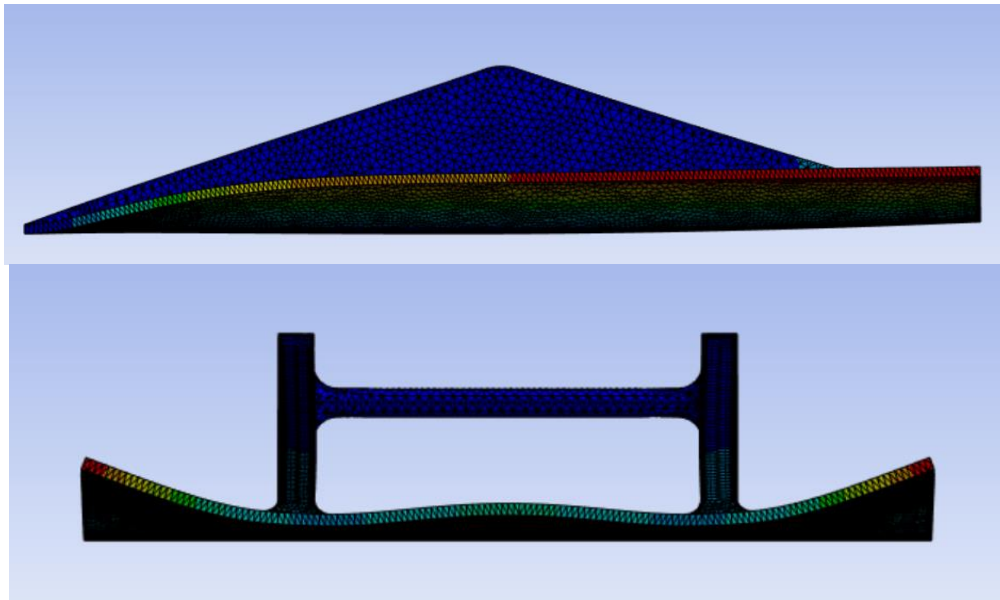


Figure 4.34. Nozzle plate resultant total deformation side (top) and front (bottom) views.

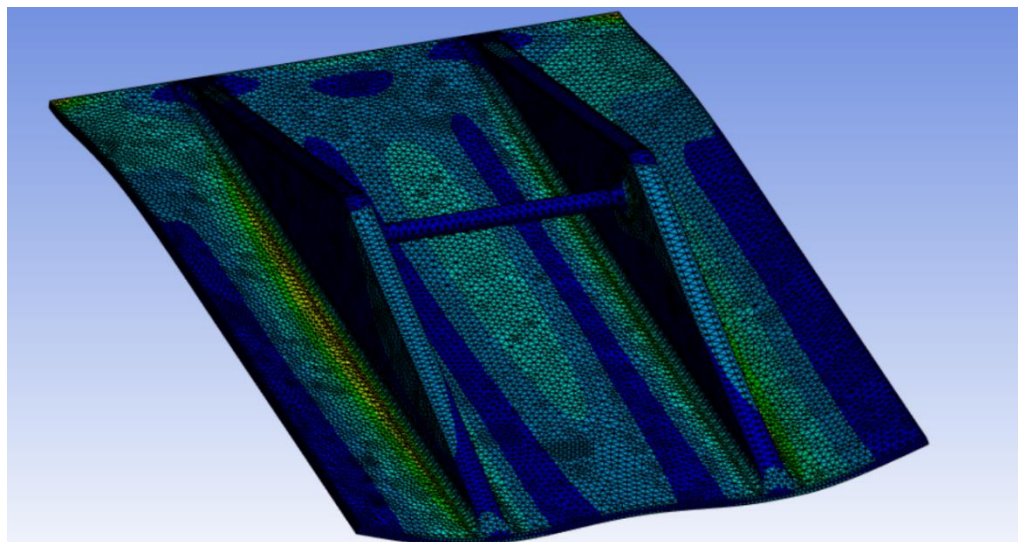


Figure 4.35. Nozzle plate resultant total stress (Von-Misses) isometric view.

As it is shown in figure 4.34, under these pressure loads, the nozzle deflects a maximum of 1.62mm at the edges of the side of the plate where the effect of the stiffeners is reduced. There is also a significant deflection around the middle of the plate, although not as high. Then, figure 4.35 shows the stress distribution of the nozzle plate. The average value of stress lies in 72.62 MPa. This is significantly higher than the 2D equivalent stress calculated and it is attributed to the three-dimensional distribution of the pressure loads in conjunction with the temperature driven stress. However, it is still lower than the 1.5 safety factor defined for Silicon Carbide. Arguably, because this is a military application, the safety factor may be lower than the one used in regular commercial aviation.

Furthermore, it's also important to study the stress concentration that happens around the connection between the rod and the stiffener and the stiffener and the plate, as shown in figure 4.36.

At these locations, stress concentrates up to a value of 510.91 MPa (SF = 1.0765) which is still lower than the defined strength for Silicon Carbide and yields the following stress concentration factor in relation with the average stress results:

$$K_t = \frac{\sigma_{max}}{\sigma_{ave}} = \frac{510.91 \text{ MPa}}{72.62 \text{ MPa}} = 7.035$$

This concentration factor is lower than what would be obtained if no fillets were used at this connection. In order to lower this value, additional thickness and roundness can be used at this location. However, another option is to use a different, stronger material for the rod and its connections with the stiffener in order to maintain a higher safety factor.

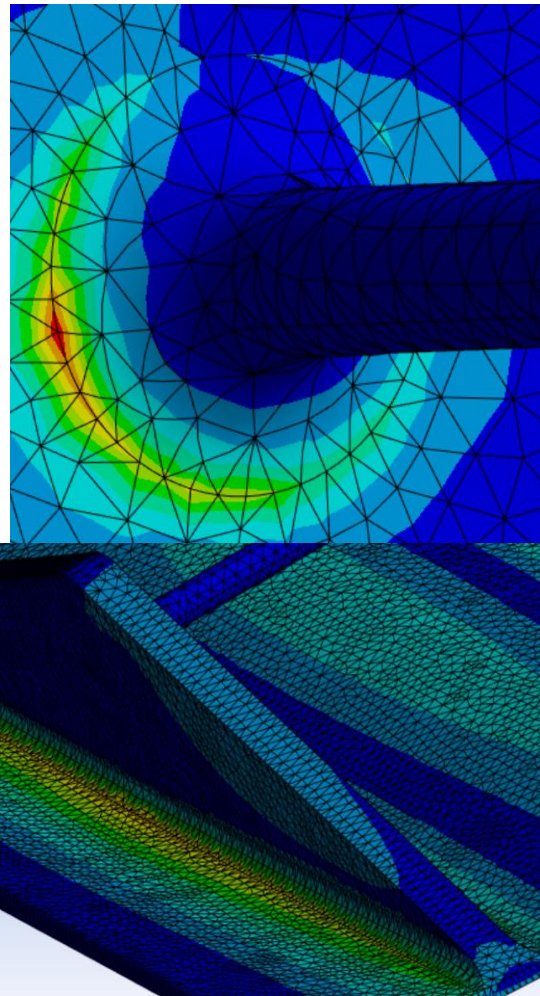


Figure 4.36. Nozzle plate resultant stress concentration around rod and stiffeners.

4.3.3. Derivation of Actuator Requirements & Preliminary Selection

Now that the overall design has been defined, the actuator force can be derived. Recalling equation (72), the actuator force in relation with the bell crank linkage is defined:

$$P_{in} = P_{out} \frac{V}{H} \rightarrow \frac{P_{out}}{P_{in}} = \frac{H}{V}$$

The ratio between the forces is known as the *Mechanical Advantage* of the system. In this case, an important assumption is made; the input and output forces act perpendicular to the direction axis of both sides of the bell crank. As shown in figure 4.37, which shows a diagram of an arbitrary bell-crank link with the defined assumption. In order for the actuator to always act perpendicular to the link, it has to mount in a pivoted support that allows it to rotate as the arm pushes or pulls from the link.

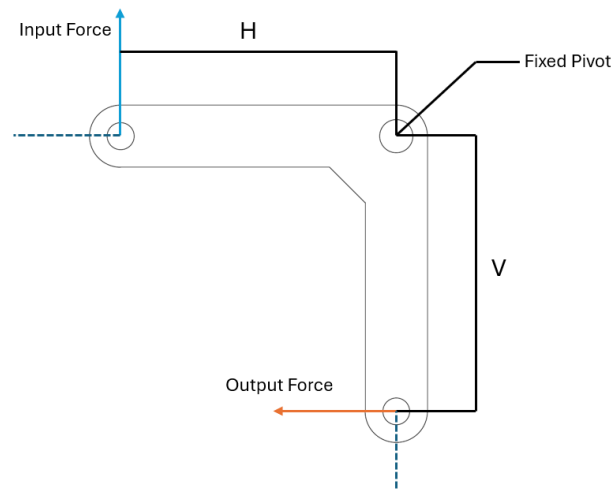


Figure 4.37. General diagram of an arbitrary bell crank link.

As the diagram in figure 4.38 shows, by taking moments from point A, the relationship between the output force and the pressure forces inside the nozzle can be derived:

$$M_A = 0 = F_p \cdot 0.45L - P_{out} \cdot h \rightarrow P_{out} = F_p \frac{0.45L}{h}$$

Replacing the output force with the input force:

$$P_{in} = F_p \frac{0.45L}{h} \frac{V}{H} \tag{76}$$

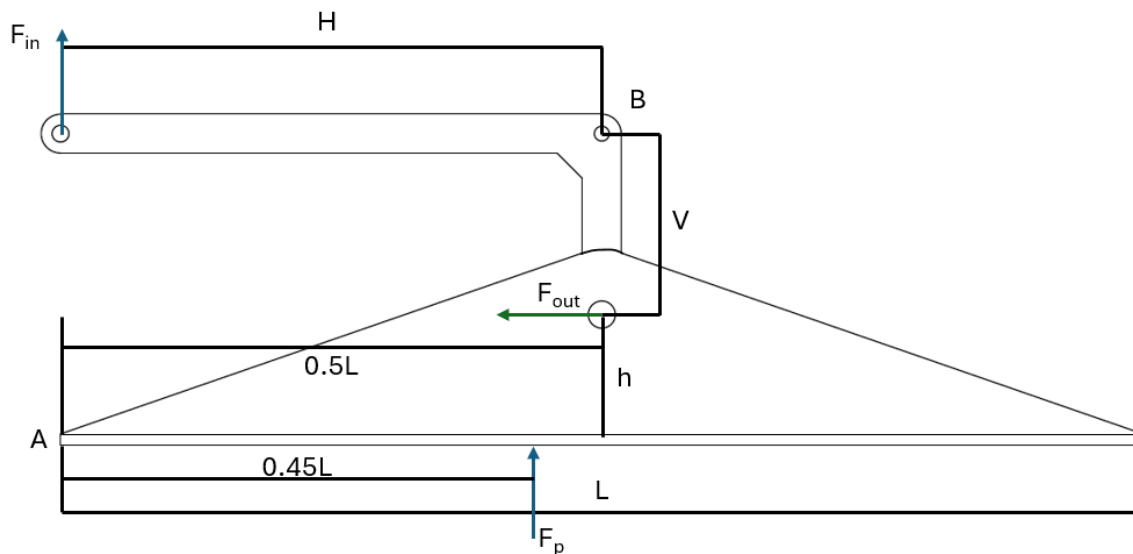


Figure 4.38. Force diagram of nozzle plate and bell crank linkage.

Where V and H are the lengths of the bell crank and h is the perpendicular distance of the bell crank output force (rod connection on the stiffeners) to point A which is the pivoted support of the nozzle with the rest of the engine. By analyzing equation (76), it is clear that there is an inverse relationship between the height of the rod and the vertical length of the bell crank. As the height decreases, the bell crank must be made longer. This has a resultant effect on both the actuator input force and the overall bending moment at A , and therefore affects the bending moment. Because the pressure forces, the height of the rod, and the length of the nozzle have already been defined, the only 2 parameters to play with are the lengths of the bell crank. In this case, clearly the horizontal length must be made longer than the vertical length in order to amplify the force, however this force amplification will result in increased moment at A , thus optimization of the bell crank design and height of the connection should be considered as further work to obtain a suitable actuator force without drastically increasing the bending moment experienced by the plate.

With that being said, for this case, the H and V dimensions of the bell crank were defined as 500mm and 110mm, respectively and the h value is 110mm. This yields a mechanical advantage of about 4.54. The diagram shown in figure 4.38, the plate is shown without its convergence angle. This angle needs to be considered for both cases studied in order to obtain the force components and their perpendicular distance to point A . The following table shows the resultant actuator input and output forces

considering the convergence angles for the Sea Level Static Case and the estimated pressure forces on the plate (368.7 kN).

Table 4.2. Resultant Actuator Output & Input Forces for the Different Nozzle Convergence Angles

Convergence Angle	Actuator Output Force	Actuator Input Force
$\Theta = 0^\circ$	1508.318 kN	331.83 kN
Dry Case: $\Theta = 12.13^\circ$	1474.8 kN	324.456 kN
Wet Case: $\Theta = 9.27^\circ$	1474.8 kN	324.456 kN

The calculations show that for both convergence angles, the resultant actuator forces are the same. This is due to the small angle difference between the two cases. In reality, because a total pressure loss due to afterburner combustion is assumed, the overall static pressure distribution for the wet case will be lower, thus lowering the required actuator force. Additionally, it is also seen that the actuator force when the plate has no rotation angle is higher than with the convergence angle.

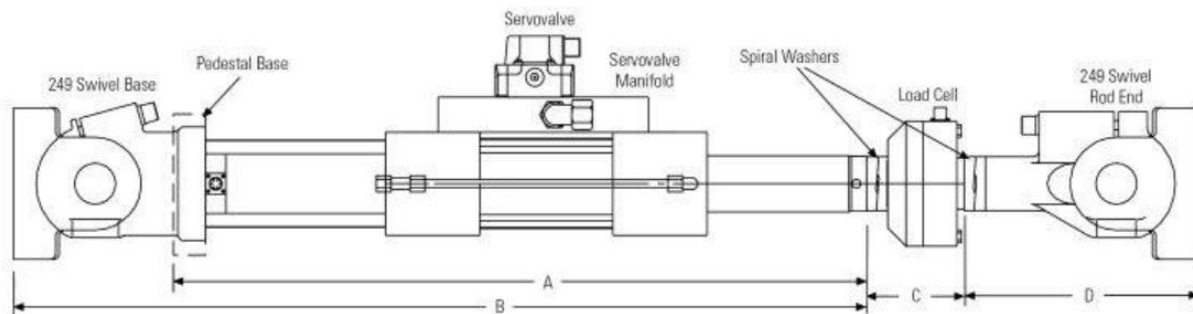
Thus, the actuator required for this specific application and configuration needs to be able to handle more than 33 tons of force during operation, operate under relatively high temperature conditions, and provide reliable performance over many cycles. For this purpose, it is clear that a hydraulic actuator is required and be integrated within the aircraft's hydraulic system. Hydraulic actuators are capable of providing enormous amounts of force while still weighing relatively little by the use of pistons and fluids.

For this purpose, a quick web search was performed to identify actuators capable of these requirements. The *MTS DuraGlide* brand was chosen due to its well-known performance and compliance with this case's requirements. Inside the brand either the 201 model or 244 can serve this purpose. In this case, the 244.41 model was chosen based on its improved reliability and cycle life. This actuator is able to produce more force than the required (500 kN) for this application and can be used in a pinned support configuration as it is required to reduce its overall stress and align itself with the line of action of the

bell-crank link (MTS) [16]. The following figures, all obtained from MTS website, show images of the actuator, as well as a list of the different 244 models and their characteristics.



Figure 4.39. MTS DuraGlide 244 hydraulic actuator picture (MTS) [16].



MODELO	TASA DE FUERZA kN	TASA DE FUERZA LBS.	ROSCA DE VARILLA (MÉTRICA)	ROSCAS DE VARILLA (USUARIO DE EE. UU.)
244.11	15	3300	M12x1.25	1/2"-20
244.12	25	5500	M12x1.25	1/2"-20
244.21	50	11000	M27x2	1"-14
244.2	67	15000	M27x2	1"-14
244.22	100	22000	M27x2	1"-14
244.23	150	35000	M27x2	1"-14
244.31	250	55000	M36x2	1 1/2"-12
244.41	500	110000	M52x2	2"-12
244.51	1000	220000	M76x2	3"-12

Figure 4.40. MTS DuraGlide 244 drawing (top) and specifications sheet (bottom)

(MTS) [16].

5. CONCLUSIONS & FUTURE WORKS

5.1. Conclusions

In general, a successful preliminary nozzle design was defined considering the selected trapezoidal shape and rectangular cross-sectional area, and justified considering the pressure forces that act on the nozzle by the jet flow exhaust that were derived from the engine thermodynamic cycle analysis.

Although many simplifications and assumptions were necessary to keep this project under a realistically doable scope of an Aerospace Engineering Bachelor's Degree, the engine model was defined following the same equations developed through the Propulsion System's and Thermodynamics courses. This model engine was then defined in a Python script which allowed for the iteration of the results as a function of altitude and flight speed by the use of object-oriented programming. The performance results show congruence with the available reference engine data (RB199 Sea Level Static performance) by considering the many simplifications and assumptions that had to be done, although it is very likely that considering 3-dimensional flow losses, the resultant performance would be even more accurate to reality (Thrust and TSFC values).

Additionally, the resultant altitude and flights speed performance loss was successfully modeled and the results, although most not completely accurate due to their exponential complexity and defined assumptions, clearly show expected behavior; where the Thrust, TSFC, and Exit Area increase significantly with afterburner use, and the Thrust decreases with increase flight speed and altitude and thus the fuel consumption increases inversely proportional to the decrease in thrust. Thus, valid for this project's scope.

Following the cycle analysis, a general variable geometry converging nozzle was selected by considering the same configuration as the reference engine. Although not optimal for supersonic flight, it was concluded that the reference engine made use of variable intake ramps in order to sustain supersonic flight even at low altitudes while still using a converging only nozzle. Following this initial definition, the nozzle geometrical shape was defined as a trapezoid with a rectangular cross-section in order to

maintain simplicity of calculations. This also allowed for a derivation a simple equation for the cross-sectional area of the nozzle along its length. By assuming the nozzle intake area and with the use of the cycle analysis resultant exit area and total temperature and pressures, the nozzle expansion behavior was successfully modeled for the Sea Level Static condition, and a structural analysis, including 2D force and moment distributions, were performed to validate the initial design.

This then allowed for the 3D CFD flow simulation which was then used to predict the overall stress and deformation where the importance of optimization iterations was a clear conclusion to avoid over-engineering of the structure, as well as to take design considerations for the concentration of stress between edges, holes, and connections.

Additionally, the importance of thermal stress and proper material selection for sustaining both pressure and temperature loads while not losing mechanical properties with high temperatures was a clear conclusion drawn from this section. For this case, Silicon Carbide composite material was selected due to its high corrosion resistance, high strength capabilities, low thermal expansion, high melting point, lack of mechanical properties loss at high temperatures, and low weight compared with other materials suited for this application.

Finally, actuator requirements were driven by designing and dimensioning the bell-crank linkage system considering the previously defined nozzle mechanical and structural configuration, where it was concluded that a hydraulic actuator was required to maintain the nozzle plate in equilibrium. The MTS *DuraGlide* 244.41 hydraulic actuator was chosen for this application based on its performance over operating cycles and force rating.

5.2. Future Works

This project contemplates a comprehensive analysis and preliminary design of a variable exhaust area propelling nozzle under the scope of an Aerospace Engineering Bachelor's Degree. It serves as a sufficiently good start to the design solution proposed; however, it can be further developed in many different ways to continue with the design and its overall implementation while also being of a much higher fidelity. These are just some of the many different aspects that can be considered to make this project even more effective:

- **Higher fidelity engine model for cycle analysis:** very little data from engine manufacturer was available, thus many assumptions had to be made. By considering significant data such as compressor pressure limitations, compressor map, turbine map, max fuel flow rate, afterburner combustion temperature, etc., an even more accurate engine model could be used to obtain more accurate results. Additionally, considering the real change of specific heat (and specific heat ratio) with temperature, the flow could be modeled more accurately.
- **Optimization of 3D nozzle shape:** a parametric study could be performed to analyze the best design solution for different conditions and mission profiles. Additionally, considering 3-Dimensional flow losses would also make this optimization of a higher fidelity.
- **Advanced 3D flow simulations:** more sophisticated CFD analysis will yield more accurate predictions of flow behavior and therefore serve to optimize the nozzle structure. By including detailed flow losses, turbulent and transient flow models, and shockwave behavior the nozzle design could be made of an ever-higher fidelity. Additionally, the iterative engine cycle analysis results could be introduced to study the flow through all the considered flight speeds and altitudes, these pressure and thermal distributions are later used to study the stress distribution of the nozzle though all the flight conditions.
- **Thermal stress analysis:** performing a detailed thermal analysis including the study of thermal distribution, stress due to thermal gradients, and refrigeration effects would definitely be an important and required addition to this design.
- **Enhanced structural analysis:** the study of dynamic loads, vibrations, fluctuating pressure, fatigue analysis, and g-loads derived stress is also an important addition that is required for a proper nozzle design and integration.
- **Optimization of nozzle structure and linkage system:** optimization of nozzle structural and mechanical design is important in order to save weight while maintaining deformation and stresses under control. Additional analysis and optimization of bell-crank design can enable this as well as including redundancies in the system such as multiple actuators in order to reduce their overall load.

- **Nozzle-Actuator kinematic analysis:** an in-depth kinematic analysis of the nozzle movement to provide the increased exit area during afterburner operation is an important addition to this project that is required in order to obtain actuator displacement, response times, nozzle plate rotation speed, and optimize the system to avoid losses and minimize stress.
- **Control system design:** a control system algorithmic design is a crucial requirement for such a project in order to control the exit area variation through fly-by-wire type systems with the use of pressure and fuel mass flow sensors. Additionally, by studying and implementing all the engine flight conditions through increased altitude and speed, the control system can be designed to work through the complete flight envelope of the aircraft.

REFERENCES

- [1] Rolls Royce plc. (1986). Afterburning. In The Jet Engine (5th ed., pp. 169–179). essay, The Technical Publications Department.
- [2] Elliott, C., & Goodwin, J. (2001). Fast jets: The history of reheat development at Derby. Rolls-Royce Heritage Trust.
- [3] Bohanon, H. R., & Wilcox, E. C. (1947). Theoretical investigation of thrust augmentation of turbojet engines by tail-pipe burning. National Advisory Committee for Aeronautics.
- [4] Nimbus227. (2022). Turbo Union RB199 turbofan engine on display at the Royal Air Force Museum Hendon. Wikipedia. Retrieved April 4, 2024, from https://en.wikipedia.org/wiki/Turbo-Union_RB199#/media/File:RB199_RAF_Museum_Hendon.jpg.
- [5] MOD, C. M. J. (2022). A IX(B) Tornado GR4 training for deployment to Afghanistan. Wikipedia. Retrieved April 2024, from https://en.wikipedia.org/wiki/Panavia_Tornado#/media/File:RAF_Tornado_GR4_MOD_4515523_3.jpg.
- [6] RB199 | rolls-royce. (n.d.). <https://www.rolls-royce.com/products-and-services/defence/aerospace/combat-jets/rb199.aspx>
- [7] RB199. MTU Aero Engines. (n.d.). <https://www.mtu.de/engines/military-aircraft-engines/fighter-aircraft/rb199/>
- [8] NASA. (n.d.). Inlet performance. NASA. <https://www.grc.nasa.gov/www/k-12/BGP/inleth.html>
- [9] ISO. (1975). International Standard Atmosphere: ISO 2533. International Organization for Standardization.
- [10] Libretexts. (2022, January 14). 2.3.3: Isa Equations. Engineering LibreTexts. https://eng.libretexts.org/Bookshelves/Aerospace_Engineering/Fundamentals_of_Aerospace_E

[ngineering \(Arnedo\)/02%3A Generalities/2.03%3A Standard atmosphere/2.3.03%3A ISA equations](#)

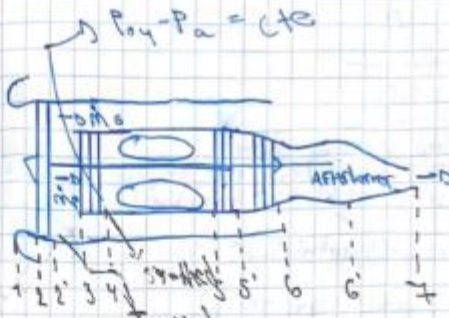
- [11] Stitt, L. E. (1990). Exhaust nozzles for propulsion systems with emphasis on supersonic cruise aircraft. National Aeronautics and Space Administration, Office of Management, Scientific and Technical Information Division.
- [12] Mattingly, J. D., Heiser, W. H., & Pratt, D. T. (2002). Aircraft Engine Design (2nd edition). American Institute of Aeronautics and Astronautics.
- [13] Gamble, E., Terrell, D., & DeFrancesco, R. (2004). Nozzle Selection and Design Criteria. In Joint Propulsion Conferences. 40th AIAA/ASME/SAE/ASEE Joint Propulsion Conference and Exhibit. doi:10.2514/6.2004-3923.
- [14] Equations, tables, and charts for compressible flow. (1953).. NACA.
- [15] Silicon carbide material properties. Imetra, Inc. (2020, June 10). <https://www.imetra.com/silicon-carbide-material-properties/>
- [16] Duraglide 244 Hydraulic Actuators. MTS. (n.d.). <https://www.mts.com/la/products/test-system-components/actuators-servo-valves/series-244-hydraulic-actuators>
- [17] F. El-Sayed, A. (2016). Fundamentals of aircraft and Rocket Propulsion. Springer London.

APPENDICES

APPENDIX 1: Engine Cycle Hand Calculations, Derivation of Equations, and Notes:

Example:

- OPR = 23.5; $\gamma_{air} = 1.2$
- TIT = 1,600K
- BPR = 1.2
- $\dot{m}_a = 70 \text{ kg/s}$
- MSL conditions
- $T_a = 15^\circ\text{C}$
- $P_a = 101,325 \text{ Pa}$



- $M=0$
- Fan driven by LP T $\dot{m}_f = 0.719 \text{ kg/s}$ $L = 44 \text{ MJ/kg}$
- HPC driven by HPT
- Converging Nozzle: $\dot{m}_{f,ab} = 4 \text{ kg/s}$
- AB T. = 1,800K
- $r = 0.2886 \text{ m}$

Calculate Thrust and exit Area with and without AB

$P_a = P_{01} \rightarrow T_a = T_{01} \rightarrow$ No RAM effect $\rightarrow 0.585 \text{ m}^2$

$\dot{m}_a = \rho A V$

$\dot{V}_a = \frac{\dot{m}_a}{\rho} = 97.68 \text{ m}^3/\text{s}$

$\frac{P_{01}}{P_{02}} = 1.2 \rightarrow P_{02} = 127.594 \text{ Pa} = P_{03}$

$BPR = 1.2 = \frac{\dot{m}_s}{\dot{m}_p} \rightarrow \dot{m}_a = \dot{m}_s + \dot{m}_p$

$\frac{\dot{m}_a}{\dot{m}_p} = BPR + 1$

$\dot{m}_p = 37.978 \text{ kg/s}$

$\dot{m}_a = 38.18 \text{ kg/s}$

$\frac{P_{01}}{P_{02}} = \left(\frac{T_{01}}{T_{02}} \right)^{\frac{\gamma}{\gamma-1}}$

$T_{02} = 288 \cdot \left(\frac{127.59 \cdot 10^3}{101325} \right)^{0.285}$

$T_{02} = 302.36 \text{ K} = T_{03}$

$\frac{P_{04}}{P_{03}} = 19.58 \rightarrow P_{04} = 2380.7322 \text{ Pa} = P_{05}$

$19.58 = \left(\frac{T_{04}}{302.36} \right)^{0.285} \rightarrow T_{04} = 709.15 \text{ K} = T_{04}$

\rightarrow Combustion @ Cte P

Combustion:

$$\dot{m}_p \cdot L = C_p (\dot{m}_p + \dot{m}_a) (T_{05} - T_{04}) \quad \checkmark \quad F =$$

$$\hookrightarrow C_{p,air} = C_{p,air}$$

$$0.719 \cdot 44 \cdot 10^6 = 1005 \cdot 32.837 (T_{05} - 708.15)$$

$\hookrightarrow T_{05} = 1675.62 \text{ K}$ \rightarrow pretty on spot with assumed value
 \rightarrow ITT

Cooling Eq: HPT \rightarrow HPC

$$\hookrightarrow (\dot{m}_a + \dot{m}_f) C_{p,air} (T_{05} - T_{05}') = \dot{m}_a C_{p,air} (T_{04} - T_{03})$$

$$\hookrightarrow (1 + \frac{\dot{m}_f}{\dot{m}_a}) (T_{05} - T_{05}') = T_{04} - T_{03}$$

$$\hookrightarrow T_{05} - T_{05}' = \frac{T_{04} - T_{03}}{1 + \frac{\dot{m}_f}{\dot{m}_a}}$$

$$\hookrightarrow T_{05}' = T_{05} - \frac{T_{04} - T_{03}}{1 + \frac{\dot{m}_f}{\dot{m}_a}}$$

$$T_{05}' = 1600 \text{ K} - \frac{708.15 - 302.36}{1.0225}$$

$$T_{05}' = 1,204.15 \text{ K}$$

$$\hookrightarrow P_{05}' = P_{04} \cdot \left(\frac{T_{05}'}{T_{05}} \right)^{\frac{\gamma}{\gamma-1}} = 2,380.73 \text{ kPa} \cdot \left(\frac{1,204.15}{1,600} \right)^{3.5}$$

$$P_{05}' = 880.38 \text{ kPa}$$

Cooling Eq: LPT \rightarrow Fan

$$\hookrightarrow (\dot{m}_a + \dot{m}_f) C_{p,air} (T_{05}' - T_{06}) = \dot{m}_a C_{p,air} (T_{02}' - T_{02})$$

$$\frac{\dot{m}_a + \dot{m}_f}{\dot{m}_a} (T_{05}' - T_{06}) = T_{02}' - T_{02}$$

$$\hookrightarrow T_{06} = - (T_{02}' - T_{02}) \frac{\dot{m}_a}{\dot{m}_a + \dot{m}_f} + T_{05}'$$

$$T_{06} = T_{05}' - \frac{C_{p,air} \cdot \frac{\dot{m}_a}{\dot{m}_a + \dot{m}_f}}{C_{p,air} \cdot \frac{\dot{m}_a}{\dot{m}_a + \dot{m}_f}} (T_{02}' - T_{02})$$

$$T_{06} = 1,199.5 - \frac{[303.36 - 288] \cdot 70}{32.587}$$

$$T_{06} = 1,171.45 \text{ K}$$

$$P_{06} = P_{05} = \left(\frac{T_{06}}{T_{05}} \right)^{\frac{\gamma}{\gamma-1}} = 880.38 \text{ kPa} = \left(\frac{1,171.45}{1204.15} \right)^{3.5}$$

$$P_{06} = 799.5 \text{ kPa}$$

Case (a): No Afterburner

- $P_{06} = P_{06} = P_{07} \rightarrow$ Ideal Nozzle
- $T_{06} = T_{06} = T_{07} \rightarrow$ No ab

Assuming Nozzle is choked:

- $M_e = 1$
- $\frac{P_{07}}{P_e} > 1.89$

$$\frac{T_{07}}{T_7} = 1 + \frac{\gamma-1}{2} M^2 = 1.2$$

$$\frac{P_{07}}{P_7} = \left(\frac{T_{07}}{T_7} \right)^{\frac{\gamma}{\gamma-1}} = 1.2^{3.5}$$

$$\frac{P_{07}}{P_7} = 1.893 \rightarrow P_e = 422.34 \text{ kPa}$$

Thus $P_e > P_a$

- $P_a = 101.325 \text{ kPa} < 422.34 \text{ kPa}$
- Nozzle is choked \downarrow

So:

$$T_e = \frac{T_{07}}{1 + \frac{\gamma-1}{2} M^2} = \frac{1,171.45}{1.2} = 976.2 \text{ K}$$

$$V_e = M_e \cdot a = \sqrt{\gamma R T_e} = \sqrt{1.4 \cdot 287 \cdot 976.2}$$

$$V_e = 626.28 \text{ m/s} ; \rho_e = \frac{P_e}{R T_e} = \frac{422.34 \cdot 10^3}{287 \cdot 976.2}$$

$$\rho_e = 1.507 \text{ kg/m}^3$$

$$A_e = \frac{\dot{m}_e}{\rho_e V_e} = \frac{\dot{m}_p + \dot{m}_c}{\rho_e V_e} = \frac{32.507}{1.507 \cdot 626.28}$$

$$A_e = 0.0345 \text{ m}^2$$

$$T_{\text{thrust}} = \dot{m}_3 (V_{\text{fan}} - V_0) + (P_{\text{fan}} - P_a) A_{\text{fan}} + \dot{M}_p (V_{\text{exit}} - V_0) + (P_e - P_a) A_e$$

↳ Because engine is low bypass, secondary flow thrust contribution is neglected

$$T = 37.818(626.28 - 0) + (422.34 \cdot 10^3 - 107.925) \cdot 0.0345$$

$$T = 31.002 \text{ N} \approx 31 \text{ N} \rightarrow \text{Very close to available data}$$

$$\text{TSFC} \approx 0.000232 \text{ kg/N}\cdot\text{s} = 0.0232 \text{ kg/kN}\cdot\text{s}$$

$$\text{↳ TSFC} =$$

cas (b): With afterburner

$$\text{↳ } T_{0c} < T_{0c}' \rightarrow T_{0c}' = T_{07}$$

$$\text{↳ } P_{0c} < P_{0c}' \rightarrow P_{0c}' = P_{07} \rightarrow \text{ideal Nozzle}$$

AB Combustion:

$$\dot{m}_{f,ab} \cdot L = C_p (T_{0c}' - T_{0c}) \cdot (\dot{m}_a + \dot{m}_p + \dot{m}_{f,ab})$$

$$\text{↳ } T_{0c}' = \frac{\dot{m}_{f,ab} \cdot L}{C_p (\dot{m}_a + \dot{m}_p + \dot{m}_{f,ab})} + T_{0c} = \frac{4 \cdot 44 \cdot 10^6}{1005 (37.8 + 6.774 + 4)} + 1177.45$$

$$T_{0c}' = 5966.88 \text{ K} \rightarrow \text{Too high?} \rightarrow \text{Less fuel is used...}$$

$$\frac{T_{0c}}{T_{0c}'} = 5.1 \rightarrow \text{VERY HIGH! ?}$$

$$P_{0c} \approx P_{0c}' \rightarrow \text{Combustion @ Cte P + 100\% efficient}$$

Is Nozzle choked?

↳ $M_0 = 1 \rightarrow \frac{T_0}{T} = 1.2$

↳ $\frac{P_0}{P_e} > 1.89$

↳ $P_0 > P_a$

↳ $\frac{P_0}{P_e} = (1.2)^{3.5} = 1.893 \checkmark$

↳ $P_e = 422.34 \text{ kPa}$

↳ $T_0 = 4,972.4 \text{ K}$

↳ $V_e = M \cdot a = \sqrt{1.4 \cdot 287 \cdot 4972} = 1413.47 \text{ m/s}$

↳ $\rho_e = \frac{P_e}{T_e R} = \frac{422.34 \cdot 10^3}{4972.4 \cdot 287} = 0.3 \text{ kg/m}^3$

↳ $A_e = \frac{\dot{m}_p + \dot{m}_f + \dot{m}_{sub}}{\rho_e \cdot V_e} = \frac{36.537}{0.3 \cdot 1413.47}$

↳ $A_e = 0.08616 \text{ m}^2$

$T = \dot{m}_e (V_e - V_0) + (P_e - P_a) A_e = 37.818 \cdot 1413.47 + (422.34 \cdot 10^3 - 101325) \cdot 0.08616$

$T = 72,630.5 \text{ N} \approx 72.63 \text{ kN}$

↳ Very close to available data, although bypass thrust was neglected. Could be due to the unrealistically high afterburner temperature increase...

↳ Not sure if those temperatures are accurate to reality, no liquid alloys must not exceed 1800K in order to prevent melting but the issue...

~~thrust generation of 2.34 times~~

↳ Available data suggests a thrust augmentation of almost ~~2.34~~ 4.825 times

$\frac{A_{e,ab}}{A_e} \approx 2.5$

↳ Area of nozzle exhaust 2.5 times larger with afterburner use

$\frac{V_{e,ab}}{V_e} \approx 2.25$ - Exhaust velocity is 2.25 larger with afterburner

- ↳ very similar to thrust increase ratio
- ↳ consistent with square root of afterburner temperature ratio

* Next iteration + Consider max afterburner temperature of 1800K

↳ $T_{0c} = 1800K$

AB Combustion:

$\dot{m}_{f,ab} \cdot L = (\dot{m}_p + \dot{m}_f) C_p (T_{0c} - T_{0c})$

↳ $\dot{m}_{f,ab} \cdot L = (\dot{m}_p + \dot{m}_f) C_p (T_{0c} - T_{0c})$

~~$\dot{m}_{f,ab} \cdot L = (\dot{m}_p + \dot{m}_f) C_p (T_{0c} - T_{0c})$~~

↳ $\dot{m}_{f,ab} \cdot L - [(\dot{m}_p + \dot{m}_f + \dot{m}_{f,ab}) C_p (T_{0c} - T_{0c})] = 0$

↳ $\dot{m}_{f,ab} \cdot L - [(\dot{m}_p + \dot{m}_f) C_p \Delta T + \dot{m}_{f,ab} C_p \Delta T]$

↳ $\dot{m}_{f,ab} (L - C_p \Delta T) - (\dot{m}_p + \dot{m}_f) C_p \Delta T = 0$

↳ $\dot{m}_{f,ab} = \frac{(\dot{m}_p + \dot{m}_f) C_p \Delta T}{L - C_p \Delta T} = \frac{32.537 \cdot 1005 \cdot (1800 - 1171.4)}{44 \cdot 10^6 - 1005 \cdot (1800 - 1171.4)}$

$\dot{m}_{f,ab} = 0.4779 \text{ kg/s}$ X

Calculate accurate fuel flows:

Combustion chamber:

$$\dot{m}_f \cdot L = (\dot{m}_a + \dot{m}_f) c_p (T_{05} - T_{04})$$

$$\hookrightarrow f \cdot L = (1 + f) c_p \Delta T$$

$$\hookrightarrow -f \cdot L + f c_p \Delta T + c_p \Delta T = 0$$

$$0 = f (c_p \Delta T - L) + c_p \Delta T = 891.85$$

$$\hookrightarrow f = \frac{-c_p \Delta T}{c_p \Delta T - L} = \frac{-1005 \cdot (1600 - 706.15)}{1005 \cdot 891.85 - 44 \cdot 10^6}$$

$f = 0.02079 \rightarrow \dot{m}_f = 0.666 \text{ kg/s}$

Afterburner chamber

$$\dot{m}_{f,ab} \cdot L = c_p (T_{06} - T_{05}) (\dot{m}_a + \dot{m}_f + \dot{m}_{f,ab})$$

$$f_{ab} \cdot L = c_p \Delta T (1 + f + f_{ab})$$

$$\hookrightarrow 0 = -f_{ab} \cdot L + c_p \Delta T (1 + f) + c_p \Delta T \cdot f_{ab}$$

$$0 = f_{ab} (c_p \Delta T - L) + c_p \Delta T (1 + f)$$

$$f_{ab} = \frac{-c_p \Delta T (1 + f)}{c_p \Delta T - L} = \frac{-1005 \cdot 628.55 \cdot 1.02079}{1005 \cdot 628.55 - 44 \cdot 10^6}$$

$f_{ab} = 0.015 \rightarrow \dot{m}_{f,ab} = 0.473 \text{ kg/s}$

$$\hookrightarrow f_{ab} \cdot L = c_{p,u} (T_{BT} - T_{05}) (1 + BPR + f + f_{ab})$$

$$0 = -f_{ab} \cdot L + c_{p,u} \Delta T (1 + BPR + f + f_{ab}) \rightarrow -f_{ab} \cdot L + c_{p,u} \Delta T \cdot f_{ab} + c_{p,u} \Delta T (1 + BPR + f) = 0$$

$$0 = f_{ab} (c_{p,u} \Delta T - L) + c_{p,u} \Delta T (1 + BPR + f)$$

$$\hookrightarrow f_{ab} = \frac{-c_{p,u} \Delta T (1 + BPR + f)}{c_{p,u} \Delta T - L}$$

Considering 1800 K AB T.

↳ $T_{05} = T_{07} \rightarrow$ Choked Nozzle \rightarrow $Ma = 1$

↳ $\frac{T_{07}}{T_7} = 1.2$

↳ $\frac{P_{07}}{P_7} = 1.2^{2.5} = 1.893$

↳ $P_7 = P_0 = 422.34 \text{ kPa} \gg P_a$

↳ $T_7 = 1,500 \text{ K}$

↳ $a = V_e = \sqrt{1500 \cdot 287 \cdot 1.4} = 776.33 \text{ m/s}$

↳ $\rho_e = \frac{422.34 \cdot 10^3}{1500 \cdot 287} = 0.987 \text{ kg/m}^3$

↳ $A_e = \frac{m_a + m_f + m_{f-b}}{\rho_e V_e} = \frac{31.818 + 0.66 + 0.473}{0.987 \cdot 776.33}$

↳ $A_e = 0.0432 \text{ m}^2 \rightarrow$ Area increases by 25%

~~Final Thrust~~

$T = 31.818 \cdot (776.33 - 0) + (422.34 \cdot 10^3 - 101.325 \cdot 11^2) \cdot 0.0432$

↳ $T = 38,569.115 \approx 38.57 \text{ kN}$

↳ With the Afterburner temperature limited at 1800 K Thrust is increased by almost 25%.

↳ Final Model should consider:

- Bypass thrust
- Secondary + Primary flow mixture @ afterburner?
- Limited Afterburner temperature
- C_p hot and C_p cold
- Iterations with altitude as a function of Mach

$$A_{c, \text{crit}} = \left[c_{c, \text{fan}} \right]^{\frac{\gamma-1}{\gamma}} - 1$$

$$\frac{T_{02}}{T_{01}} - 1$$

$$\frac{T_{02}}{T_{01}} - 1 = \left[c_{c, \text{fan}} \right]^{\frac{\gamma-1}{\gamma}} - 1$$

$$T_{02} = \left[\frac{(c_{c, \text{fan}})^{\frac{\gamma-1}{\gamma}} - 1}{\eta_{\text{comp}}} + 1 \right] T_{01}$$

$$\eta_T = \frac{1 - \frac{T_{05, \text{out}}}{T_{04, \text{in}}}}{1 - \left(\frac{P_{05}}{P_{04}} \right)^{\frac{\gamma-1}{\gamma}}} \quad \eta_T = \frac{1 - \frac{T_{05, \text{out}}}{T_{04, \text{in}}}}{\eta_T}$$

$$\rightarrow \left(\frac{P_{05}}{P_{04}} \right)^{\frac{\gamma-1}{\gamma}} = \frac{1 - \frac{T_{05}}{T_{04}}}{\eta_T} - 1$$

$$\left(\frac{P_{05}}{P_{04}} \right)^{\frac{\gamma-1}{\gamma}} = \frac{\frac{T_{05}}{T_{04}} - 1}{\eta_T} + 1$$

$$\frac{P_{05}}{P_{04}} = \left[\frac{\frac{T_{05}}{T_{04}} - 1}{\eta_T} + 1 \right]^{\frac{\gamma}{\gamma-1}}$$

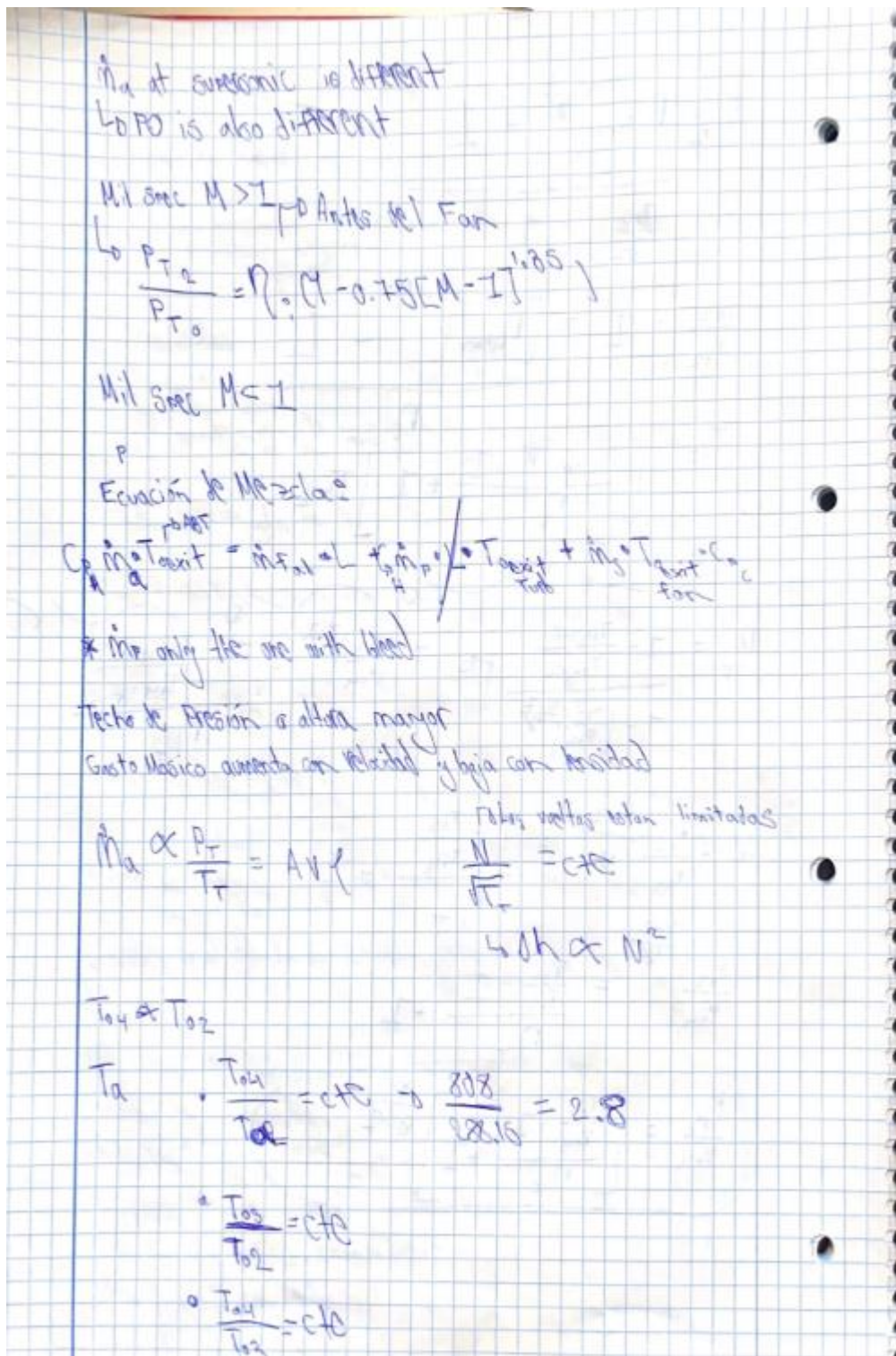


Tabla:

X
L

$\left\{ \begin{array}{l} \text{Velocidad} \\ \text{Presión} \\ \text{Temperatura Estática} \end{array} \right\}$
 distribución de presiones, temperaturas y velocidad a lo largo de la tubería

$$C_{FH} \cdot \dot{m}_a \cdot T_{04} = \dot{m}_{\text{tab}} \cdot L + C_{FH} \cdot \dot{m}_p \cdot T_{05} + \dot{m}_g \cdot C_{FG} \cdot T_{05}$$

$$\left[\frac{\text{N}}{\text{kgm}} \cdot \frac{\text{kg}}{\text{s}} \cdot \text{K} \right] = \left[\frac{\text{kg}}{\text{s}} \cdot \frac{\text{m}}{\text{kg}} \right] + \left[\frac{\text{N}}{\text{kgm}} \cdot \frac{\text{kg}}{\text{s}} \cdot \text{K} \right]$$

$\left[\frac{\text{N}}{\text{s}} \right] \quad \left[\frac{\text{N}}{\text{s}} \right] + \left[\frac{\text{N}}{\text{s}} \right]$

$$C_{FH} [\dot{m}_a + \dot{m}_g] \cdot T_{04} = \dot{m}_{\text{tab}} \cdot L + C_{FH} \cdot \dot{m}_p \cdot T_{05} + \dot{m}_g \cdot C_{FG} \cdot T_{05}$$

$$(1 + \text{BPR}) T_{04} = f_{\text{tab}} \cdot \frac{L}{C_{FH}} + T_{05} + \text{BPR} \cdot \frac{C_{FG}}{C_{FH}} \cdot T_{05}$$

$$f_{\text{tab}} = \left[(1 + \text{BPR}) T_{04} - T_{05} - \text{BPR} \cdot \frac{C_{FG}}{C_{FH}} \cdot T_{05} \right] \cdot \frac{C_{FH}}{L}$$

$$f_{\text{tab}} = \frac{(1 + \text{BPR}) T_{04} \cdot C_{FH}}{L} - \frac{T_{05} \cdot C_{FH}}{L} - \text{BPR} \cdot C_{FG} \cdot \frac{T_{05}}{L}$$

APPENDIX 2: Engine Thermodynamic Cycle Iteration Script

```
#Complete Thermodynamic Cycle Analysis of turbofan engine with and
without afterburner:

#Import working libraries:
import matplotlib.pyplot as plt
import numpy as np

#Start by setting sea level conditions:
P_MSL= 101325 #Pascals [Pa]
T_MSL= 288.15 #Kelvin [K]
D_MSL = 1.225 #[kg/m^3]

#Define Constants (idealization):
gamma = 1.4 #Specific heat ratio for air
R = 287 #Gas constant for air [J/kg*K]
g0 = 9.80665 #Standard acceleration due to gravity [m/s^2]
Cp_cold= 1005 #Specific heat at constant pressure while cold [J/kg*K]
Cp_hot = 1170 #Specific heat at constant pressure while hot [J/kg*K]
L = 44000000 #Heating value of Kerosene (J/kg)

#Define Given Data & Input Parameters:
BPR = 1.2 #Bypass Ratio of the Engine
OPR = 23.5 #Overall Pressure Ratio of the compressors (LPC + HPC)
rc_fan = 1.2 #Compression Ratio of Fan section only (assumed)
mdot_air_max = 70 #Mass flow rate of air [kg/s]
D = 0.72 #Fan Diameter [m]
TIT = 1600 # Turbine Inlet Temperature [K]
ABT = 2500 #Afterburner Temperature [K] (assumed)
altitudes = (0, 1000, 2000, 4000, 8000, 12000, 16000) #Altitude Array
in meters
Mach_numbers = np.linspace(0, 2, 50) #Array of Mach numbers for
analysis
```

```
#Some initial calculations/conversions:
mdot_p_max = (mdot_air_max/(BPR+1)) #Obtain primary mass flow of air
[kg/s]
mdot_s_max = mdot_air_max - mdot_p_max #Obtain secondary mass flow of
air [kg/s]
A_fan = np.pi*(D/2)**2 #Calculate Fan Area [m^2]
rc = OPR/rc_fan
V_MSL_M0= mdot_air_max/(A_fan*D_MSL)

#Define ISA Equations for Temperature:
def ISA_T(altitude):
    if altitude < 11000: #Function up to tropopause (11km)
        return 288.15 - 0.0065*altitude
    else:
        return 216.65 #Constant T after 11km

#Define ISA Equations for Pressure:
def ISA_P(altitude):
    if altitude < 11000: #Function up to tropopause (11km)
        return 101325 * (1 - 0.0065 * altitude / 288.15)**5.256
    else: #11km and beyond
        return 22632.06 * np.exp(-0.00015769 *(altitude-11000))

#Define ISA Equations for Density:
def ISA_D(altitude):
    if altitude < 11000: #Function up to tropopause (11km)
        return 1.225 *((1- 0.000022558*altitude)**4.2559)
    else: #11km and beyond
        return 0.3639 * np.exp(-0.00015769*(altitude-11000))

#Define Function for air mass flow rate as a function of altitude:
def mdot_air(altitude):
```

```
    if altitude == 0: #Function for MSL where mass flow rate is
maximum
        return mdot_air_max
    else: #Function based on altitude considering change in density
        mdot_air = A_fan*V_MSL_M0*ISA_D(altitude)
        return mdot_air

#Define Function to calculate speed of sound given temperature:
def speed_of_sound(T):
    return np.sqrt(R*gamma*T)

#Define Function to calculate flight speed given mach number:
def flight_speed(M,Ta):
    a = speed_of_sound(Ta)
    return a*M

#Define Functions for Ram Effect:
def RAM_T(M,T):
    T01 = (1+((gamma-1)/2)*(M**2))*T #Calculates total T (T01) based
on Mach number and ambient T (Ta)
    return T01
def RAM_P(M,P):
    P01 = ((1+((gamma-1)/2)*(M**2))**(gamma/(gamma-1)))*P #Calculates
total P (P01) based on Mach number and ambient P (Pa)
    return P01

#Define Functions for Fan Stage (2-3):
def fan(T01, P02, rc_fan):
    #Considering and ideal (100% effient) inlet, no pressure losses
    T02 = T01 #No work or heat added thus no change in total
temperature in the inlet
    P03 = P02*rc_fan #Calculates total pressure after fan from fan
compression ratio
```



```
T03 = (((rc_fan**((gamma-1)/gamma)-1)/0.82)+1)*T02 #Calculates
total temperature after fan from adiabatic efficiency of fan
return T03, P03

#Define Functions for Core Compressor Stage (3-4):
def comp(T03,P03,rc):
    P04 = P03*rc #Calculates total pressure after core compressor from
compressor ratio
    T04 = (((rc**((gamma-1)/gamma)-1)/0.82)+1)*T03 #Calculates total
temperature after core compressor from compressor efficiency
return T04, P04

#Define Functions for Combustion Stage (4-5):
def comb(T04, P04, TIT, L, mdot_p, Cp_hot):
    P05 = P04*0.95 #Combustion losses of 5%
    f = (Cp_hot*(TIT-T04))/(L-Cp_hot*(TIT-T04)) #Calculate fuel-to-air
ratio from combustion with given Turbine Inlet Temperature
    mdot_f = f*mdot_p #Calculate fuel flow rate during combustion
return P05, f, mdot_f

#Define Function For HPT (5-5`): Coupling Equation with HPC
def HPT(TIT, T04, T03, P05, Cp_hot, Cp_cold, f):
    T05_exit = TIT-(((Cp_cold/Cp_hot)*(1/(1+f)))*(T04-T03)) #Calculates
HPT outlet total temperature
    P05_exit = P05*(((T05_exit/TIT) - 1 )/0.87)+1)**(gamma/(gamma-
1))) #Calculates HPT exit pressure with turbine efficiency
return T05_exit, P05_exit

#Define Function for LPT (5'-6): Coupling equation with LPC (Fan):
def LPT(T05_exit,T03, T02, P05_exit, Cp_hot, Cp_cold, f, BPR):
    T06 = T05_exit - ((Cp_cold/Cp_hot)*((BPR+1)/(1+f))*(T03-T02))
#Calculates LPT outlet total temperature
```

```
P06 = P05_exit*(((T06/T05_exit) - 1 )/0.87)+1)**(gamma/(gamma-1))) #Calculates LPT outlet total pressure with isentropic evolution
return T06, P06

#Define exit nozzle function with no afterburner(6-7):
def nozzle(T06, P06,Pa):
    T07 = T06 #No afterburner combustion
    P07 = P06 #Ideal exit nozzle (no losses)
    #Assuming that exit nozzle is choked (Me = 1):
    Pe = P07/1.893
    EGT = T07/1.2 #Exhaust Gas Temperature calculated considering exit
Mach =1
    Ve = np.sqrt(gamma*R*EGT) #Calculate exhaust speed once EGT is
calculated considering that Mach = 1
    De = Pe/(R*EGT) #Calculates exhaust gas density with given exit
pressure and temperature

    NPR = P07/Pa #Calculates Nozzle Pressure Ratio
    return EGT, Pe, Ve, De, P07, NPR

#Define exit nozzle function WITH afterburner (6'-7):
def nozzle_ab(T06, ABT, P06, L, Cp_hot, mdot_p, f, BPR, T03, Pa):
    T07 = ABT #After combustion total temperature is constant
    P07 = P06*0.92 #Combustion losses of 8%
    #fab = (Cp_hot*(ABT-T06)*(1+BPR+f))/(L-Cp_hot*(ABT-T06))
#Calculates fuel to air mixture of afterburner considering ducted fan
mixture of air at exit nozzle
    fab = ((1+BPR)*ABT*Cp_hot/L)-(T06*Cp_hot/L)-(BPR*Cp_cold*T03/L)
    mdot_fab = mdot_p*fab
    #Assuming that exit nozzle is choked (Me = 1):
    Pe_ab = P07/1.893
    EGT_ab = T07/1.2 #Exhaust Gas Temperature calculated considering
exit Mach =1
```

```
Ve_ab = np.sqrt(gamma*R*EGT_ab) #Calculate exhaust speed once EGT
is calculated considering that Mach = 1
De_ab = Pe_ab/(R*EGT_ab) #Calculates exhaust gas density with
given exit pressure and temperature

NPR_ab = P07/Pa #Calculates Nozzle Pressure Ratio
return EGT_ab, Pe_ab, Ve_ab, De_ab, fab, mdot_fab, P07, NPR_ab

#Define Analysis Function:
def perform_analysis(altitudes, Mach_numbers):
    results = [] #Results list for later appending without afterburner
    results_ab = [] #Results list for later appending with afterburner
    cte = 0

    for altitude in altitudes: #Iterate through each defined altitude
        Ta = ISA_T(altitude)
        Pa = ISA_P(altitude)
        rho_air = ISA_D(altitude)
        mdot = mdot_air(altitude)
        mdot_p = (mdot/(BPR+1))*0.9 #10 air bleed
        mdot_s = (mdot - mdot_p) #20% bleed

        print(f"Altitude: {altitude}m, Temperature: {Ta:.2f}K,
Pressure: {Pa:.2f}Pa, Density: {rho_air:.2f}kg/m^3") #Print statement
to check values

        thrust_results = [] # Temporary list to store thrust results
        thrust_results_ab = [] # Temporary list to store thrust
results with afterburner
        exit_area_results = [] # Temporary list to store exit area
results
        exit_area_results_ab = [] # Temporary list to store exit area
results with afterburner
```

```
P0_nozzle_results = [] #Temporary List to store total pressure
at nozzle exit
P0_nozzle_results_ab = []
TSFC_results = []
TSFC_results_ab = []
NPR_results = []
NPR_results_ab = []
T0_nozzle_results = []

for Mach in Mach_numbers: #iterate through each Mach number
    #Calculate Flight speed from given mach numbers
    V0 = flight_speed(Mach, Ta)

    #RAM effect consideration
    T01 = RAM_T(Mach, Ta)
    P01 = RAM_P (Mach, Pa)

    if Mach > 1:
        P02 = P01*(1-0.75*((Mach-1)**1.35))
    else:
        P02 = P01

    #Fan Stage (2-3)
    T03, P03 = fan(T01, P02, rc_fan)

    #Compressor Stage (3-4)
    T04, P04 = comp(T03,P03,rc)

    #Combustion (4-5):
    P05, f, mdot_f = comb(T04, P04, TIT, L, mdot_p, Cp_hot)

    #HPT Stage (5-5'):
```

```
T05_exit, P05_exit = HPT(TIT, T04, T03, P05, Cp_hot,
Cp_cold, f)

#LPT Stage (5'-6):
T06, P06 = LPT(T05_exit, T03, T01, P05_exit, Cp_hot,
Cp_cold, f, BPR)

#Nozzle Exit WITHOUT AfterBurner:
EGT, Pe, Ve, De, P07, NPR = nozzle(T06, P06, Pa)
#Exit area WITHOUT AfterBurner:
Ae = (mdot+ mdot_f) * (np.sqrt(T06)/P07) *
(np.sqrt(R/gamma)) * ((gamma+1)/2)**((gamma+1)/(2*(gamma-1)))
#Thrust Without Afterburner
Thrust = ((mdot*0.7) + mdot_f)*Ve -mdot*V0 + (Pe - Pa)*Ae
#Considering only primary flow at nozzle
#TSFC Without Afterburner:
TSFC = (mdot_f/Thrust)*3600 # [kg/N hr]

print(f"Vexit:{Ve:.2f}, T07:{T06:.2f}, P07:{P07:2f},
Aexit:{Ae:.2f}, EGT:{EGT:.2f},Pexit:{Pe:.2f}, mdot:{mdot+mdot_f:.2f}")

# Limit computation for the case without afterburner up to
Mach = 0.9
if Mach <= 0.9:
    thrust_results.append(Thrust)
    exit_area_results.append(Ae)
    P0_nozzle_results.append(P07)
    TSFC_results.append(TSFC)
    NPR_results.append(NPR)
    T0_nozzle_results.append(T06)
```

```
#Nozzle Exit WITH AfterBurner:
EGT_ab, Pe_ab, Ve_ab, De_ab, fab, mdot_fab, P07_ab, NPR_ab
= nozzle_ab(T06, ABT, P06, L, Cp_hot, mdot_p, f, BPR, T03, Pa)
#Exit area WITH Afterburner:
Ae_ab = (mdot+ mdot_f +mdot_fab) * (np.sqrt(ABT)/P07_ab) *
(np.sqrt(R/gamma)) * ((gamma+1)/2)**((gamma+1)/(2*(gamma-1)))
#Thrust WITH AfterBurner:
Thrust_ab = (mdot*0.8 +mdot_f+mdot_fab)*Ve_ab - V0*mdot +
(Pe_ab-Pa)*Ae_ab
Thrust_ab = max(1, Thrust_ab)
# TSFC WITH Afterburner:
TSFC_ab = ((mdot_f + mdot_fab) / Thrust_ab)*3600 # Avoid
division by zero

# Append results for each Mach number
thrust_results_ab.append(Thrust_ab)
exit_area_results_ab.append(Ae_ab)
P0_nozzle_results_ab.append(P07_ab)
TSFC_results_ab.append(TSFC_ab)
NPR_results_ab.append(NPR_ab)

# Append results for each altitude
results.append({
    'altitude': altitude,
    'thrust': thrust_results,
    'exit_area': exit_area_results,
    'P07' : P0_nozzle_results,
    'TSFC_dry' : TSFC_results,
    'NPR' : NPR_results,
    'T06': T0_nozzle_results
```

```
    })
    results_ab.append({
        'altitude': altitude,
        'thrust_ab': thrust_results_ab,
        'exit_area_ab': exit_area_results_ab,
        'P07_AB': P0_nozzle_results_ab,
        'TSFC_wet': TSFC_results_ab,
        'NPR_ab' : NPR_results_ab
    })
    return results, results_ab

#Defining Plotting Functions
def plot_thrust_vs_mach(results, results_ab):
    linestyle = ['-', 'dotted']
    markers = ['o', 's', '^', 'D', 'v', '>', '<']

    for result in results:
        altitude = result['altitude']
        thrust_results = result['thrust']
        Mach_numbers = np.linspace(0, 0.9, len(thrust_results)) #
Adjusted for the limited case

        marker = markers[results.index(result) % len(markers)]

        plt.plot(Mach_numbers, thrust_results,
linestyle=linestyle[0], marker=marker, label=f'Altitude {altitude}m
(Without AB)')

    for result_ab in results_ab:
        altitude = result_ab['altitude']
        thrust_results_ab = result_ab['thrust_ab']
        Mach_numbers_ab = np.linspace(0, 2.5,
len(thrust_results_ab)) # Full range for with afterburner
```

```
marker = markers[results_ab.index(result_ab) % len(markers)]

plt.plot(Mach_numbers_ab, thrust_results_ab,
linestyle=linestyles[1], marker=marker, label=f'Altitude {altitude}m
(With AB)')

plt.xlabel('Mach Number')
plt.ylabel('Thrust (N)')
plt.title('Thrust vs. Mach Number')
plt.legend()
plt.grid(True)
plt.show()

def plot_exit_area_vs_mach(results, results_ab):
    linestyles = ['- ', 'dotted']
    markers = ['o', 's', '^', 'D', 'v', '>', '<']

    for result in results:
        altitude = result['altitude']
        exit_area_results = result['exit_area']
        Mach_numbers = np.linspace(0, 0.9, len(exit_area_results)) #
Adjusted for the limited case

        marker = markers[results.index(result) % len(markers)]

        plt.plot(Mach_numbers, exit_area_results,
linestyle=linestyles[0], marker=marker, label=f'Altitude {altitude}m
(Without AB)')

    for result_ab in results_ab:
        altitude = result_ab['altitude']
        exit_area_results_ab = result_ab['exit_area_ab']
        Mach_numbers_ab = np.linspace(0, 2.5,
len(exit_area_results_ab)) # Full range for with afterburner
```



```
        marker = markers[results_ab.index(result_ab) % len(markers)]

        plt.plot(Mach_numbers_ab, exit_area_results_ab,
linestyle=linestyles[1], marker=marker, label=f'Altitude {altitude}m
(With AB)')

    plt.xlabel('Mach Number')
    plt.ylabel('Exit Area (m^2)')
    plt.title('Exit Area vs. Mach Number')
    plt.legend()
    plt.grid(True)
    plt.show()

def plot_total_pressure_nozzle(results, results_ab):
    linestyles = ['- ', 'dotted']
    markers = ['o', 's', '^', 'D', 'v', '>', '<']

    for result in results:
        altitude = result['altitude']
        P0_nozzle_results = result['P07']
        Mach_numbers = np.linspace(0, 0.9, len(P0_nozzle_results)) #
Adjusted for the limited case

        marker = markers[results.index(result) % len(markers)]

        plt.plot(Mach_numbers, P0_nozzle_results,
linestyle=linestyles[0], marker=marker, label=f'Altitude {altitude}m
(Without AB)')

    for result_ab in results_ab:
        altitude = result_ab['altitude']
        P0_nozzle_results_ab = result_ab['P07_AB']
```

```
Mach_numbers_ab = np.linspace(0, 2.5,
len(P0_nozzle_results_ab)) # Full range for with afterburner

marker = markers[results_ab.index(result_ab) % len(markers)]

plt.plot(Mach_numbers_ab, P0_nozzle_results_ab,
linestyle=linestyles[1], marker=marker, label=f'Altitude {altitude}m
(With AB)')

plt.xlabel('Mach Number')
plt.ylabel('Total Pressure (Pa)')
plt.title('Nozzle Exit Total Pressure vs. Mach Number')
plt.legend()
plt.grid(True)
plt.show()

def plot_TSFC(results, results_ab):
    linestyles = ['- ', 'dotted']
    markers = ['o', 's', '^', 'D', 'v', '>', '<']

    for result in results:
        altitude = result['altitude']
        TSFC_results = result['TSFC_dry']
        Mach_numbers = np.linspace(0, 0.9, len(TSFC_results)) #
Adjusted for the limited case

        marker = markers[results.index(result) % len(markers)]

        plt.plot(Mach_numbers, TSFC_results, linestyle=linestyles[0],
marker=marker, label=f'Altitude {altitude}m (Without AB)')

    for result_ab in results_ab:
        altitude = result_ab['altitude']
        TSFC_results_ab = result_ab['TSFC_wet']
```

```
Mach_numbers_ab = np.linspace(0, 2.5, len(TSFC_results_ab)) #  
Full range for with afterburner  
  
marker = markers[results_ab.index(result_ab) % len(markers)]  
  
plt.plot(Mach_numbers_ab, TSFC_results_ab,  
linestyle=linestyles[1], marker=marker, label=f'Altitude {altitude}m  
(With AB)')  
  
plt.xlabel('Mach Number')  
plt.ylabel('TSFC (kg/N hr)')  
plt.title('TSFC vs. Mach Number')  
plt.legend()  
plt.grid(True)  
plt.show()  
  
def plot_NPR(results, results_ab):  
    linestyles = ['-', 'dotted']  
    markers = ['o', 's', '^', 'D', 'v', '>', '<']  
  
    for result in results:  
        altitude = result['altitude']  
        NPR_results = result['NPR']  
        Mach_numbers = np.linspace(0, 0.9, len(NPR_results)) #  
Adjusted for the limited case  
  
        marker = markers[results.index(result) % len(markers)]  
  
        plt.plot(Mach_numbers, NPR_results, linestyle=linestyles[0],  
marker=marker, label=f'Altitude {altitude}m (Without AB)')  
  
    for result_ab in results_ab:  
        altitude = result_ab['altitude']
```

```
NPR_results_ab = result_ab['NPR_ab']
Mach_numbers_ab = np.linspace(0, 2.5, len(NPR_results_ab)) #
Full range for with afterburner

marker = markers[results_ab.index(result_ab) % len(markers)]

plt.plot(Mach_numbers_ab, NPR_results_ab,
linestyle=linestyles[1], marker=marker, label=f'Altitude {altitude}m
(With AB)')

plt.xlabel('Mach Number')
plt.ylabel('Nozzle Pressure Ratio')
plt.title('NPR vs. Mach Number')
plt.legend()
plt.grid(True)
plt.show()

def plot_T07(results):
    linestyles = ['-']
    markers = ['o', 's', '^', 'D', 'v', '>', '<']

    for result in results:
        altitude = result['altitude']
        T07_results = result['T06']
        Mach_numbers = np.linspace(0, 0.9, len(T07_results)) #
Adjusted for the limited case

        marker = markers[results.index(result) % len(markers)]

        plt.plot(Mach_numbers, T07_results, linestyle=linestyles[0],
marker=marker, label=f'Altitude {altitude}m (Without AB)')

plt.xlabel('Mach Number')
```

```
plt.ylabel('T06')
plt.title('T06 vs. Mach Number')
plt.legend()
plt.grid(True)
plt.show()
#Perform Analysis and Plot:
results, results_ab = perform_analysis(altitudes, Mach_numbers)

plot_thrust_vs_mach(results, results_ab)
plot_exit_area_vs_mach(results, results_ab)
plot_total_pressure_nozzle(results, results_ab)
plot_TSFC(results, results_ab)
plot_NPR(results, results_ab)
plot_T07(results)
```

APPENDIX 3: Resultant Thrust, Exit Area, and TSFC Increase Calculations

Handwritten calculations on grid paper showing thrust and exit area data for various altitudes. The calculations are organized into two main sections: Thrust (TAR) and Exit Area (A_e).

Thrust Calculations:

- 0 m: Dry = 35 kN, Wet = 80 kN → TAR = 1.77 → % = 77.7%
- 1000 m: Dry = 47.5 kN, Wet = 72.5 kN → TAR = 1.75 → % = 74.7%
- 2000 m: Dry = 38 kN, Wet = 66 kN → TAR = 1.74 → % = 73.7%
- 4000 m: Dry = 37.5 kN, Wet = 64.5 kN → TAR = 1.73 → % = 73%
- 8000 m: Dry = 27 kN, Wet = 55.5 kN → TAR = 1.69 → % = 69%
- 12000 m: Dry = 27 kN, Wet = 51.5 kN → TAR = 1.67 → % = 67.7%
- 16000 m: Dry = 26 kN, Wet = 44 kN → TAR = 1.676 → % = 67.64%

Exit Area Calculations:

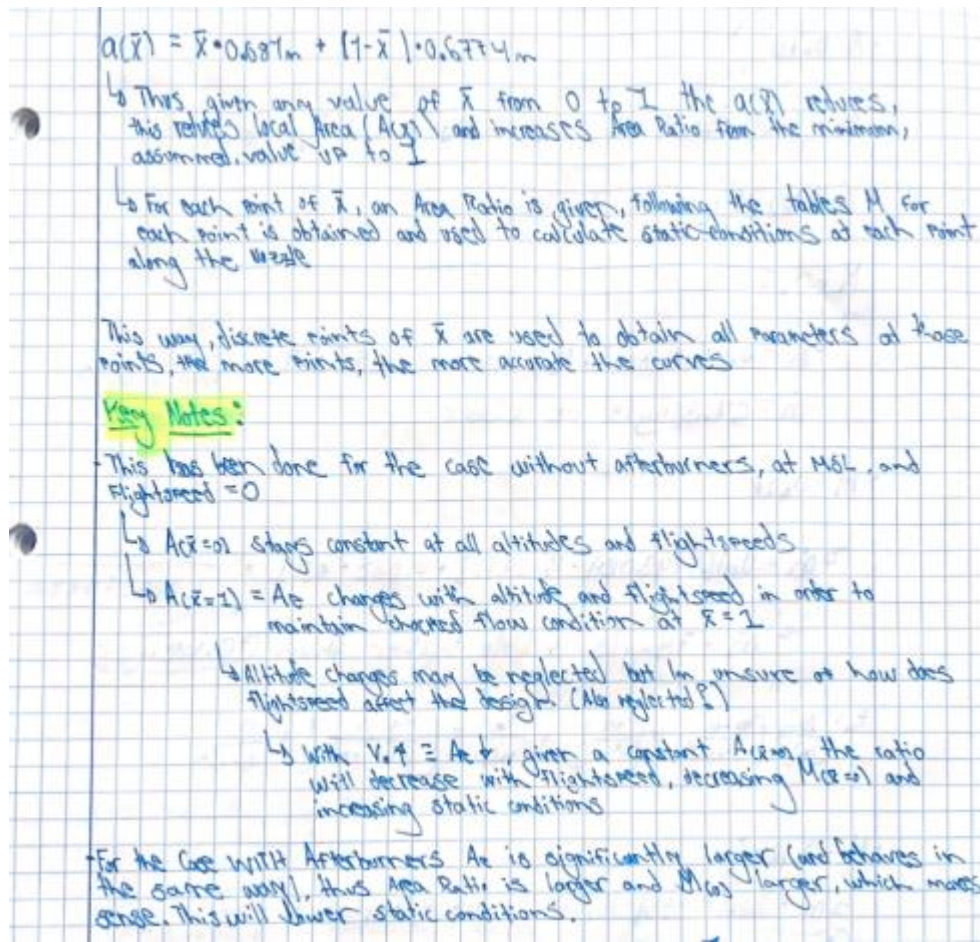
- 0 m: Dry = 0.0732 m², Wet = 0.142 m² → % = 99.18%
 Dry = 0.1092 m², Wet = 0.174325 m², % =
- 1000 m: Dry = 0.0724 m², Wet = 0.1395 m² → % = 92.7%
 Dry = 0.1035 m², Wet = 0.172 m², % =
- 2000 m: Dry = 0.0717 m², Wet = 0.1373 m² → % = 97.5%
 Dry = 0.102 m², Wet = 0.1695 m², % =
- 4000 m: Dry = 0.07045 m², Wet = 0.1338 m² → % = 89.92%
 Dry = 0.102 m², Wet = 0.1657 m², % =
- 8000 m: Dry = 0.0689 m², Wet = 0.1284 m² → % = 82.87%
 Dry = 0.098 m², Wet = 0.1595 m², % =
- 12000 m: Dry = 0.06855 m², Wet = 0.126 m² → % = 83.8%
 Dry = 0.09745 m², Wet = 0.1557 m², % =
- 16000 m: Dry = 0.06855 m², Wet = 0.116 m² → % = 83.8%
 Dry = 0.09745 m², Wet = 0.1557 m², % =

ISFC Ref: Dry = 0.055 kg/N.hr 0 % = 23.6%

Wet = 0.224 kg/N.hr 0 % = 25%

- 0 m: Dry = 0.04905 kg/N.hr 0 % = 247.8% → 3.42 X
Wet = 0.16765 kg/N.hr
- 1000 m: Dry = 0.04965 kg/N.hr 0 % = 230.35% → 3.35 X
Wet = 0.167 kg/N.hr
- 2000 m: Dry = 0.05025 kg/N.hr 0 % = 237.24% → 3.37 X
Wet = 0.16645 kg/N.hr
- 4000 m: Dry = 0.0514 kg/N.hr 0 % = 227.98% → 3.22 X
Wet = 0.16545 kg/N.hr
- 8000 m: Dry = 0.0529 kg/N.hr 0 % = 204.45% → 3.04 X
Wet = 0.1641 kg/N.hr
- 12,000 m: Dry = 0.0557 kg/N.hr 0 % = 193.5% → 2.93 X
Wet = 0.1685 kg/N.hr
- 16,000 m: Dry = 0.0557 kg/N.hr 0 % = 193.5% → 2.93 X
Wet = 0.1685 kg/N.hr

APPENDIX 4: Resultant Static Pressure, Temperature, and Velocity Hand Calculations along Adimensionalised Nozzle Length & Notes



$a(\bar{x}) = \bar{x} \cdot 0.6871 \text{ m} + (1 - \bar{x}) \cdot 0.6774 \text{ m}$

- ↳ Thus, given any value of \bar{x} from 0 to 1, the $a(\bar{x})$ reduces, this reduces local area ($A(x)$), and increases Area Ratio from the minimum, assumed, value up to 1
- ↳ For each point of \bar{x} , an Area Ratio is given, following the tables M for each point is obtained and used to calculate static conditions at each point along the nozzle

This way, discrete points of \bar{x} are used to obtain all parameters at those points, the more points, the more accurate the curves

Key Notes:

- This has been done for the case without afterburners, at MSL, and flight speed = 0
 - ↳ $A(x=0)$ stays constant at all altitudes and flight speeds
 - ↳ $A(x=1) = A_e$ changes with altitude and flight speed in order to maintain choked flow condition at $x=1$
 - ↳ Altitude changes may be neglected but I'm unsure as how does flight speed affect the design (Also neglected?)
 - ↳ With $V \uparrow \equiv A_e \uparrow$, given a constant $A(x=0)$, the ratio will decrease with flight speed, decreasing $M(x=1)$ and increasing static conditions

*For the case with afterburners A_e is significantly larger (and behaves in the same way), thus Area Ratio is larger and $M(x)$ larger, which makes sense. This will lower static conditions.

Fix $a(x)$ and $A(x)$:

$$a(x) = \bar{x} \cdot a + (1 - \bar{x})A$$

$$A(x) = (\bar{x} \cdot a + (1 - \bar{x})A) \cdot b$$

→ At $\bar{x} = 1$: $A(x=1) = A_e = 0.1042 \text{ m}^2 = (a + 0) \cdot b$
 ↳ Assuming $b = D_{\text{noz}} = 0.72 \text{ m}$
 ↳ $a = 0.14472 \text{ m}$

At $\bar{x} = 0$ → $A(x=0) = 0.40715 \text{ m}^2 = (0 + A) \cdot b$
 ↳ $A = 0.565486771 \text{ m}$

Thus

$$a(x) = \bar{x} \cdot 0.14472 \text{ m} + (1 - \bar{x}) \cdot 0.565486771 \text{ m}$$

$$A(x) = [\bar{x} \cdot 0.14472 \text{ m} + (1 - \bar{x}) \cdot 0.5655 \text{ m}] \cdot 0.72 \text{ m}$$

Now that we got everything right, let's chose values of \bar{x} from 0 to 1 to obtain $A(x)$ and local Area Ratio. With the Area Ratio for each point using tables, we can approximate the Mach Number and with Mach Number obtain static parameters as a function of \bar{x}

Sea Level Static: $M_0 = 0$; $T_0 = 1149.64 \text{ K}$; $P_0 = 567,106.68 \text{ Pa}$
 $A_e = 0.1042 \text{ m}^2$

\bar{x}	$A(x)$	$\frac{A_e}{A(x)}$	$M(x)$	$T(x)$	$P(x)$	$V(x)$
0	0.40715	0.256	0.15	1,138.92	589,264.49	107.45 m/s
0.1	0.3769	0.276	0.16	1,137.87K	587,060.11	108.18 m/s
0.2	0.34669	0.3	0.18	1,136.876	584,4309	127.624 m/s
0.3	0.3165	0.3246	0.2	1,134.56	581,509.8	135 m/s
0.4	0.2862	0.3643	0.22	1,132.67K	578,314.17	148.415-15
0.5	0.25595	0.4075	0.24	1,130.67K	574,821.33	167.76 m/s
0.6	0.2254	0.46219	0.28	1,125.48K	587,087.1	188.333 m/s
0.7	0.19505	0.534	0.33	1,119.26K	525,912.95	227.3-15
0.8	0.16471	0.63232	0.4	1,108.379	807,909.9	266 m/s
0.9	0.1345	0.77422	0.53	1,082.8	488,382.34	349.58 m/s

\bar{x}	$A(x)$	$A(x)/A(x=1)$	$M(x)$	$T(x)$	$P(x)$	$V(x)$
0.92	0.118486	0.9113	0.57	1,073.66	454,956.3	374.41 m/s
0.94	0.122371	0.85146	0.61	1,064.415	441,118.7	399.925 m/s
0.96	0.116318	0.79582	0.67	1,049.42	419,338.53	435.06 m/s
0.98	0.110259	0.945	0.76	1,025.2	386,806.7	487.77 m/s
0.99	0.1072205	0.9717	0.82	1,008.07	364,549.6	527.87 m/s
1	0.1042	1	1	983.03	299,820.9	618.81 m/s

Now with Afterburners: Sea Level Static

$\rightarrow T_{0e} = T_{0T} = 2,500K$; $P_{0e} = 521,738.15 Pa$; $V_e = 914.92 m/s$
 $A_e = 217492 m^2$; $P_e = 23814.45 Pa$; $T_e = 2083.33 K$
 $\dot{m} = 73.69$

↳ Lets check at exit: $\bar{x} = 1$

$$\dot{m} = \sqrt{\frac{1.4}{287}} \cdot \frac{521,738.15}{\sqrt{2,500}} \cdot 0.77472 \cdot \frac{7}{1.728}$$

↳ $\dot{m} = 73.69$ → Perfect

↳ Lets check at inlet: $\bar{x} = 0$

Using tables: $\frac{A_e}{A_{00}} = \frac{0.17472}{0.40715} = 0.4297$ → $M_{00} \approx 0.26$

$$\rightarrow \dot{m} = \sqrt{\frac{1.4}{287}} \cdot \frac{521,738.15}{\sqrt{2,500}} \cdot 0.40715 \cdot 0.26 \cdot \frac{7}{1.041119943}$$

↳ $\dot{m} = 74.7 \text{ kg/s}$ → Good Enough

Area function is now different:

$$A(x) = \bar{x} \cdot a + (1 - \bar{x})A \rightarrow A(x) = [\bar{x} \cdot a + (1 - \bar{x})A]b$$

↳ At $\bar{x} = 0 \rightarrow A(x=0) = 0.40715 m^2 = A \cdot b \rightarrow b = 0.72 m$
 $\rightarrow A = 0.565486111 m$

↳ At $\bar{x} = 1 \rightarrow A_e = 0.17472 m = a \cdot b$
 $\rightarrow a = 0.242666 \bar{b}$

Thus $\rightarrow A(x) = \bar{x} \cdot 0.242666 m + (1 - \bar{x}) \cdot 0.565486111 m$
 $A(x) = [\bar{x} \cdot 0.242666 m + (1 - \bar{x}) \cdot 0.565486111 m] \cdot 0.72 m$

\bar{x}	$Ac(\bar{x})$	$M(\bar{x})$	$T(\bar{x})$	$P(\bar{x})$	$V(\bar{x})$
0	0.40715	0.26	2,466.65K	497,782.3Pa	258.84m/s
0.1	0.3889	0.28	2,467.4K	494,187Pa	278.45m/s
0.2	0.3606 0.357427	0.3 0.32	2,455.8K	490,187.18	298m/s
0.3	0.337427	0.32	2,449.82	486,110.65	317.48m/s
0.4	0.314138	0.35	2,440.2	479,358.82	346.56m/s
0.5	0.290983	0.38	2,429.82	472,254.4	375.47m/s
0.6	0.267692	0.42	2,414.8	462,115.15	419.7m/s
0.7	0.244449	0.47	2,394.22	448,475.57	460.98m/s
0.8	0.221206	0.54	2,362.23	427,851.52	526.07m/s
0.9	0.197963	0.65	2,305.27	392,779.8	625.52m/s
0.92	0.1933144	0.68	2,288.37K	382,829.47	652.04m/s
0.94	0.1896658	0.73	2,259.21	366,026.67	695.9m/s
0.96	0.1840132	0.77	2,234.9	352,406.56	729.66m/s
0.98	0.1793686	0.83	2,197.26K	332,084.46	779.87m/s
0.99	0.1771443	0.88	2,164.72	315,190.83	820.7m/s
1	0.17472	1	2,083.3	275,624.76	914.92m/s

APPENDIX 5: Static Parameters Graphs Along Adimensionalised Nozzle Length & Area Ratio as a Function of Mach Number Graph Script

```
#Define X' Values from 0 to 1
x_prime_1 = np.arange(0,0.9,0.1)
x_prime_2 = np.arange(0.9,1,0.02)
x_prime_3 = np.array([0.99])
x_prime_4 = np.array([1.0])

#Concatenate all the arrays in a single one:
X_prime = np.concatenate((x_prime_1,x_prime_2,x_prime_3,x_prime_4))
#print(X_prime) for checking

#Calculate Nozzle Area based on X' for DRY case: Nozzle has been
approximated to a simple trapezoid
A_local = (0.144722222222*X_prime + (1-X_prime)*0.565486111)*0.72
A_local_ab = (0.242666666666*X_prime+(1-X_prime)*0.565486111)*0.72
#print for checking print(A_local) print(A_local_ab)

#Computing Area Ratio as a function of Mach to get visual aid:
M = np.arange(0,5,0.1)
Area_ratio = M * (((gamma+1)/2)/(1+(M**2)*(gamma-
1)/2))**((gamma+1)/(2*(gamma-1)))
# Plotting
plt.figure(figsize=(8, 6))
plt.plot(M, Area_ratio, color='b')
plt.title('Area Ratio vs Mach Number')
plt.xlabel('Mach Number')
plt.ylabel('Area Ratio')
plt.grid(True)
plt.show()

#Input all calculated parameters for each of the X_prime points:
```

```
static_temp =
[1138.52,1137.81,1136.276,1134.56,1132.67,1130.61,1125.98,1119.26,1108
.178,1082.8,1073.86,1064.425,1049.42,1025.2,1008.07,953.0333333333]
static_press =
[558264.45,557060.111,554430,551509.37,548304.27,544821.33,537051.1,52
5912.95,507908.9,468362.34,454956.3,441118.7,419738.53,386806.7,364649
.65,299580.92]
flow_velocity =
[101.45,108.18,121.624,135,148.415,161.76,188.333,221.3,266.9,349.58,3
74.41,398.925,435.06,487.77,521.87,618.81]
#for the case WITH Afterburners:
static_temp_ab =
[2466.65,2461.4,2455.8,2449.82,2440.2,2429.82,2414.8,2394.22,2362.23,2
305.21,2288.37,2259.21,2234.9,2197.26,2164.72,2083.333333333333]
static_press_ab =
[497782.3,494087,490157.18,486000.65,479358.82,472254.4,462115.15,4484
75.57,427851.52,392779.8,382829.47,366026.67,352466.56,332084.46,31519
0.83,275624.76]
flow_velocity_ab =
[258.84,278.45,298,317.48,346.56,375.47,413.7,460.98,526.01,625.04,652
.5,695.5,729.66,779.87,820.7,914.92]

# Plotting for DRY CASE:
fig, ax1 = plt.subplots(figsize=(10, 6))

# Plot static temperature

color = 'tab:red'
ax1.set_xlabel("X'")
ax1.set_ylabel('Static Temperature [K]', color=color)
line1, = ax1.plot(X_prime, static_temp, color=color, label='Static
Temperature (Dry)')
ax1.tick_params(axis='y', labelcolor=color)
```

```
# Create a secondary y-axis for static pressure
ax2 = ax1.twinx()
color = 'orange' # Changed color to orange for better readability
ax2.set_ylabel('Static Pressure [Pa]', color=color)
line2, = ax2.plot(X_prime, static_press, color=color, label='Static
Pressure (Dry)')
ax2.tick_params(axis='y', labelcolor=color)

# Create a tertiary y-axis for velocity of flow
ax3 = ax1.twinx()
color = 'tab:blue'
ax3.spines['right'].set_position(('outward', 60))
ax3.set_ylabel('Flow Speed [m/s]', color=color)
line3, = ax3.plot(X_prime, flow_velocity, color=color, label='Flow
Speed (Dry)')
ax3.tick_params(axis='y', labelcolor=color)

# Combine legends
lines = [line1, line2, line3]
labels = [line.get_label() for line in lines]
ax1.legend(lines, labels, loc='center left')

plt.title('Static Parameters vs X\'for the Dry Engine')
plt.grid(True)
plt.show()

# Plotting for the case WITH afterburners
fig2, ax4 = plt.subplots(figsize=(10, 6))

# Plot static temperature with afterburners
color = 'tab:red'
ax4.set_xlabel("X'")
ax4.set_ylabel('Static Temperature [K]', color=color)
```

```
line4, = ax4.plot(X_prime, static_temp_ab, color=color, label='Static  
Temperature (Wet)')  
ax4.tick_params(axis='y', labelcolor=color)  
  
# Create a secondary y-axis for static pressure with afterburners  
ax5 = ax4.twinx()  
color = 'orange' # Changed color to orange for better readability  
ax5.set_ylabel('Static Pressure [Pa]', color=color)  
line5, = ax5.plot(X_prime, static_press_ab, color=color, label='Static  
Pressure (Wet)')  
ax5.tick_params(axis='y', labelcolor=color)  
  
# Create a tertiary y-axis for velocity of flow with afterburners  
ax6 = ax4.twinx()  
color = 'tab:blue'  
ax6.spines['right'].set_position(('outward', 60))  
ax6.set_ylabel('Flow Speed [m/s]', color=color)  
line6, = ax6.plot(X_prime, flow_velocity_ab, color=color, label='Flow  
Speed (Wet)')  
ax6.tick_params(axis='y', labelcolor=color)  
  
# Combine legends for the case WITH afterburners  
lines4, labels4 = ax4.get_legend_handles_labels()  
lines5, labels5 = ax5.get_legend_handles_labels()  
lines6, labels6 = ax6.get_legend_handles_labels()  
ax4.legend(lines4 + lines5 + lines6, labels4 + labels5 + labels6,  
loc='center left')  
  
plt.title('Static Parameters vs X\' for the Wet Engine')  
plt.grid(True)  
plt.show()
```

APPENDIX 6: Exit Area Dimensioning Based on 1D Nozzle Flow Theoretical Losses

Example Dimensioning based on 1D Flow: No AB, MSL

$\dot{m} = 70.62 \text{ kg/s}$ $F_g = 45.11 \text{ kN}$
 $P_T = 567,106,68 \text{ Pa}$
 $T_T = 1142,64 \text{ K}$
 $A_0 = 0,1042 \text{ m}^2$ $\rightarrow \frac{A_0}{A^*} = 0,250$
 $M_0 = 0,15$
 $P_0 = 101,825 \text{ Pa}$
 $\lambda = 1$ \rightarrow Given Gross Thrust Coefficient from Diagram
 $\rightarrow \frac{F_g \text{ Gross}}{F_g \text{ Ideal}} = 0,985$

From Equations:

$$\frac{F_g}{P_0 \cdot A_{\text{exit}}} = \left\{ \frac{2 \times 14^2}{1,4 - 1} \left(\frac{2}{1,4} \right)^4 \left[1 - \left(\frac{1}{5,6} \right)^{0,285} \right]^2 \right\}^{1/2}$$

$$= \left\{ 9,8 \cdot 0,335 \left[0,3879 \right]^2 \right\}^{1/2}$$

$\frac{F_g}{P_0 \cdot A_{\text{exit}}} = 1,1285$

Considering $\theta = 20^\circ$: $C_{\text{wall}} = 0,965$ $\rightarrow C_d = \frac{A_0}{A_{\text{exit}}}$
 $C_0 \cdot C_v = 0,99$ $\rightarrow A_{\text{exit}} = 0,108 \text{ m}^2$

$$\frac{F_g}{P_0 \cdot A_{\text{exit}}} = 0,99 \cdot 1,4 \cdot \frac{2 \cdot 14 \cdot 567,10668}{567,10668} \cdot 1^2 + \frac{1}{0,045} (0,528 - 0,17857)$$

$$= 0,73017 + 0,86210362$$

$\frac{F_g}{P_0 \cdot A_{\text{exit}}} = 1,09427362$

$$\eta_F = \frac{F_j / A_{c,act} \cdot P_T}{F_g / A_{c,act} \cdot P_T}$$

$$\eta_F \approx 0.97 \quad \rightarrow \quad F_g = 43.68 \text{ kN}$$

Considering $A_{c,act} = 0.108 \text{ m}^2$:

$$A_{c,act} = \frac{A_{c,act}}{b} = \frac{0.108 \text{ m}^2}{0.72 \text{ m}}$$

$$\frac{A_c}{A_{c,act}} = 0.265$$

$$A_{c,reactive} = 0.15 \text{ m}$$

This represents a 3.65% difference with the "ideal" geometry

Now for the afterburning case = MSL

$$\dot{m} = 73.6 \text{ kg/s} \quad F_g = 80 \text{ kN}$$

$$P_T = 2.500$$

$$P_T = 52.1738.15 \text{ Pa}$$

$$P_T = 2.35.614.45 \text{ Pa}$$

$$A_c = 0.17472 \text{ m}^2 \rightarrow \frac{A_c}{A_{c,act}} = 0.429$$

$$M_{act} = 0.26$$

$$\theta = 10^\circ \rightarrow 10^\circ \text{ difference for operating afterburners}$$

$$NPR = 5.15$$

$$\frac{F_{j,comb}}{F_{j,ideal}} \approx 9.56$$

From equations:

$$\frac{F_j}{A_c \cdot P_T} = \left\{ \frac{2 \times 1.4^2}{0.4} \cdot 0.26^3 \cdot \left[1 - \left(\frac{1}{5.15} \right)^{0.265} \right]^2 \right\}^{1/2}$$

$$= \left\{ 9.8 \cdot 0.26^3 \cdot [0.9732] \right\}^{1/2}$$

$$\frac{F_j}{A_c \cdot P_T} = 1.10638$$

Considering $\theta = 10^\circ \rightarrow C_{0, \max} = 0.979$
 $\hookrightarrow C_v \cdot C_0 = 0.995$ $\hookrightarrow A_{e, \text{eff}} = 0.17846 \text{ m}^2$

$$\frac{F_g}{A_e P_T} = 0.995 \cdot 1.4 \cdot 0.52826 \cdot 7^\circ + \frac{1}{0.979} \cdot (0.52826 - 0.19497)$$

$\frac{F_g}{A_e P_T} = 1.07763$

Thus:

$\eta_F = 0.9735$ $\rightarrow F_g = 77,886.12 \text{ N}$

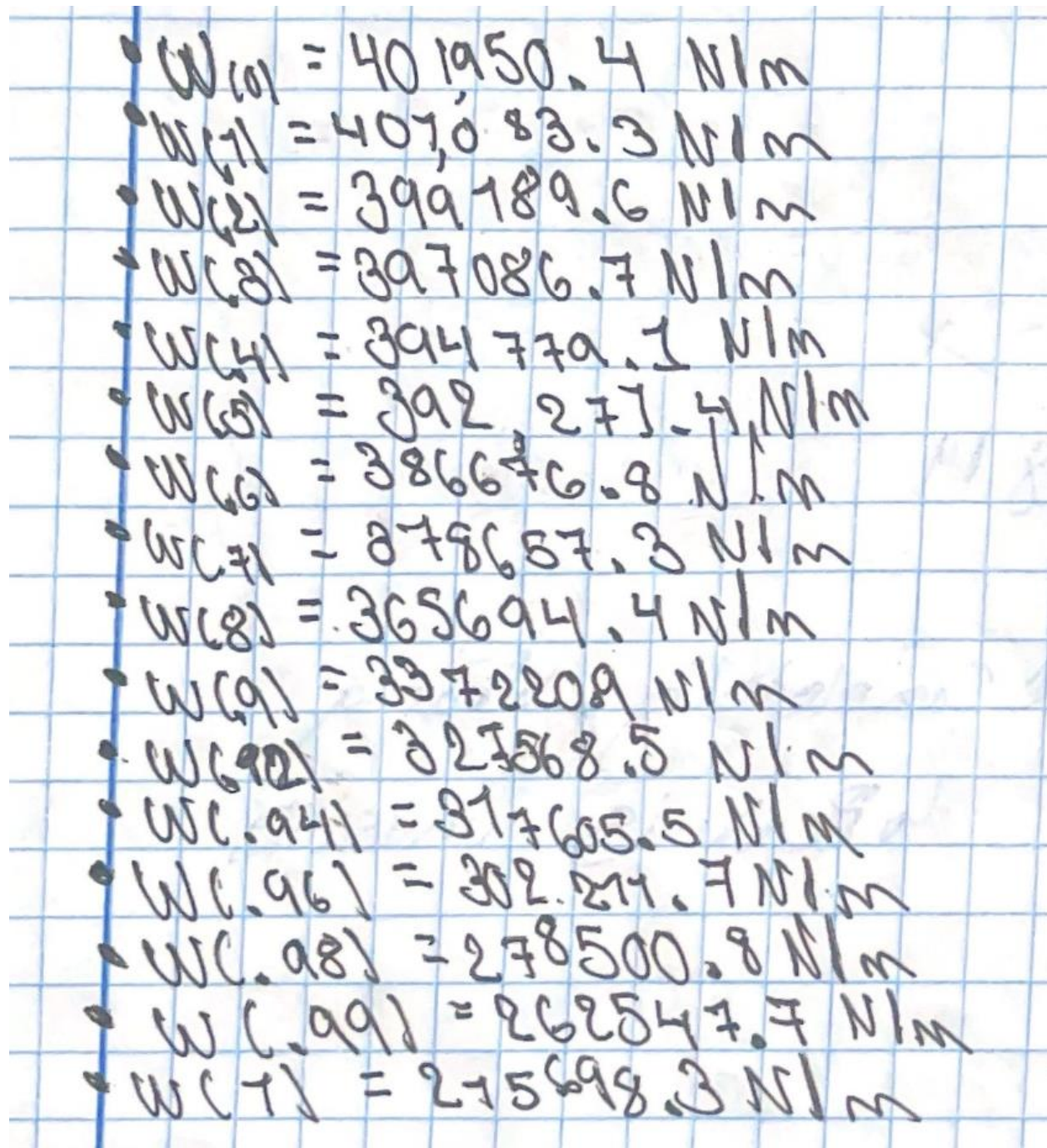
Considering $A_{e, \text{eff}} = 0.17846 \text{ m}^2$, $b = 0.72 \text{ m}$

$\hookrightarrow A_{e, \text{effective}} = 0.24786 \text{ m}^2$

\hookrightarrow This represents a 2.14% increase with the "ideal" geometry

$\frac{A_{e, \text{eff}}}{A_{e, \text{ideal}}} = 0.4383$

APPENDIX 7: Nozzle 2D pressure Distribution Resultant Force Calculation for Sea Level Static Case and no Afterburner:



Handwritten calculations on a grid background showing a list of resultant force values (WC) in N/m for various nozzle sections:

- $WC_{01} = 401950.4 \text{ N/m}$
- $WC_{11} = 407083.3 \text{ N/m}$
- $WC_{21} = 399189.6 \text{ N/m}$
- $WC_{31} = 397086.7 \text{ N/m}$
- $WC_{41} = 394779.1 \text{ N/m}$
- $WC_{51} = 392271.4 \text{ N/m}$
- $WC_{61} = 386676.8 \text{ N/m}$
- $WC_{71} = 378687.3 \text{ N/m}$
- $WC_{81} = 365694.4 \text{ N/m}$
- $WC_{91} = 3372209 \text{ N/m}$
- $WC_{921} = 323868.5 \text{ N/m}$
- $WC_{941} = 317605.5 \text{ N/m}$
- $WC_{961} = 302211.7 \text{ N/m}$
- $WC_{981} = 278500.8 \text{ N/m}$
- $WC_{991} = 262547.7 \text{ N/m}$
- $WC_{T1} = 215698.3 \text{ N/m}$

Recalculating F_{ext}:

$\vec{F} = \int_A p \cdot \vec{n} \, dA$ $\rightarrow dA = dx \, dy$
 $A = p(x) \cdot x \cdot b \rightarrow \int dA = p(x) \cdot dx \cdot b$
 $\rightarrow F = p(x) \cdot b \, dx$
 $\rightarrow p(x) \cdot b = w(x)$

Discretizing:

$F = \sum w(x_i) \cdot \Delta x_i$

$\rightarrow F = \int_{x_1}^{x_2} w(x) \, dx = \sum w(x_i) \cdot \Delta x_i$

$\rightarrow F_{ext} = 385,467 \, \text{N} = 385 \, \text{kN}$ $\rightarrow F_{ext} = 368,703,929 \, \text{N}$

Centroid:

$\bar{x} = \frac{\sum F_i x_i}{\sum F_i} = 0.437 = 0.44 \, \text{m}$

$\rightarrow F_{ext} = 368,704 \, \text{N}$
 $\rightarrow B_y = 324,456 \, \text{N}$
 $\rightarrow A_y = 44,244 \, \text{N}$
 $\rightarrow \bar{x} \approx 0.45 \, \text{m}$

Reactions:

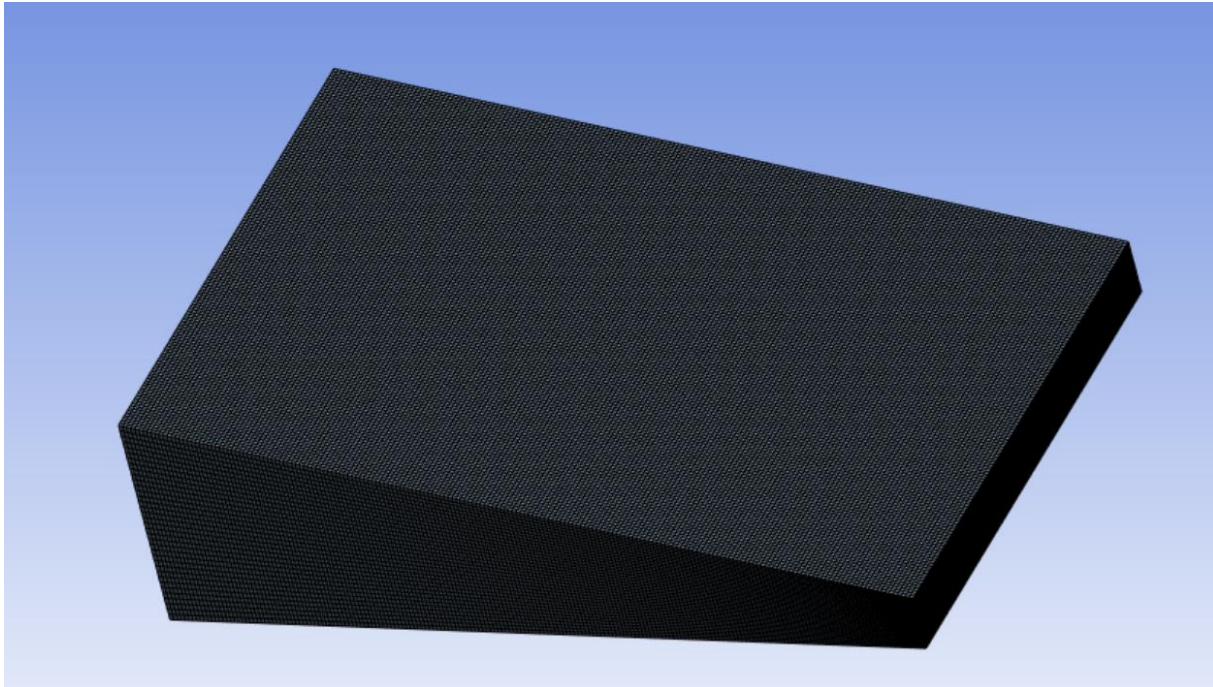
$\uparrow \sum F_y = 0 = -A_y + F - B_y$
 $\sum F_x = 0$
 $\circlearrowleft M_A = 0 = F \cdot 0.44 \, \text{m} - B_y \cdot 0.5 \, \text{m}$

$\rightarrow B_y = 0.88 F = 338.8 \, \text{kN}$
 $\rightarrow A_y = 0.12 F = 46.2 \, \text{kN}$

Obtain SF and BM:

$t = 80 \, \text{mm}$
 $\text{Max BM} = 34,723 \, \text{kN} \cdot \text{m}$
 $\text{Max SF} = 169,9 \, \text{kN}$
 $\rightarrow \sigma_{max} = 327,65 \, \text{MPa}$
 $\rightarrow \tau_{max} = 77,8 \, \text{MPa}$

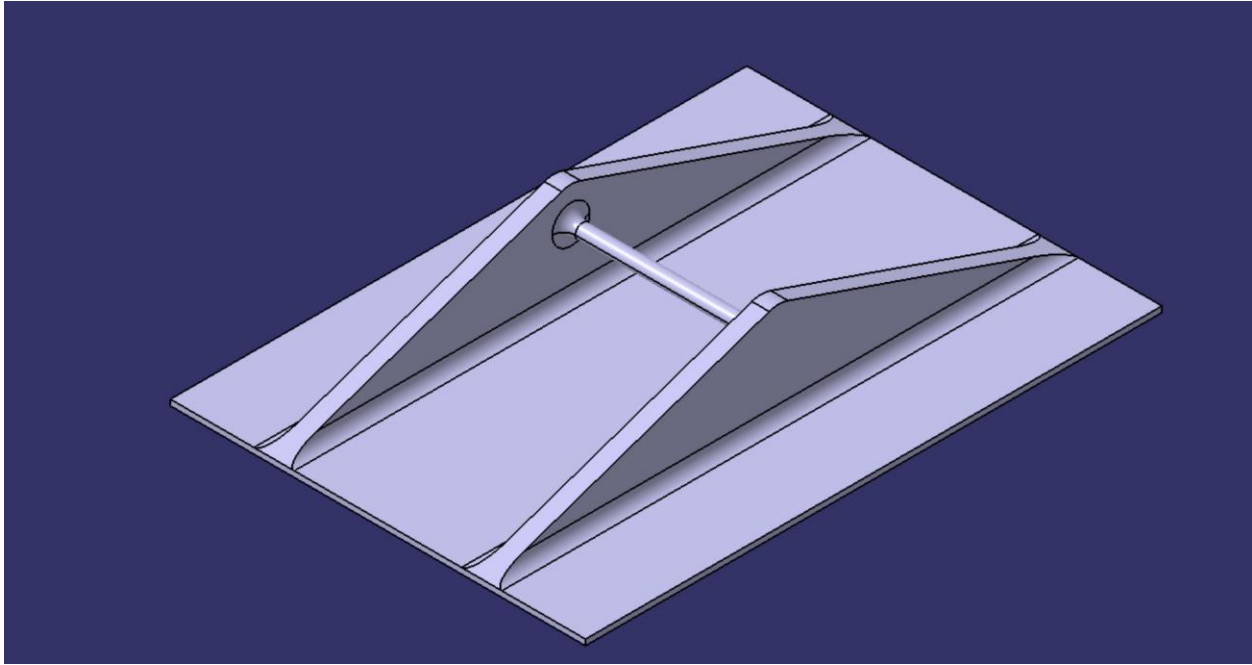
APPENDIX 8: Nozzle Fluid Domain Mesh & Details



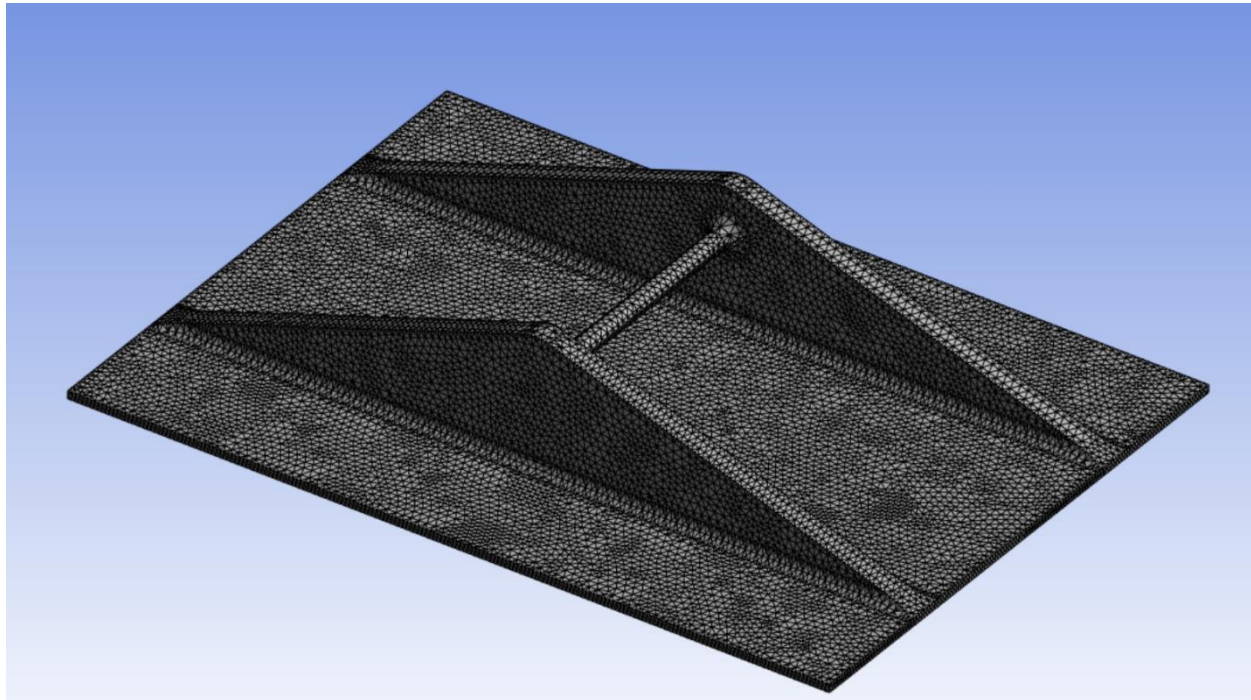
Details of "Mesh" ⌵ 📌 🗄 ➤

Solver Preference	Fluent
Element Order	Linear
<input type="checkbox"/> Element Size	5.e-003 m
Export Format	Standard
Export Preview Surface Mesh	No
+ Sizing	
- Quality	
Check Mesh Quality	Yes, Errors
<input type="checkbox"/> Target Skewness	Default (0.9)
Smoothing	Medium
Mesh Metric	Orthogonal Quality
<input type="checkbox"/> Min	0.97763
<input type="checkbox"/> Max	0.99998
<input type="checkbox"/> Average	0.99215
<input type="checkbox"/> Standard Deviation	6.8397e-003
+ Inflation	
+ Advanced	
- Statistics	
<input type="checkbox"/> Nodes	1067635
<input type="checkbox"/> Elements	1026432

APPENDIX 9: Final Nozzle Structure CAD Model don in CATIA V5











APPENDIX 10: Nozzle Structure Mesh & Details



Details of "Mesh" ▼ 📏 🗑️ 🔍

<input type="checkbox"/> Defaults	
Physics Preference	Mechanical
Element Order	Program Controlled
<input type="checkbox"/> Element Size	5.e-003 m
<input checked="" type="checkbox"/> Sizing	
<input type="checkbox"/> Quality	
Check Mesh Quality	Yes, Errors
Error Limits	Aggressive Mechanical
<input type="checkbox"/> Target Element Quality	Default (5.e-002)
Smoothing	Medium
Mesh Metric	Element Quality
<input type="checkbox"/> Min	0.13038
<input type="checkbox"/> Max	0.99994
<input type="checkbox"/> Average	0.74601
<input type="checkbox"/> Standard Deviation	0.13516
<input checked="" type="checkbox"/> Inflation	
<input checked="" type="checkbox"/> Advanced	
<input type="checkbox"/> Statistics	
<input type="checkbox"/> Nodes	185433
<input type="checkbox"/> Elements	100952

APPENDIX 11: Material Properties Definition in Workbench (Silicon Carbide)

Properties of Outline Row 4: Silicon_Carbide			
	A	B	C
1	Property	Value	Unit
2	 Material Field Variables	 Table	
3	 Density	3100	kg m ⁻³ ▼
4	 Isotropic Secant Coefficient of Thermal Expansion		
5	 Coefficient of Thermal Expansion	4E-06	C ⁻¹ ▼
6	 Isotropic Elasticity		
7	Derive from	Young's Modulus and Po... ▼	
8	Young's Modulus	410	GPa ▼
9	Poisson's Ratio	0.14	
10	Bulk Modulus	1.8981E+11	Pa
11	Shear Modulus	1.7982E+11	Pa
12	 Tensile Yield Strength	550	MPa ▼
13	 Compressive Yield Strength	3900	MPa ▼

APPENDIX 12: Resultant Equivalent Stress & Total Deformation Distribution Tabular Data

- Equivalent Stress:

Tabular Data				
	Time [s]	<input checked="" type="checkbox"/> Minimum [Pa]	<input checked="" type="checkbox"/> Maximum [Pa]	<input checked="" type="checkbox"/> Average [Pa]
1	1.	1.1631e-002	5.1091e+008	7.2619e+007

- Total Deformation:

Tabular Data				
	Time [s]	<input checked="" type="checkbox"/> Minimum [m]	<input checked="" type="checkbox"/> Maximum [m]	<input checked="" type="checkbox"/> Average [m]
1	1.	0.	1.6179e-003	2.9538e-004

APPENDIX 13: Resultant Pressure Force Calculation utilizing Trapezoidal Rule

x	w	Fi	Fi*xi
0	401950,4	40151,685	0
0,1	401083,3	40013,645	4001,3645
0,2	399189,6	34813,815	6962,763
0,3	297086,7	34593,29	10377,987
0,4	394779,1	39352,525	15741,01
0,5	392271,4	38947,41	19473,705
0,6	386676,8	38266,705	22960,023
0,7	378657,3	37217,585	26052,3095
0,8	365694,4	35145,765	28116,612
0,9	337220,9	6647,894	5983,1046
0,92	327568,5	6451,74	5935,6008
0,94	317605,5	6198,172	5826,28168
0,96	302211,7	5807,125	5574,84
0,98	278500,8	2705,2425	2651,13765
0,99	262547,7	2391,23	2367,3177
1	215698,3		0
Net Force	368703,829		
centroid	0,44945		

APPENDIX 14: Actuator Force Calculations

$$\theta = 9.27^\circ \rightarrow \begin{aligned} d_{rx} &= 0.02802 \text{ m} \\ d_{ry} &= 0.51119 \text{ m} \\ d_{Lx} &= 0.434254 \text{ m} \\ d_{Ly} &= 0.070878 \text{ m} \end{aligned}$$

$$0 = F_p \cdot \cos 9.27^\circ \cdot 0.434254 \text{ m} + F_p \cdot \sin 9.27^\circ \cdot 0.070878 - P' \cdot \cos 9.27^\circ \cdot 0.02802 \text{ m} - P' \cdot \sin 9.27^\circ \cdot 0.51119 \text{ m}$$

$$0 = F_p \cdot 0.44 - P' \cdot 0.11$$

$$\hookrightarrow P' = F_p \cdot 4 = 1,474.8 \text{ kN}$$

$$\hookrightarrow P = 1,474.8 \text{ kN} \cdot \frac{0.11 \text{ m}}{0.5 \text{ m}}$$

$$\boxed{P = 324.456 \text{ kN}}$$

$$\theta = 0^\circ \quad \begin{aligned} d_r &= 0.10 \text{ m} \\ d_L &= 0.45 \text{ m} \end{aligned} \quad \rightarrow \quad 0 = F_p \cdot 0.45 - P' \cdot 0.11 \text{ m}$$

$$\hookrightarrow P = 4.091 \cdot F_p \approx 1,509.38 \text{ kN}$$

$$\hookrightarrow P = 1,509.38 \text{ kN} \cdot \frac{0.11}{0.5}$$

$$\boxed{P = 337.83 \text{ kN}}$$

$$\theta = 12.13^\circ \rightarrow \begin{aligned} d_{rx} &= 0.002479 \text{ m}, \quad d_{Lx} = 0.430176 \text{ m} \\ d_{ry} &= 0.511957 \text{ m}, \quad d_{Ly} = 0.092457 \text{ m} \end{aligned}$$

$$0 = F_p \cdot \cos 12.13^\circ \cdot 0.430176 \text{ m} + F_p \cdot \sin 12.13^\circ \cdot 0.092457 \text{ m} - P' \cdot \cos 12.13^\circ \cdot 0.002479 \text{ m} - P' \cdot \sin 12.13^\circ \cdot 0.511957 \text{ m}$$

$$r_p \approx 0.44 \quad \rightarrow \quad 0 = F_p \cdot 0.439 - P' \cdot 0.11$$

$$\hookrightarrow P' = F_p \cdot 4 = 1,474.8 \text{ kN}$$

$$\hookrightarrow \boxed{P = 324.456 \text{ kN}}$$